University of Calgary

PRISM Repository **https://prism.ucalgary.ca**

The Vault Open Theses and Dissertations

2015-01-29

Kinetic Study of the CO2 Capture using Calcium-Based Sorbents and its Application for Hydrogen Production in Gasification Process

Sedghkerdar, Mohammad Hashem

Sedghkerdar, M. H. (2015). Kinetic Study of the CO2 Capture using Calcium-Based Sorbents and its Application for Hydrogen Production in Gasification Process (Doctoral thesis, University of Calgary, Calgary, Canada). Retrieved from https://prism.ucalgary.ca. doi:10.11575/PRISM/26705 http://hdl.handle.net/11023/2045

Downloaded from PRISM Repository, University of Calgary

UNIVERSITY OF CALGARY

Kinetic Study of the CO_2 Capture using Calcium-Based Sorbents and its Application for Hydrogen Production in Gasification Process

by

Mohammad Hashem Sedghkerdar

A THESIS

SUBMITTED TO THE FACULTY OF GRADUATE STUDIES

IN PARTIAL FULFILMENT OF THE REQUIREMENTS FOR THE

DEGREE OF DOCTOR OF PHILOSOPHY

GRADUATE PROGRAM IN CHEMICAL AND PETROLEUM ENGINEERING

CALGARY, ALBERTA

JANUARY, 2015

© Mohammad Hashem Sedghkerdar 2015

Abstract

Carbon dioxide (CO_2) capture and sequestration (CCS) from flue gas obtained from fossil fuel power plants appears to be essential to decrease CO_2 emissions into the atmosphere. Calcium-looping cycle represents a promising technology for CO_2 capture. The intrinsic kinetics of the carbonation reaction for the calcines from two types of limestone (Havelock and Cadomin) was studied. The order of the carbonation reaction changed from first order to zero order when the CO_2 partial pressure exceeded ~ 0.7 atm for both types of limestone. The rate of carbonation reaction increased with increasing temperature up to 675°C and decreased with further increases. The obtained intrinsic kinetic parameters (e.g., order of reaction, activation energy, and per-exponential factor), were applied in global kinetic study of the carbonation reaction.

The global kinetic study performed using the grain model and the changing grain size (CGS) model. In the CGS model, the physical structure of the sorbent particle changes during the reaction. The overall sorbent conversion obtained with the CGS model showed better agreement with the experimental data than the results obtained using the grain model. The presence of sawdust as a biomass during calcination step decreased the negative effects of calcium-based sorbent sintering by enhancement of calcium dioxide (CaO) surface area, which resulted in an improvement in the carbonation initial rate.

Four CO_2 carriers included one calcined natural limestone (Cadomin) and three modified calcium-based sorbents; Cadomin-calcium aluminate cement pellets (CD-CA-14), Cadomin-silica-sol pellets (CD-Si), and Cadomin-mesostructred silica core/shell pellets (CD-CS), were examined through 31 carbonation–calcination cycles. The presence of the Mayenite phase ($Ca_{12}Al_{14}O_{33}$) in the CD-CA-14 pellets led to slower decay in sorbent activity with increased

numbers of cycles. The CD-CS pellets showed the best performance in the retention of CO_2 uptake activity with only 46% activity loss.

Finally, CO_2 capture sorbents were integrated with steam gasification of coal to capture CO_2, which consequently produced high purity hydrogen. The experimental results showed that the presence of sorbent in the steam gasification of coal enhanced the molar fraction of H_2 to more than 80%, with almost all CO_2 fixed into the sorbent structure. The steam gasification of coal integrated with CO_2 capture exhibited an optimal condition at 675°C.

Acknowledgements

First and foremost, I would like to express my gratitude to Allah (SWT) for providing me the ability to think and study. Prayers and peace be upon prophet Mohammad (SAW) and his Ahl al-Bayt (AS) for showing me the aim of life and the way to thank Allah (SWT). Regarding Imam Reza (AS) narration "who thanks creature, would thank Allah (SWT)", I would like to sincerely appreciate people who support and help me to be able to make this thesis.

I would like to express my heartfelt thanks to my supervisor, Dr. Nader Mahinpey for providing me the opportunity to do my doctoral program under his supervision. I am grateful to my supervisor for his continuous financial support, unconditional motivation, and encouragement during my PhD career. I am always thankful for his patience and invaluable guidance to shape my research in a better way.

I would like to take this opportunity to thank my supervisor committee members, Dr. Hector Siegler and Dr. Pedro Pereira Almao for their helpful comments. I am grateful to my examiner, Dr. Hugo de Lasa, Dr. Ed Nowicki, and Dr. Hassan Hassanzadeh for their time and useful comments.

I am very grateful to my mother, Gohari Shakoor and my father, Mohammad Jafar who passed away during my PhD program in November 2011 for their constant support and affection throughout my life. I am indebted to my wife, Zahra for her love, support, patience, understanding, and encouragement throughout my PhD program which helped me to focus on my research work. I will be thankful to my sisters, Elham and Najmeh for their constant help during my life.

The financial support from Carbon Management Canada for this PhD work is highly appreciated. I would also like to thank Dr. Michael Schoel for his help and guidance in using SEM facility.

My special appreciation goes to all the friendly Energy and Environment Research Group (EERG) members. In particular, I would like to acknowledge Dr. Davood Karami, Mr. Ehsan Mostafavi, and Mr. Rico Silbermann for their collaboration and assistance with performing experiments and analyzing the results.

Dedication

I dedicate this thesis to my beloved wife.

Table of Contents

List of Tables

List of Figures and Illustrations

List of Symbols, Abbreviations and Nomenclature

Symbols

a	product layer parameter, dimensionless
$C_{CO_2,g}$	CO_2 concentration in the CaO grain
$C_{CO_2,eq}$	equilibrium CO_2 concentration
$C_{CO_2,R}$	CO_2 concentration in the particle
$C_{CO_2,s}$	CO_2 concentration at the reaction surface
C_b	CO_2 concentration in the bulk
D_{CO_2}	molecular diffusivity of CO_2
D_e	effective diffusivity of CO_2 in the particle
D_g	gas diffusivity
D_K	knudsen diffusivity
D_{PL}	product layer diffusivity
D_{PL0}	initial product layer diffusivity
E	activation energy
k_0	pre-exponential factor
k_s	intrinsic surface rate constant
k_1	rate constant
k_{-1}	rate constant
k_2	rate constant
m(0)	mass of CaO at time zero
m(t)	mass of CaO at time t

MW_{CaO}	molar weight of CaO
n	reaction order
n_d	number of grains in the particle
N_{CaO}	mole of CaO at time t
N_{CaO_0}	mole of CaO at t=0
NP	number of experimental data points
P	total pressure
$Purity$	purity of CaO in calcined limestones
P_{CO_2}	partial pressure of CO_2
$P_{CO_2.eq}$	equilibrium partial pressure of CO_2
R_g	gas constant
r	reaction rate
r_0	reaction rate at time zero
r_c	radius of the unreacted core of the grain
r_g	grain radius
r_g'	expanded grain radius
r_i	radius of un-reacted grain core
R_p	radius of particle
S	specific surface area
S_0	specific surface area at t=0
t	time
T	temperature

X	conversion of CaO
W_{CO_2}	CO_2 molar mass transfer
$W_{CO_2,0}$	CO_2 molar mass transfer with no CO_2 diffusion resistance
X	local conversion
X_o	overall conversion
Z	molar density ratio for product to reactant

Greek letters

$\rho_{m,CaO}$	CaO molar density
θ	fraction of site occupied by $CaO.CO_2$ complex
ε	particle porosity
ε_0	initial particle porosity
ν	molar volume
φ	local Thiele modulus
φ_0	overall Thiele modulus
η	effectiveness factor

Abbreviations

BET	Brunauer-Emmett-Teller method
BJH	Barret-Joyner-Halenda method
CD	Cadomin limestone
CD-CA-14	Cadomin-calcium aluminate cement pellet
CD-Si	Cadomin-silica-sol pellet
CD-CS	Cadomin-mesostructred silica core/ shell pellets

PTGA	Pressurized Thermogravimetric Analyzer
SEM	Scanning Electron Microscopy
TGA	Thermogramivetric Analyzey
XRD	X-ray Diffraction

Chapter One: **Introduction**

1.1 Overview

The world energy demand is projected to increase by 40% between 2007 to 2030 at an annual rate of 1.5%. Although energy generation from renewable resources is projected to grow, fossil fuels will continue to meet a major portion of the worldwide energy needs in the near future [1]. The increasing use of fossil fuels to meet required energy demand has led to higher CO_2 emissions as a greenhouse gas into the atmosphere. Due to their low cost, availability, and existing reliable technology for energy production, fossil fuels currently supply over 85% of the energy used worldwide [2-3].

The rising CO_2 concentration reportedly accounts for at least half of the greenhouse effect that causes global warming [4]. The growing need to reduce anthropogenic CO_2 emissions has led to a global push towards the development of efficient, economical, and realistic carbon capture and sequestration (CCS) technologies for application to fossil fuel-based power plants [5]. In consideration of how best to improve CO_2 capture, three technological pathways are being developed: into post-combustion, pre-combustion, and oxy-fuel combustion, which are illustrated in Fig. 1.1.

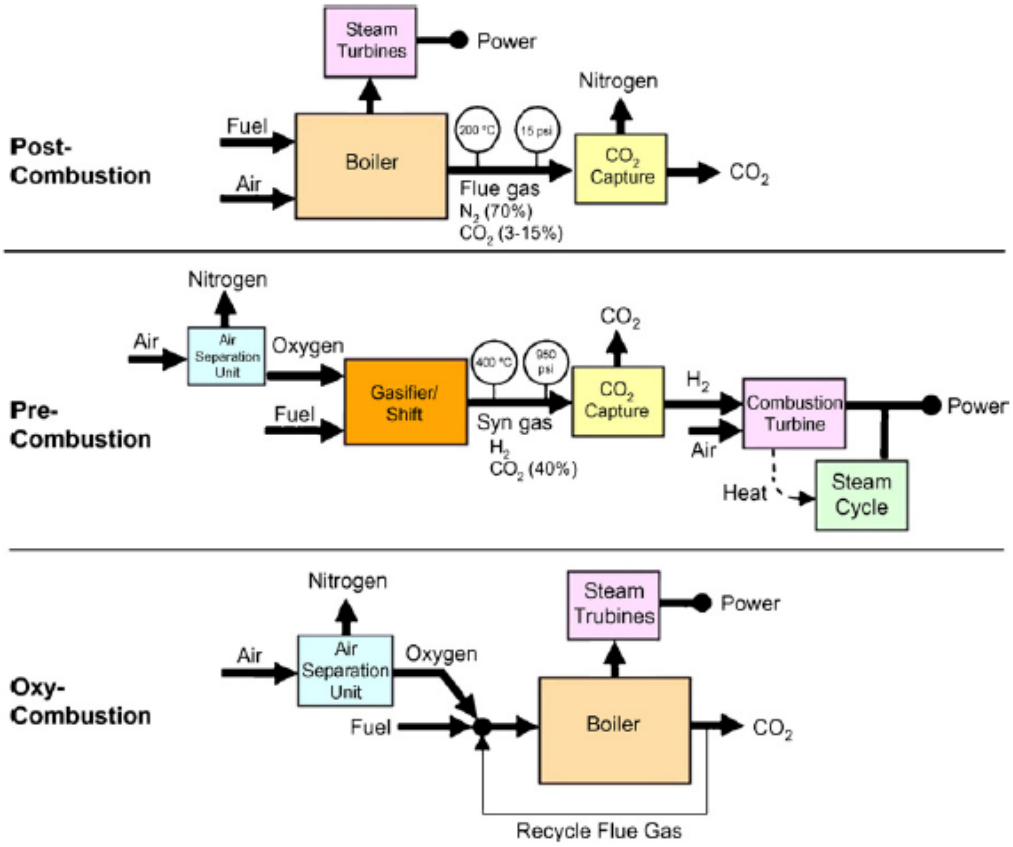

Fig. 1.1 Block diagrams illustrating post-combustion, pre-combustion, and oxy-fuel combustion systems (Taken form [6]).

In post-combustion, the CO_2 is separated from other flue gas produced by combustion. Among the post-combustion technologies, amine-based CO_2 wet scrubbing is believed to be the most technologically mature, but it requires high capital and operational costs [7].

In pre-combustion, the CO_2 is recovered from certain process streams before the fuel is burned. One very promising approach to pre-combustion is the integrated gasification combine cycle (IGCC) supplemented by shift conversion. Whereby, fossil fuel is gasified with oxygen to produce synthesis gas (syngas), a mixture of mainly carbon monoxide (CO) and hydrogen (H_2). The syngas, is sent to a shift reactor to convert CO to H_2 and CO_2 in the presence of steam. The

CO_2 is then separated using chemical absorption, chemical adsorption or membrane in the separation unit. Thus, three units are needed in an IGCC: a gasification reactor, a water gas shift reactor, and a separation unit.

In oxy-fuel combustion, the fuel is burned with oxygen and recycled flue gas to produce a concentrated stream containing CO_2 and steam, which CO_2 is then dried, compressed, and transported for sequestration. Although oxy-fuel obviates the need for a separate CO_2 capture stage, it requires an Air Separation Unit (ASU), which is energy intensive and expensive [8].

Given the advantages of gasification in producing syngas for a range of chemical processes and the overall energy efficiency and environmental factors in power generation, considerable work was conducted over many decades on the gasification of a wide range of feed stocks. Despite these efforts, however, many unanswered questions and uncertainties remain regarding the optimal ways of conducting gasification integrated with an efficient CO_2 capture scheme. Significant research questions remain in the following areas: 1) understanding of the behavior of different solid sorbents, pelletized sorbents, and core-shell sorbents for CO_2 capturing and respective kinetics; 2) studying the effects of various temperatures, pressures, and particle sizes on the carbonation/calcination cycle; 3) a detailed kinetic study of carbonation reaction; 4) the effect of additives as binders such as alumina to the sorbent for enhancing the lifetime and cyclic operation through long series of calcination/carbonation cycles; and 5) the integrated gasification with the CO_2 capture process and respective kinetics in the presence of sorbents.

In this research, several objectives are undertaken to formulate strategies to determine the optimized conditions for integrated gasification with CO_2 capture to decrease the emissions of CO_2, while generating H_2 as an environmentally clean source of energy:

- To study the intrinsic kinetics of the carbonation reaction with two types of commercial natural limestone, Havelock and Cadomin and investigate different key parameters such as temperature, partial pressure, and total pressure (Chapter 2).
- To study the detailed global kinetics of a CO_2 capture process with a calcium-based sorbent as a non-catalytic gas-solid reaction using both the grain and the changing grain size (CGS) models (Chapter 3).
- To focus on the presence of biomass through the calcination period and its effect on the sorbent surface morphology and carbonation kinetics (Chapter 4).
- To synthesize new calcium-based solid sorbents prepared by various procedures, and investigate their CO_2 capture activity and cyclic stability through 31 carbonation–calcination cycles. Natural Cadomin limestone was used as the base of the sorbents (Chapter 5).
- To investigate H_2 production from the steam gasification of Boundary Dam (BD) coal integrated with CO_2 capture using calcined natural Cadomin limestone in a horizontal fixed bed reactor. In order to identify basic kinetic information, the effects of the reaction parameter such as temperature and molar ratio of sorbent-to-carbon in BD coal ([Ca]/[C]) were investigated (Chapter 6).

1.2 Literature review

Energy may be the most important factor that sustains human civilization and influences society in the 21st Century. Before the 18th century, the consumption of energy was limited to applications such as residential heating and cooking, and ancient metallurgical activities. Energy was mainly generated from naturally available sources with or without preliminary pre-treatment due to the lack of advanced knowledge of mining and energy conversion technology [9].

However, the UK-based industrial revolution that spreaded throughout the entire world led to gradual transformation of the small-scale manual labor and draft-animal-based economies into an advanced large-scale machine-based manufacturing. During this transition, numerous modern industries, such as textile, aviation, and chemical industries began to emerge. Large-scale manufacturing and advancements in technology resulted in long-term economic prosperity and growing world population [10-11]. Therefore, the demand for stable and abundant energy was projected to increase, dramatically. Due to its low cost and availability, fossil fuel became the main source of the world's energy supply in the 18^{th}, 19^{th}, and 20^{th} centuries [12].

The term "global warming" was first used by Wally Broecker in his paper published in Science in 1975 and described it as a result of CO_2 emissions from burning chemical fuels [13]; a great deal of research works and debates have been taken place about this topic since then [14-18]. Today, despite the doubts and debates, it is widely accepted that the anthropogenic decrease of CO_2 into the atmosphere is the main solution to prevent global warming [19]. As far as reducing the huge contribution of fossil fuel combustion in anthropologic CO_2 emissions, many investigations and much research continue to be conducted on the development of clean and renewable sources of energy such as solar energy, geothermal power, nuclear energy, and wind power [20-21]. Although a great deal of effort is being expended to investigate on alternative sources of energy, such as renewable resources from the late 20^{th} century which are projected to grow, fossil fuels still produce a major portion of the energy needs today and will continue to do so in the near future, due to their cost efficiency and existing reliable technology for energy production [22]. Therefore, the growing need for the reduction of anthropogenic CO_2 emissions has led to a global push to develop efficient, economical, and realistic CCS technologies for application to fossil fuel-based power plants [22]. In CCS, the CO_2 is first captured during fossil

fuel conversion, which is the most costly stage and is then compressed and geologically sequestered in deep subsurface rock formations for long-term storage.

There are three types of technological approaches under development with respect to the capture of CO_2: post-combustion, pre-combustion, and oxy-fuel combustion processes [21-25]. Post-combustion technology, which is proven, commercially available, and low-temperature separate CO_2 from the flue gases produced by combustion using wet scrubbing with amine solvents (i.e., mono-ethanolamine, MEA) [26]. However, this approach introduces serious loss in efficiencies and economic penalties, including the high cost of manufacturing the solvent [27]; degradation of the solvent due to undesired reactions with certain compounds such as oxygen (O_2) and sulfur dioxide (SO_2) in the flue gas [28]; and the disposal of the large quantities of waste solvent which causes both environmental and health safety concerns.

In oxy-fuel combustion, the fuel is burned with pure oxygen instead of air (as in conventional combustion processes) and recycled flue gas to produce a concentrated stream containing CO_2 and steam, which is then dried, compressed, and transported for sequestration. Although oxy-fuel combustion obviates the need for a separate CO_2 capture stage, it does requires an ASU in order to provide a vast quantity of O_2, which is energy intensive and expensive [8]. Due to the strong exothermic reaction of combustion with pure O_2, more safety management is required, thereby causing additional capital and operating costs.

In pre-combustion, the fuel reacts with steam and/or oxygen to produce mainly syngas, which is a mixture of CO and H_2 (Eq. (1.1)). The produced syngas is sent to the shift reactor to convert CO to H_2 and CO_2 in the presence of steam through the water-gas-shift reaction (Eq. (1.2)). CO_2 is then separated from H_2 in a separation unit using a physical or chemical absorption process.

$C + H_2O \rightarrow CO + H_2$ $\Delta H^o_{298} = 132\ kJ/mol$ (1.1)

$CO + H_2O \rightarrow CO_2 + H_2$ $\Delta H^o_{298} = -41.5\ kJ/mol$ (1.2)

Given the disadvantages of wet scrubbing CO_2 capture and oxy-fuel combustion, a wide range of research is being pursued for alternative CO_2 capture technologies. One promising technology involves the use of solid sorbents and can be performed under wider operating conditions. Among the solid sorbents for capturing CO_2, calcium-based solid materials are the least costly, most abundant sorbents for the capture of CO_2 for high-temperature operations through the calcium-looping cycle [29-30]. In addition, a calcium-based sorbent has a high initial activity for CO_2 capture compared to an amine solution. In the calcium-looping cycle process, a calcium-based sorbent, typically derived from limestone or dolomite, reacts via a reversible reaction, as presented in Eq. (1.3). The schematic diagram of the calcium-looping cycle is shown in Fig. 1.2.The forward exothermic reaction is known as the carbonation step and the backward step is known as the calcination.

$CaO\ (s) + CO_2\ (g) \leftrightarrow CaCO_3(s)$ $\Delta H^o_{298} = -178\ kJ/mol$ (1.3)

where CaO is calcium oxide and CaCO3 is calcium carbonate or limestone.

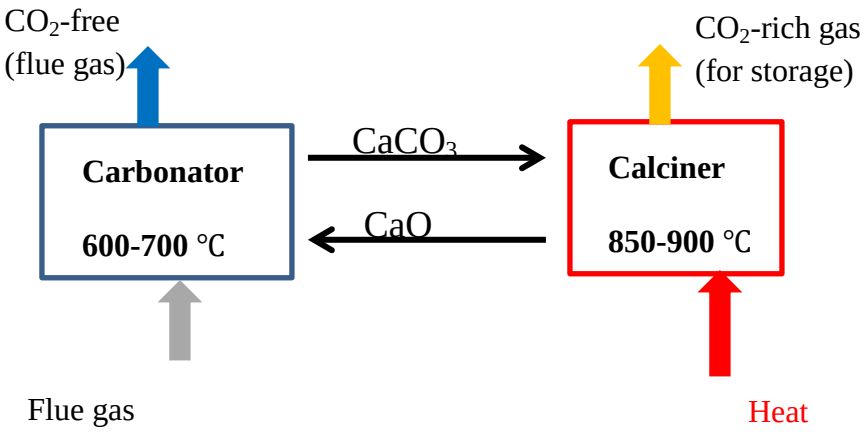

Fig. 1.2 Schematic diagram of a Calcium-looping cycle

Fig. 1.3 shows the equilibrium vapor pressure of CO_2 as a function of temperature. The carbonation reaction occurs when the partial pressure of CO_2 is greater than the equilibrium partial pressure at a given temperature; and, those partial pressures lower than that of the equilibrium favor the calcination reaction.

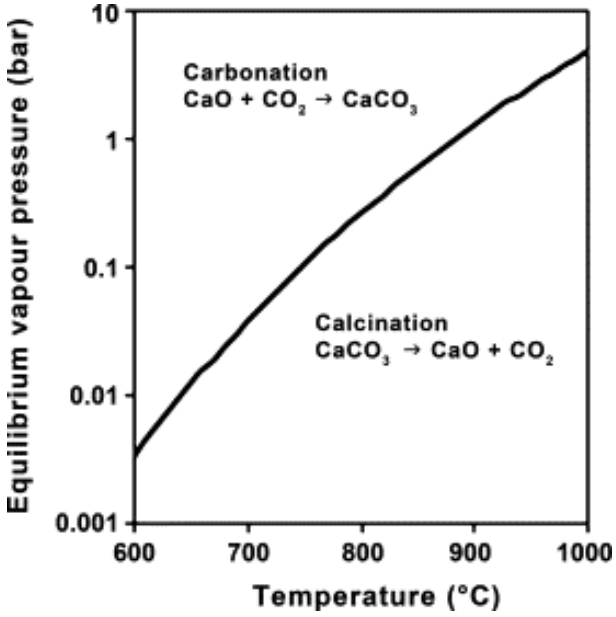

Fig. 1.3 Equilibrium vapor pressure of CO_2 over CaO as a function of temperature [36]

Some of the important applications of calcium-based sorbents for CO_2 capture processes include hydrogen production by reaction-integrated novel gasification (HyPr-Ring) [31-33] and fluidized bed combustors for in situ CO_2 capture [34-35]. In these applications, gasification is integrated with the CO_2 capture process to capture the CO_2 stream at high temperatures, which is mainly produced from the water-gas-shift reaction. According to LeChâtelier's principle, the equilibrium is shifted forward and results in an improvement of the gasification process to produce H_2 rich gas and a concentrated CO_2 stream suitable for sequestration [31-35].

1.2.1 Kinetic study of carbonation reaction with CaO-based sorbents

Heterogeneous catalytic and non-catalytic reactions play a significant role in industrial applications, such as the coal gasificaion process, metals preparation from oxides, and nitrogenation of calcium carbide to produce cyanamide. The capture of CO_2 with a calcium-based sorbent is categorized as a heterogeneous non-catalytic gas-solid reaction. Therefore, assignation of the conditions of the reversible carbonation reaction (Eq. (1.3)) has to strike equivalence between high temperature, which aids the rate of reaction; and low temperature, which favors the equilibrium conversion.

A non-catalytic gas-solid reaction with no gaseous product takes places in three steps: first, external mass transfer of the gaseous reactant through the gas film formed surrounding the solid particle; second, internal mass transfer of the gaseous reactant through the particle and product layer; and, lastly, the reaction at the reaction surface. Alternatively, Barker [36] showed that the carbonation reaction that produces a solid product takes place in two regimes. The first regime involves a rapid chemical the reaction of reactant gas with solid particles at the fresh CaO surface, which produces a sharp interface between the product layer and the un-reacted inner core of the CaO particle. This is followed by the second regime, which is a slow reaction characterized by the formation of a $CaCO_3$ layer that impedes the reactant gas diffusion. In the first stage, the reaction is controlled kinetically; and after formation of the product layer, the diffusion controls the whole reaction. The intrinsic kinetic of the carbonation reaction as a gas-solid reaction focuses on the first stage of the reaction, which is controlled kinetically in the absence of pore diffusion; whereas both the kinetic control and diffusion control regimes are considered in the global kinetic study using intrinsic kinetic parameters such as activation energy, the pre-exponential factor, and the order of reaction.

1.2.1.1 Intrinsic kinetic study

Bhatia and Perlmutter [37] performed an early intrinsic kinetic study of the carbonation reaction in 1983. They found a zero-activation energy for the carbonation reaction using an atmospheric thermogravimetric analyzer (ATGA) with CO_2 concentrations in the range of 0 to 10 mole%. Similarly, Von Nitsch [38] obtained a zero-activation energy for the initial carbonation reaction at 800-850°C. However, Sun et al. [39] reported activation energies of 29 and 24 kJ/mol for limestone and dolomite, respectively, in the temperature range of 500 to 650°C. In another study, Kyaw et al. [40] found activation energies of 78 kJ/mol for a limestone and 35 kJ/mol for a dolomite.

Another issue regarding the intrinsic kinetic study of the carbonation reaction is the uncertainty in the order of reaction. Bhatia and Perlmutter [37] and Sun et al. [39] claimed that a first-order intrinsic rate changed to zero order, when the CO_2 partial pressure exceeded 0.1 atm; however, Yu and Fan [41] observed a shift in the order of the carbonation reaction from one to zero at CO_2 partial pressures higher than 1 atm.

1.2.1.2 Global kinetic study

There are many parameters that affect the carbonation reaction, such as temperature, physical structure of the solid particles, and particle size. Therefore, an appropriate mathematical model is required to reliably represent the behavior of the interaction between gaseous and solid reactants. The desired mathematical model should be the closest representation of reality without mathematical complexities.

There are several mathematical models proposed to model non-catalytic gas-solid reactions in the standard textbooks [42-43]. The un-reacted shrinking core model and the grain model are used mostly for a non-catalytic gas-solid reaction for a non-porous and a porous solid

reactant, respectively. The un-reacted shrinking core model is an early model proposed for the gas-solid reaction [44] and is well-explained in chemical reaction engineering textbooks. In this model, the reaction takes place at the sharp interface between the outer layer (product layer) and the inner un-reacted core of the particle. As the reaction proceeds, the reaction zone moves into the solid particle but the overall particle size remains constant. A schematic diagram of the un-reacted shrinking core model is shown in Fig. 1.4.

Although the un-reacted shrinking core model does not exactly demonstrate the whole mechanism of a non-catalytic gas-solid reaction, it is widely accepted as the most popular and simple model used for gas-solid reactions. This model has been used by several researchers to interpret their experimental results [45-47].

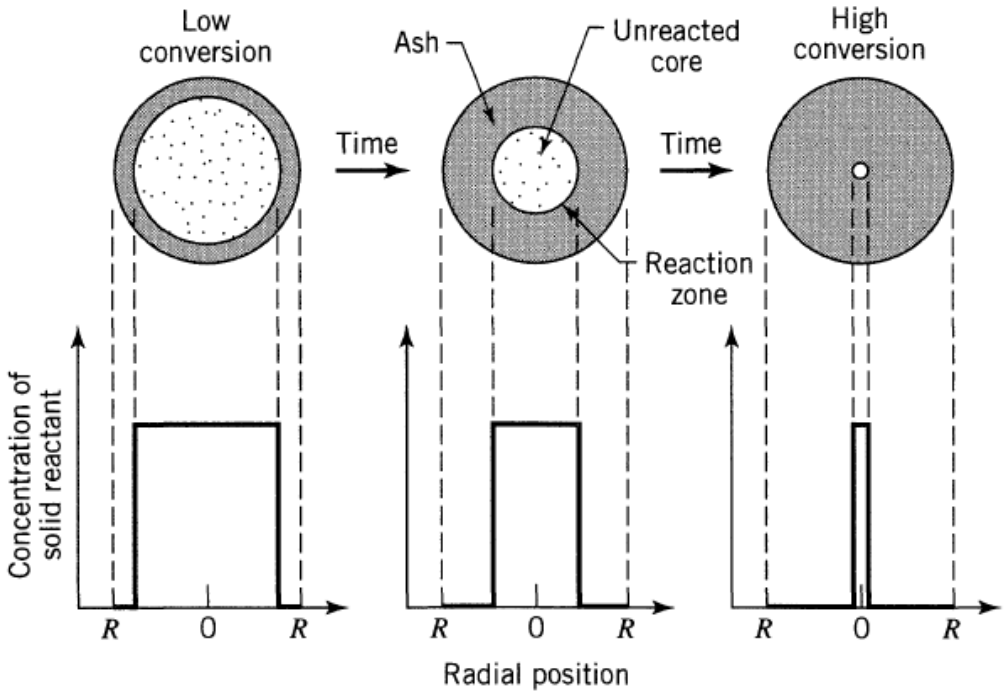

Fig. 1.4 Schematic diagram of the un-reacted shrinking core model [43]

On the other hand, the grain model, considers a spherical porous solid particle consisting of a large number of small non-porous grains (Fig. 1.5). In this model, the non-porous grains are

located next to each other within the solid particle and the reactant gas has to diffuse through the pores between grains to reach the grains. Similarly to the un-reacted shrinking core model, the reaction takes place at the surfaces of the grains in the grain model. The grain model has been analyzed in detail by Szekely and Evans [48] and is discussed at greater length in Chapter 3 of this thesis. The grain model has been used by numerous researchers due to its potential determine the radial profile of the reactant gases in solid particles. This model has been applied to a variety of gas-solid reactions, such as metal oxide-based solid sorbent with different reactant gases [49-51].

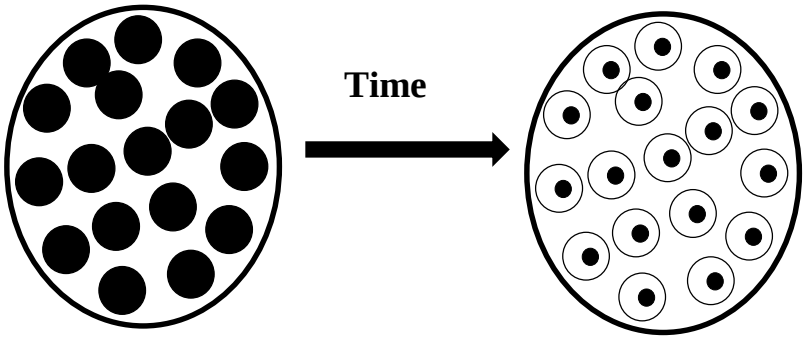

Fig. 1.5 Schematic diagram of the grain model [42]

1.2.2 Pre-treatment of calcium-based sorbents using different methods and materials

The result of a calcium-looping cycle using a natural calcium-based sorbent such as limestone or dolomite shows two major limitations: 1) the loss of sorbent activity in the CO_2 uptake over multiple carbonation-calcination cycles; and, 2) the mechanical fragility of natural sorbents leads to excessively high sorbent losses in fluidized bed systems [52]. The loss of sorbent activity due to sintering of the porous CaO during high temperature calcination and

attrition causing an elutriation of fines with the increasing number of cycles are the two most important issues with the calcium-looping cycle [53-55]. Sintering is accompanied by an expansion of the crystallite dimensions, leading to decreases in the particle specific surface area and porosity. Sintering may also cause a decrease in the pore openings, with the pores eventually closing completely and making the active species inaccessible to the reactants.

Several methods have been proposed to improve the initial physical properties of the sorbent to counteract the negative effects of sorbent sintering: these methods include steam hydration, thermal pre-treatment of the sorbent, and pelletization.

Most research investigations have performed the calcium-looping cycle process using a thermogravimetric analyzer (TGA) in a laboratory or a pilot-scale fluidized bed combustion (FBC). The most commonly employed experimental conditions have been isothermal, under nitrogrn (N_2), air, argon (Ar), or diluted CO_2 flow during the calcination stage, in order to be able to regenerate sorbent at lower temperature and under CO_2 during carbonation step. The proposed approaches to decrease sorbent sintering and the investigation results are presented in the following sections.

1.2.3 Supported calcium oxides

Many studies have proposed the addition of a support material called binders to prevent sorbent sintering and to maintain the sorbent activity through multiple cycles. Recent research works showed that the presence of aluminium oxide (Al_2O_3) in the form of Mayenite ($Ca_{12}Al_{14}O_{33}$), improves the durability of calcium-based sorbents. Manovic et al. [56-57] showed that the pelletization of sorbents using calcium aluminate cement as a binder significantly improved the performance of the calcium-looping cycle. Calcium aluminate cement was shown to enrich the physical strength of the sorbent and, as a source of Al_2O_3, developed a nanoporous

structure for enhanced CO_2 capture activity. In a long series of 1000 carbonation-calcination cycles, such pellets indicated a high residual activity of 28%, while the residual activity of natural sorbent was reported to be 7.5% and 16%.

Kaolin, which is a natural source of Al_2O_3 and widely available, has been attractive for use as a binder for calcium-based sorbent [58]. However, investigations indicated that natural kaolin is an unstable binder for pelletization of calcium-based sorbent, due to its negative effect on the sorbent morphology. In contrast, aluminium hydroxide ($Al(OH)_3$) binder obtained from kaolin leaching showed a strong positive impact on calcium-based pellet surface morphology with respect to the surface area and pore volume, resulting in a significant improvement in the calcium-looping cycle [59].

Manovic et al. [60] investigated different binders, including sodium and calcium bentonites, and concluded that these binders increased the sintering rate due to the formation of calcium-silica (spurrite, $Ca_5(SiO_4)_2CO_3$). Albrecht et al [61] showed that a mixture of 20 wt% magnesium oxide (MgO) with 80 wt% CaO could maintain residual activity of 24% after 1250 cycles. In another study, Li et al. [62] reported that a mixture of CaO with 26% MgO in a series of 100 carbonation-calcination cycles showed 45% residual activity.

It is widely accepted that the performance of dolomite-derived CaO is better than limestone-derived CaO for the calcium-looping cycle process due to the presence of MgO that inhibits the sorbent sintering. Manovic and Anthony [63] concluded that calcination under realistic conditions, for instance in a FBC capture plant (> 900 °C and > 90% CO_2) [64], appears to compromise the performance of sorbent in the calcium-looping cycle and the use of a binder enhances the sorbent cost.

Li et al. [62] proposed an activation strategy to improve the performance of sorbent over long series of carbonation-calcination cycles, including limestone treatment with acetic acid as an organic acid, and then generating CaO by heating. However, Ridha et al. [65] suggested that natural limestone (100-1000 μm) treated with organic acid tended to disintegrate under real fluidized bed operating conditions. Therefore, a new activation approach was proposed consisting of the combination of acetification with pelletization. Pellets prepared from acetified powdered Havelock limestone using 10 vol% acetic acid and with $Al(OH)_3$ binder (at a ratio of 5.5) exhibited 44% improvement in both the surface area and pore volume, which would be useful for superior performance in the calcium-looping cycle [66].

1.2.4 Hydration

Hydration has been proposed as one of the most promising approaches to overcome the problem of decay in sorbent performance in the calcium-looping cycle process. The idea of reactivating calcium-based material particles by means of hydration was suggested by Argonne National Laboratories in 1980 to enhance the utilization of calcium-based sorbent materials for SO_2 capture in a FBC [67]. In this case, the higher molar volume of calcium sulfate ($CaSO_4$) compared to CaO favors pore blockage and the formation of the product layer of $CaSO_4$ around CaO. Therefore, the diffusion of reactant gas through the product layer and reaching CaO inside the particle is slow, resulting in a low conversion in the FBC system (between 30 and 45%). In such cases, hydration would be useful to regenerate the used calcium-based sorbent by penetrating H_2O through the layer of $CaSO_4$ and reacting with CaO in the core of the particle to form calcium hydroxide ($Ca(OH)_2$). The higher molar volume of $Ca(OH)_2$ compared to that of CaO, leads to particle swelling and cracking on the surface of CaO. As a result, the fresh CaO in the interior can react with SO_2 [68].

Although the deactivation mechanisms in the CO_2 capture process through the carbonation reaction and the SO_2 capture through the sulfation reaction differ, the hydration process can be applied to reactivate calcium-based sorbents used in the calcium-looping cycle process. The exothermic hydration reaction of calcium-based sorbent is shown in Eq. (1.4):

$$CaO+H_2O \rightarrow Ca(OH)_2 \qquad \Delta H = -178\ kJ/mol \qquad (1.4)$$

Hydration of calcium-based sorbents can occur using both water and steam, both of which have been investigated by several researchers. Hughes et al. [69] reported an improvement in the sorbent activity in the capture of CO_2 using the hydration method to regenerate spent CaO sorbent from the calcium-looping cycle process and achieved a conversion of 52% after 20 carbonation-calcination cycles. They suggested that high pressure steam hydration enhanced the surface area of the sorbent due to formation of cracks in the sorbent particle, creating channels extending to the interior of the sorbent particle.

Fennell et al. [70] suggested a hydration method with water at room temperature to regenerate used sorbent in a fluidized bed through 30 carbonation-calcination cycles. They used this method after the regeneration step and reported a CaO conversion of higher than 50%. Although the reactivated spent sorbent showed superior performance in capturing CO_2, the reactivated sorbent particles were very fragile and could not be used in FBC systems.

Manovic and Anthony [71] applied a mixture of CO_2 and steam during carbonation step at different temperatures (350-800°C). The results showed that the carbonation conversion improved with the addition of steam, which was more pronounced at lower temperatures. In this case, the steam increases the carbonation conversion via solid-state diffusion through the product layer.

Ramkumar and Fan [72] applied steam during the calcination step and found that hydration was effective in sorbent reactivity, due to the reduction in the extent of sintering. Kuramoto et al. [73] have studied the effect of an intermediate hydration treatment of a calcium-based sorbent with steam at high temperature and pressure using TGA for a specific application in a novel hydrogen production process called HyPr-RING. Lin et al. [31-33] proposed the HyPr-RING process, in which both hydration and carbonation of sorbent occurs in the gasifier under operation conditions. The results showed an improvement in reactivity and durability of the sorbents for the calcium-looping cycle process. Moreover, the heat produced from both the hydration and carbonation can balance the endothermic gasification reaction.

1.2.5 CO_2 removal and hydrogen production

Hydrogen as a clean source of energy will play a significant role in the future providing energy that can be used in transport, industrial, and residential application, where fossil fuels are currently used. Hydrogen has several advantages compared to fossil fuels, such as non-toxicity, high heating value per unit weight, and safe transportation. There are additional benefits for the switch to hydrogen from fossil fuels, including enhancement of energy security due to a greater variety of resources for supply, and greater energy efficiency with the progress in hydrogen fuel cell technology [74]

To meet worldwide demand, hydrogen will need to be produced from all available resources, such as fossil fuels, biomass, or even water. Hydrogen can be produced through thermochemical processes using diverse feed stocks such as coal, natural gas, and petroleum. Currently, hydrogen is produced via: (a) steam methane reforming (48%), (b) coal gasification (18%), (c) oil reforming (30%), and (d) electrolysis (4%).

Coal, as the most abundant source of energy on earth, is a potential resource for the production of hydrogen, which can enhance energy security and reduction of CO_2. Approximately 67% of the coal produced worldwide is used in coal-based power plants [75]. There are two major coal-based power generation technologies: conventional coal combustion plants and coal gasification plants. Pulverized coal (PC) technology is a conventional coal combustion, where the heat generated from burning the coal is used to produce steam to drive a steam turbine-generator (Fig. 1.6). In a PC power plant, only 33% of the coal heat value is converted into electricity. The low efficiency of the PC power plant results in increasing the emission of the pollutant gases (mainly CO_2) per unit of energy generated [7].

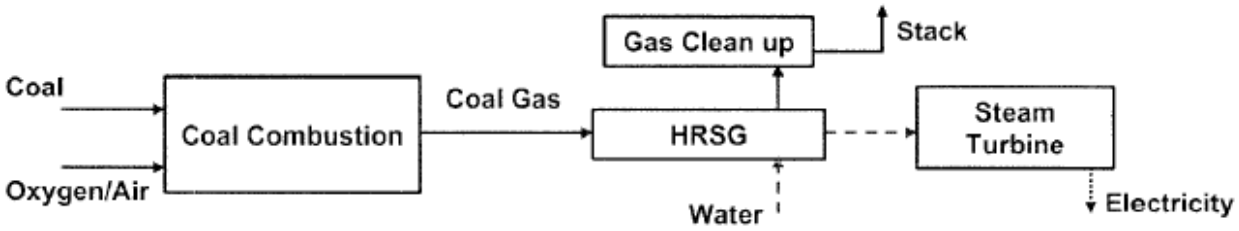

Fig. 1.6 Schematic diagram of a conventional combustion power plant

The integrated gasification combined cycle (IGCC) is a coal gasification technology. In IGCC, coal is gasified at high temperature (800-1200°C) to produce a mixture of fuel gases (CO, CO_2, H_2, and methane (CH_4)). The produced gases are subsequently cleaned-up (sulfur removal, conversion of CO to CO_2, CO_2 separation, and methanation) and fired in a gas-turbine generator and the exhaust gas of turbine is then used to generate steam to utilize in a steam-turbine generator.

IGCC power plants are more efficient (> 50%) at converting the heat value of coal to electricity, which decreases the fuel consumption and CO_2 emissions (40%) per unit of energy generated [76]. Other environmental advantages of coal gasification include producing much

lower SO_x (sulfur oxides), and NO_x (nitric oxide and nitrogen dioxide) emissions. In addition, the syngas produced from coal gasification can be used in several catalytic processes, such as the Fisher-Tropsch process to produce other value-added chemicals and light fuels. Despite the high efficiency of the coal gasification, the high carbon to hydrogen ratio of coal results in high CO_2 emission. Therefore, the reduction of CO_2 emissions is critical to minimize the effect of the coal gasification process on global warming.

In the IGCC process, the coal gasifier produces syngas, which is then introduced into a shift reactor that is usually operating at a temperature around 450^{o}C for CO conversion through the water gas shift reaction (Eq. (1.2)). While higher temperatures enhance the kinetics of the water gas shift reaction, its exothermic nature adversely affects H_2 production, and the H_2 yield decreases with rising temperature [77]. Therefore, the water gas shift reaction requires a lower temperature than that of the gasification process for CO conversion.

The IGCC process requires a unit for CO_2 separation from H_2 after the CO conversion. There are several technologies to capture CO_2, such as polymeric membranes, and chemical solvents, such as amine-based solutions, which are applied at low temperatures (less than 100°C). These low temperature syngas cleanup processes are energy intensive, due to the gas cooling and reheating requirements for capturing and releasing CO_2, respectively. It has been reported that syngas cleaning at high temperatures saves up to 15% of the total thermal efficiency of the gasification process [76]. Therefore, researchers have attempted to study high temperature CO_2 removal to maximize H_2 production.

Materials that are capable of capturing CO_2 at high temperatures can be high temperature membrane, such as a ceramic membrane, and solid sorbents. Ceramic membranes are expensive, and susceptible to poisoning. Moreover, membranes suffer from a considerable pressure drop

[78]. A huge challenge therefore exists in developing low cost membranes suitable for the capture of CO_2 at high temperature.

A promising technique to drive the water gas shift reaction forward for enhanced H_2 generation is the removal of CO_2 from the reaction mixture a using solid material. According to thermodynamic analysis, if CO_2 is removed during the water gas shift reaction, CO is converted to H_2 at a comparatively high temperature [79]. This is achieved based on the process in which CO_2 reacts with a solid metal oxide sorbent to produce a metal carbonate (Eq. (1.5)).

$$MxO + CO_2 \rightarrow MxCO_3 \quad (1.5)$$

Once the metal oxide has reached an appropriate conversion level, it can be thermally regenerated to the metal oxide and CO_2 by heating the metal carbonate as follows:

$$MxCO_3 \rightarrow MxO + CO_2 \quad (1.6)$$

There are several advantages for the use of a reaction based CO_2 separation process. The CO_2 separation can be performed under flue gas (800-1200°C and atmospheric or sub-atmospheric pressure) conditions. This is a unique advantage over processes such as absorption and membrane separation, where either low temperatures and/or high pressures are required to increase separation efficiencies. Another advantage of reaction based CO_2 separation processes is that metal oxides have high adsorption capacities. For comparison purposes, mono-ethanolamine (MEA) captures 60g of CO_2/kg, silica gel adsorbs 13.2g of CO_2/kg, and activated carbon adsorbs 88g of CO_2/kg, while CaO captures 393g of CO_2/kg [80]. The final benefit for using a reaction based CO_2 separation process is the capability of generating a nearly pure stream of CO_2, because the only off gas leaving the sorbent after regeneration (calcination) is CO_2 [81].

The choice of a suitable metal oxide is critical in determining the viability of the CO_2 separation process. Table 1.1 presents the approximate calcination temperatures, at atmospheric pressure.

Table 1.1 Calcination temperature of various metal carbonates [82]

	$CaCO_3$	$MgCO_3$	$ZnCO_3$	$PbCO_3$	$CuCO_3$	$MnCO_3$
Calcination temperature (^oC)	800	385	340	350	260	440

Based on the exit gas temperature from both combustors and gasifiers, calcium carbonate is the best candidate as a sorbent, In addition, the higher carbonation temperature reduces the amount of heat needed to be removed from the exit gas to attain the carbonation temperature.

1.3 Objectives and layout of the thesis

The overall objective of this thesis is the integration of coal gasification and CO_2 capture using a solid sorbent and, at the same time, produce high purity hydrogen. Hence, two topics have been studied in this investigation. The first topic focuses on the capture of CO_2 using a solid sorbent and the second addresses the application of the solid sorbent in the gasification process to capture CO_2 and produce high purity hydrogen.

Therefore, the specific objectives of this thesis are as follows:

- To study the intrinsic kinetic of the CO_2 capture process using a solid sorbent;
- To describe CO_2 capture experimental data using a mathematical model of the gas-solid reaction;
- To improve the activity and durability of solid sorbents for the calcium-looping cycle process;
- To investigate the effect of sawdust on the CO_2 capture process; and

- To study the integrated coal gasification and CO_2 capture technology to produce hydrogen

Chapter 2 focuses on the first objective, which is the investigation of the intrinsic kinetic of the CO_2 capture process using a solid sorbent through the carbonation reaction. In this chapter, a detailed description of the intrinsic kinetics of the carbonation reaction with two types of commercial limestone, Havelock and Cadomin, using an ATGA and a pressurized thermogravimetric analyzer (PTGA) is presented. The kinetic parameters, such as activation energy, the pre-exponential factor, and the order of reaction, are calculated using experimental data. Moreover, the effect of numerous key parameters, such as temperature, partial pressure, and total pressure, on the kinetic of carbonation reaction is investigated.

Chapter 3 describes the CO_2 capture experimental data through the carbonation reaction as a non-catalytic gas-solid reaction using a mathematical model, (e.g., the grain model and the changing grain size (CGS) model). The effects of temperature, particle size, and porosity of the sorbent on the kinetics of the carbonation reaction are investigated, which is quite difficult experimentally. In addition, the modeling results using both the grain and CSG models are validated and compared with our own experimental data points, as presented in Chapter 2.

There are extensive research works which have been devoted to investigate the effects of various gases, such as CO_2, syngas, and steam on the kinetics of calcination and carbonation reactions, the influence of biomass during calcination and on the carbonation reaction rate has not been reported. Chapter 4 investigates the effects of sawdust as a biomass during high temperature calcination on the surface morphology of the calcium-based sorbent, and consequently on the carbonation kinetics.

Chapter 5 focuses on the improvement of the activity and durability of the solid sorbents for the calcium-looping cycle process. The advantages of looping cycles in the capture of CO_2 are the generation of a pure CO_2 stream, overall energy cost and efficiency, and environmental benefits; however, considerable challenges remain to be investigated. The loss of sorbent activity, due to sintering and attrition, with the increasing number of cycles are the most important issues [13-14]. In this chapter, some methods are proposed to modify the physical structure of natural calcium-based sorbents to counteract the negative effects of sorbent sintering. Therefore, modified sorbents using pelletization and core/shell procedures are prepared and their CO_2 capture activity and cyclic stability through 31 carbonation–calcination cycles are compared to the natural calcium-based sorbent. This study presents a collaborative work with CanmetEnergy, Natural Resources Canada in Ottawa and Université Laval.

Chapter 6 discusses the application of the calcium-based sorbent in the coal gasification process to capture CO_2 and consequently produce hydrogen. The integrated gasification combined cycle (IGCC) supplemented with shift conversion is a very promising approach for pre-combustion capture.

In recent years, a new gasification method for H_2 production from coal using a CO_2 solid sorbent, i.e., hydrogen production reaction integrated novel gasification (HyPr-RING), was proposed by Lin et al. [31-33]. This chapter provides a detailed study on H_2 production from the integration of the steam gasification of coal with CO_2 capture using calcium-based sorbents. The effects of temperature and molar ratio of sorbent-to-carbon in coal are investigated.

Finally, the conclusions and recommendations for future work are presented in Chapter 7.

1.4 Outcome of the thesis

The author has published four peer-reviewed journal papers and submitted a fifth manuscript as the first author as well as two additional peer-reviewed papers as the second author. A list of these publications follows:

Published peer-reviewed journal papers (First author):

1. **Sedghkerdar, M. H.**, Mostafavi, E., Mahinpey, N., Investigation of the kinetics of carbonation reaction with CaO-based sorbents using experiments and Aspen Plus simulation, Chem. Eng. Comm. 202 (2015) 746-755.

2. **Sedghkerdar, M. H.**, Mahinpey, N., Ellis, N., The effect of sawdust on the calcination and the intrinsic rate of the carbonation reaction using a Thermogravimetric Analyzer (TGA), Fuel proc. Technology 106 (2013) 533-538.

3. **Sedghkerdar, M. H.**, Mahinpey, N., Sun, Z., Kaliaguine, S., Novel synthetic sol-gel CaO-based sorbent using porous mesostructured silica as CO_2 carriers in cyclic capture processes, Fuel 127 (2014) 101-108.

4. **Sedghkerdar, M. H.**, Mostafavi, E., Mahinpey, N., Sorbent Enhanced Hydrogen Production from Steam Gasification of Coal Integrated with CO_2 Capture, Int. J. Hydrogen Energy 39 (2014) 17001-17008.

5. **Sedghkerdar, M. H.**, Mahinpey, N., A modified grain model in studying the CO_2 capture process with a calcium-based sorbent: a semi-analytical approch, Ind. Eng. Chem. Res. (2015) In press, DOI10.1021/ie503989n.

Published peer-reviewed journal (Second author):

6. Mostafavi, E., **Sedghkerdar, M. H.**, Mahinpey, N., Thermodynamic and kinetic study of CO_2 capture with calcium based sorbents: experimental and modeling, Ind. Eng. Chem. Res. 52 (2013) 4725-4733.

7. Sun, Z., **Sedghkerdar, M. H.**, Saayman, J., Mahinpey, N., Ellis, N., Zhao, D., and Kaliaguine, S., A facile fabrication of mesoporous core/shell CaO based pellets with enhanced reactive stability and resistance to attrition in cyclic CO_2 capture, J. Mat. Chem. A 2 (2014) 16577-16588

1.5 References

[1] Energy Information Administration (EIA), International Energy Outlook. Washington, D.C.: U.S. Department of Energy, DOE/EIA-0484 (2009).

[2] Energy Information Administration (EIA), Annual Energy Outlook (2006a). http://www.eia.doe.gov/oiaf/aeo/.

[3] Energy Information Administration (EIA), International Energy Outlook (2006b). http://www.eia.doe.gov/oiaf/ieo/index.html.

[4] Houghton, J. T., Meira Filho, L. G., Callander, B. A., Harris, N., Kattenberg, A., Maskell, K., Climate Change 1995, The science of climate change. Cambridge University Press, Cambridge, UK (1996).

[5] Metz, B., Davidson, O., de Coninck, H., Loos, M., Meyer, L., Special report on carbon dioxide capture and storage. Intergovernmental panel on climate change, Cambridge University Press: New York (2005).

[6] Obersteiner, M., Azar, C., Kauppi, P., Mollerstern, M., Moreira, J., Nilsson, S., Read, P., Riahi, K., Schlamadinger, B., Yamagata, Y., Yan, J., and Ypersele, J. P., Azar, C., Kauppi, P., Managing climate risk. Science 294 (2001) 786b.

[7] Tontiwachwuthikul, P., Research and development activities on high efficiency separation process technologies for carbon dioxide removal from industrial source at University of Regina, Canada. Energy Convers. Manage. 37 (1996) 935-940.

[8] Rao, A. B., Rubin, E. S., A technical, economic, and environmental assessment of amine-based CO_2 capture technology for power plant greenhouse gas control. Environ. Sci. Technol. 36 (2002) 4467-4475.

[9] Hubbert, M. K., Energy from fossil fuels. Science 109, (1949) 103-109.

[10] Beck, R. B., Black, L., Krieger, L. S., World history: patterns of Interaction Illinois. McDougal Littell, (2001).

[11] Meier, G. M., Rauch, J. E., Leading issues in economic development. Oxford, University Press, U.S.A, (2005).

[12] Snedden, R., Energy from fossil fuels. Heinemann-Raintree, (2005).

[13] Broecker, W. S., Climatic change: are we on the brink of a pronounced global warming. Science 189 (1975) 460-463.

[14] IPCC, Climate change 2007: Synthesis report. Contribution of working groups I, II and III to the fourth assessment report of the intergovernmental panel on climate change. In: Pachauri KP, Reisinger A, editors. IPCC: Geneva, Switzerland, (2007).

[15] Pielke, R., Wigley, T., Green, C., Dangerous assumptions. Nature 452 (2008) 531-532.

[16] IEA. Prospects for CO_2 capture and storage. Paris, France, OECD/IEA, (2004).

[17] Herzog, H., Eliasson, B., Kaarstad, O., Capturing greenhouse gases. Scientific American 282 (2000) 72-79.

[18] Herzog, H. J., What future for carbon capture and sequestration. Environ. Sci. Technol. 35 (2001) 148A-153A.

[19] Liverman, D. M., Conventions of climate change: constructions of danger and the dispossession of the atmosphere. J. Historical Geo. 35 (2009) 279-296.

[20] Dincer, I., Renewable energy and sustainable development: a crucial review. Renew. Sustain. Energy Rev. 4 (2000) 157-175.

[21] Fan, L. S., Chemical looping systems for fossil energy conversion; John Wiley & Sons, Inc., Hoboken (2010).

[22] Figueroa, J. D., Fout, T., Plasynski, S., McIlvried, H., Srivastava, R. D., Advances in CO_2 capture technology—The U.S. Department of Energy's Carbon Sequestration Program. Int. J. Greenh. Gas Control 2 (2008) 9–20.

[23] Hossain, M. M., de Lasa, H. I., Chemical-looping combustion (CLC) for inherent CO2 separations—a review. Chem. Eng. Sci. 63 (2008) 4433–4451.

[24] Kanniche, M., Gros-Bonnivard, R., Jaud, P., Valle-Marcos, J., Amann, J.M., Bouallou, C., Pre-combustion, post-combustion and oxy-fuel combustion in thermal power plant for CO_2 capture. Appl. Therm. Eng. 30 (2010) 53–62.

[25] Scheffknecht, G., Al-Makhadmeh, L., Schnell, U., Marier, J., Oxy-fuel coal combustion—A review of the current state-of-the-art. Int. J. Greenh. Gas Control 55 (2011) 516-535.

[26] Yang, H., Xu, Z., Fan, M., Gupta, R., Slimane, R. B., Bland, A. E., Wright, I., Progress in carbon dioxide separation and capture: A review. J. Environ. Sci. 20 (2008) 14-27.

[27] Rao, A. B., Rubin, E. S., Keith, D. W., Morgan, M. G., Evaluation of potential cost reductions from improved amine-based CO_2 capture systems. Energy Policy 34 (2006) 3765-3772.

[28] Xu, G., Jin, H. G., Yang, Y. P., Xu, Y. J., Lin, H., Duan, L. Q., A comprehensive techno-economic analysis method for power generation systems with CO_2 capture. Int. J Energy Res. 34 (2010) 321-332.

[29] Abanades, J. C., Alvarez, D., Anthony, E. J., Lu, D., In situ capture of CO_2 in a fluidized bed combustor, In: Proceedings of the 17th International Fluidized Bed Combustion Conference, ASME, Jacksonville, Florida, USA (2003) 133–135.

[30] Silaban, A., Narcida, M., Harrison, D.P., Characteristics of the reversible reaction betweem CO_2 (g) and calcined dolomite. Chem. Eng. Comm. 146 (1996) 149–162.

[31] Lin, S. Y., Suzuki, Y, Atano, H. H., Harada, M., Hydrogen production from hydrocarbon by integration of water-carbon reaction and carbon dioxide removal (HyPr-RING method). Energy Fuels 15 (2001) 339-343.

[32] Lin, S. Y., Harada, M., Suzuki, Y., Hatano, H., Developing an innovative method, HyPr-RING to produce hydrogen from hydrocarbons, Energy Conservation and Management 43 (2002) 1283–1290.

[33] Lin, S. Y., Process analysis for hydrogen production by reaction integrated novel gasification (HyPr-RING). Energy Conv. Manag. 46 (2005) 869-880.

[34] Abanades, J. C., Anthony, E. J., Alvarez, D., Lu, D., Salvador, C., Capture of CO_2 from combustion gases in a fluidized bed of CaO. AIChE J. 50 (2004) 1614–1622.

[35] An, H., Song, T., Shen, L., Qin, C., Yin, J., Feng, B., Coal gasification with in situ CO_2 capture by the synthetic CaO sorbent in a 1 kWth dual fluidised-bed reactor. Int. J. Hydrogen Energy 37 (2012) 14195–14204.

[36] Baker, E. H., The calcium oxide-carbon dioxide system in the pressure range 1–300 atmospheres. J. Chem. Soc. (1962) 464–470.

[37] Bhatia, S. K., Perlmutter, D. D., Effect of the product layer on kinetics of the CO_2—lime reaction. AIChE J. 29 (1983) 79–86.

[38] Von Nitsch, W., On the pressure dependence of CaO carbonation. Elektrochem 66 (1970) 17 (in German).

[39] Sun, P., Grace, J. R., Lim, C. J., and Anthony, E. J., Determination of intrinsic rate constants of the CaO-CO_2 reaction. Chem. Eng. Sci. 63 (2008) 47–56.

[40] Kyaw, K., Kanamori, M., Matsuda, H., Hansatani, M., Study of carbonation reactions of Ca-Mg oxides for high temperature energy storage and heat transformation. J. Chem. Eng. Japan 29 (1996) 112-118.

[41] Yu, F. C., Fan, L. S., Kinetic study of high-pressure carbonation reaction of calcium-based sorbents in the calcium looping process (CLP). Ind. Eng. Chem. Res. 50 (2011) 11528–11536.

[42] Szekely, J., Evans, J. W., Sohn, H. Y., Gas-solid reactions. Academic Press, New York (1976).

[43] Levenspiel, O., Chemical Reaction Engineering. Third ed. Wiley, New York (1972).

[44] Yagi, S. and Kunii, D., Studies on combustion of carbon particles in flames and fluidized beds, Proceedings of 5th (int.) Symbosium on Combustion, Reinhold, New York, (1955) 231.

[45] Ishida, M., Wen, C.Y., Comparison of zone-reaction model and unreacted-core shrinking model in solid–gas reactions—I Isothermal analysis. Chem. Eng. Sci. 26 (1971) 1031–1041.

[46] Ishida, M.,Wen, C. Y., Shirai, T., Comparison of zone-reaction model and unreacted-core shrinking model in solid–gas reactions—II Nonisothermal analysis. Chem. Eng. Sci. 26 (1971) 1043–1048.

[47] Nikulshina, V., Galvez, M. E., Steinfeld, A., Kinetic analysis of the carbonation reactions for the capture of CO2 from air via the $Ca(OH)_2$-$CaCO_3$-CaO solar thermochemical cycle. Chem. Eng. J.129 (2007) 75-83.

[48] Szekely, J., Evan, J. W., Studies in gas-solid reactions: Part I. A structural model for the reaction of porous oxides with a reducing gas, Metallurgical Transactions 2 (1971) 1691-1698.

[49] Patisson, F., Ablitzer D., Physicochemical and thermal modeling of the reaction between a porous pellets and a gas, Powder Technology 128 (2002) 300–305.

[50] Stendardo, S., Foscolo, P. U., Carbon dioxide capture with dolomite: A model for gas–solid reaction within the grains of a particulate sorbent. Chem. Eng. Sci. 64 (2009) 2343-2352.

[51] Gibson, J. B., Harrison, D. P., The reaction between hydrogen sulfide and spherical pellets of zinc oxide. Ind. Eng. Chem. Proc. Des. 19 (1980) 231-237.

[52] Croiset, E. and Thambimuthu, K. V., Coal combustion in O_2/CO_2 mixtures compared to air. Canad. J. Chem. Eng. 78 (2000) 402-407.

[53] Blamey, J., Anthony, E. J., Wang, J., Fennell P. S., The calcium looping cycle for large-scale CO_2 capture. Prog. Energy Combust. Sci. 36 (2010) 260–279.

[54] Lysikov, A. I., Salanov A. N., Okunev A. G., Change of CO_2 carrying capacity of CaO in isothermal recarbonation-decomposition cycles. Ind. Eng. Chem. Res. 46 (2007) 4633–4638.

[55] Abanades, J. C., The maximum capture efficiency of CO_2 using a calcination/carbonation cycle of $CaO/CaCO_3$. Chem. Eng. J. 90 (2002) 303– 306.

[56] Manovic, V., Anthony, E. J., Long-term behavior of CaO-based pellets supported by calcium aluminate cements in a long series of CO_2 capture cycles. Ind. Eng. Chem. Res. 48 (2009) 8906–8912.

[57] Manovic, V., Anthony, E. J., CaO-based pellets supported by calcium aluminate cements for

[58] Tang, A., Su, L., Li, C., Wei, W., Effect of mechanical activation on acid-leaching of kaolin residue. Appl. Clay Sci. 48 (2010) 296–299.

[59] Wang, K., Guo, X., Zhao, P., Zheng, C., Cyclic CO2 capture of CaO-based sorbent in the presence of metakaolin and aluminum (hydr) oxides. Appl. Clay Sci. 50 (2010) 41–46.

[60] Manovic V., Anthony, E. J., Screening of binders for pelletization of CaO-based sorbents for CO_2 capture. Energy Fuels 23 (2009) 4797–4804.

[61] Albrecht, K. O., Wagenbach, K. S., Satrio, J. A., Shanks, B. H., Wheellock, T. D., Development of a CaO-Based CO_2 sorbent with improved cyclic stability. Ind. Eng. Chem. Res. 47 (2008) 7841-7848.

[62] Li, L., King, D. L., Nie, Z., Howard, C., Magnesia-stabilized calcium oxide absorbents with improved durability for high temperature CO_2 capture. Ind. Eng. Chem. Res. 48 (2009) 10604-10613.

[63] Manovic, V, Anthony, E. J., CO_2 carrying behavior of calcium aluminate pellets under high temperature/high- CO2 concentration calcination conditions. Ind. Eng. Chem. Res. 49 (2010) 6916-6922.

[64] Abanades, J. C., Anthony, E. J., Wang, J., Oakey, J. E., Fluidized bed combustion systems integrating CO2 capture with CaO. Environ. Sci. Technol. 39 (2005) 2861-2866.

[65] Ridha, F. N., Manovic, V., Macchi, A., Anthony, E. J., High-temperature CO2 capture cycles for CaO-based pellets with kaolin-based binders. Int. J. Greenh. Gas Control 6 (2012a) 164–170.

[66] Ridha, F. N., Manovic, V., Anthony, E. J., Macchi, A., The morphology of limestone-based pellets prepared with kaolin-based binders. Mat. Chem. Phys. 138 (2013) 78-85.

[67] Shearer, J. A., Smith, G. W., Moulton, D. S., Smyk, E. B., Myles, K. M., Swift, W. M., Johnson, I., Hydration process for reactivating spent limestone and dolomite sorbent for reuse in fluidized-bed coal combustion. Proceedings of the sixth international conference on fluidized-bed Combustion, April (1980) 9-11.

[68] Laursen K., Duo W., Grace J.R., Lim, C.J., Characterization of steam reactivation mechanisms in limestones and spent calcium sorbents. Fuel (2001) 1293-1306.

[69] Hughes, R.W., Lu, D., Anthony E.J., Improved long-term conversion of limestone-derived sorbents for in situ capture of CO_2 in a fluidized bed combustor. Ind. Eng. Chem. Res. 43 (2004) 5529-5539.

[70] Fennell, P. S., Davidson, J. F., Dennis, J. S., Hayhurst, A. N., Regeneration of sintered limestone sorbents for the sequestration of CO_2 from combustion and other systems, J. Energy Inst. 80 (2007) 116–119.

[71] Manovic, V., Anthony, E. J., Carbonation of CaO-based sorbents enhanced by steam addition. Ind. Eng. Chem. Res. 49 (2010) 9105-9110.

[72] Ramkumar, S., Fan, L.-S., Thermodynamic and experimental analyses of the three-stage calcium looping process. Ind. Eng. Chem. Res. 49 (2010) 7563-7573.

[73] Kuramoto, K., Fujimoto, S., Morita, A., Shibano, S., Suzuki, Y., Hatano, H., Shi- Ying, S., Harada, M., Takarada, T., Repetitive carbonation-calcination reactions of ca-based sorbents for efficient CO_2 sorption at elevated temperatures and pressures. Ind. Eng. Chem. Res. 42 (2003) 975-981.

[74] Giaconia, A., Thermochemical production of hydrogen, Adv. in hydrogen production, storage and distribution (2014) 263-280.

[75] Energy Information Administration (EIA), International energy outlook (2006). ww.eia.doe.gov/oiaf/ieo/index.html.

[76] Tsakomakas, N.G., Pilavachi, P.A., Polyzakis, A.L., An economic comparison assessment of lignite and biomass IGCC power plants, Appl. Therm. Eng. 38 (2012) 26–30.

[77] Holt, N. A. H., Gasification & IGCC - design issues & opportunities, proceedings of GCEP advanced coal workshop provo. (2005).

[78] Kreutz, T. G., Williams, R.H., Socolow, R.H., Chiesa, P., Lozza, G., Production of hydrogen and electricity from coal with CO_2 capture. Sixth Green house gas Control Technologies Conference, Kyoto, Japan, (2002).

[79] Roark, S. E., Mackay, R., Sammells, A.F., Hydrogen separation membranes for vision 21 energy plants. Proceedings of the International Technical Conference on Coal Utilization & Fuel Systems 27 (2002) 101-112.

[80] Lin, S., Harada, M., Suzuki, Y., Hatano, H., Hydrogen production from coal by separating carbon dioxide during gasification. Fuel 81 (2002) 2079-2085.

[81] Gupta, H., Fan, L.S., Carbonation-calcination cycle using high reactivity calcium oxide for carbon dioxide separation from flue gas. Ind. Eng. Chem. Res. 41 (2002) 4035-4042.

[82] Kim, M., Pettersen, J., Bullard, C. W., Fundamental process and system design issues in CO_2 vapor compression systems. Prog. Energy Combust. Sci. 30 (2004) 119-174.

Chapter Two: **Investigation of the kinetics of carbonation reaction with CaO-based sorbents using experiments and Aspen Plus simulation**

Chem. Eng. Comm. 202 (2015) 746-755

2.1 Presentation of the article

This paper provides a detailed description of the comprehensive intrinsic kinetics of the carbonation reaction with two types of commercial limestone, Havelock and Cadomin, using an ATGA and a pressurized thermogravimetric analyzer (PTGA). A grain model was applied to measure the kinetic parameters using experimental data. In addition, the effects of numerous key parameters on the kinetics of the carbonation reaction were investigated, such as temperature, partial pressure, and total pressure. The obtained experimental data were compared to the thermodynamic and kinetic modeling results obtained from the Aspen Plus simulator. The results indicated that, the order of carbonation reaction was related to the CO_2 partial pressure, changing from first order to zero order when the CO_2 partial pressure exceeded ~ 0.7 atm for both types of limestone. The rate of carbonation reaction increased with increasing temperature up to 675°C and then decreased with further increases of temperature.

The main part of this work including all experiments and analyses of experimental data, were conducted by Mohammad H. Sedghkerdar under the supervision of Dr. Nader Mahinpey; and Mr. Ehsan Mostafavi performed the thermodynamic and kinetic modeling using the Aspen Plus simulator.

Investigation of the kinetics of carbonation reaction with CaO-based sorbents using experiments and Aspen Plus simulation

This article has been accepted in Chem. Eng. Comm. Journal, 202 (2015) 746-755

Mohammad Hashem Sedghkerdar, Ehsan Mostafavi, Nader Mahinpey

Department of Chemical and Petroleum Engineering, Schulich School of Engineering, University of Calgary, Calgary, AB, Canada T2N 1N4

2.2 Abstract

The intrinsic kinetics of the carbonation reactions for two limestones (Havelock and Cadomin) were studied using an atmospheric thermogravimetric analyzer (ATGA) and a pressurized thermogravimetric analyzer (PTGA). A grain model was applied to measure the kinetic parameters. The order of the carbonation reaction was related to the carbon dioxide (CO_2) partial pressure, changing from the first order to the zero order when the CO_2 partial pressure exceeded ~ 0.7 atm for both limestones. The rate of carbonation reaction increased with increasing temperature up to 675°C and decreased with further increases. No significant effect of particle size was found on the rate of carbonation reaction. Thermodynamic and kinetic simulations of the carbonation reaction using the Aspen Plus simulator was performed, obtaining the optimal temperature of 650°C. The activation energies were 32.1 and 20.3 kJ/mol for the tested Havelock and Cadomin limestones, respectively. The simulation results from the kinetic model were in good agreement with the experimental data, showing the reversible characteristic of the carbonation reaction. The shift in the mechanism of the carbonation reaction with temperature and the shift in the reaction order with CO_2 partial pressure were demonstrated by both the experiments and simulation.

2.3 Introduction

The anthropogenic increase of carbon dioxide (CO_2) in the atmosphere has been suggested as a main contributor to global warming [1-2]. The growing need for the reduction in anthropogenic CO_2 emission has led to a global push towards the development of efficient, economical and realistic CO_2 capture technology, which comprises 60-70% of the costs of carbon capture and storage (CCS) for application to fossil fuel-based power plants [2].

Three technological approaches are under development to consider how best to improve CO_2 capture: post-combustion, pre-combustion, and oxy-fuel processes [3-6]. Post-combustion is currently one of the proven, commercially available, low-temperature technologies to separate CO_2 from the flue gases produced by combustion using wet scrubbing with amine solvents (i.e., mono-ethanolamine, MEA) [7]. However, this approach introduces harsh efficiency and economic penalties; therefore, there has been considerable recent interest in dry processes for CO_2 capture [2].

Among the solid sorbents for capturing CO_2, calcium-based solid materials are the least costly, most abundant sorbents for the capture of CO_2 for high-temperature operations [8-9]. Some of the important applications of calcium-based sorbents for CO_2 capture processes include hydrogen production by reaction-integrated novel gasification (HyPr-Ring) [10-12] and fluidized bed combustors for in situ CO_2 capture [13-14]. In these applications, gasification is integrated with the CO_2 capture process to capture the CO_2 stream at high temperatures. which is mainly produced from the water-gas-shift reaction; therefore, based on LeChâtelier's principle, the equilibrium is shifted forward, resulting in improvement of the gasification process for producing hydrogen (H_2) rich product gas and a concentrated CO_2 stream suitable for sequestration [10-14].

The carbonation reaction is a gas-solid reaction that produces a solid product and takes place in two regimes. The first regime involves a rapid chemical reaction of gas with solid at the fresh lime surface. This is followed by the second regime, which is a slow reaction that is characterized by the formation of a calcium carbonate ($CaCO_3$) layer that impedes the reactant gas diffusion.

There are a limited number of published studies on the intrinsic kinetics of the carbonation reaction; however, several uncertainties with respect to intrinsic kinetic parameters, such as activation energy and the order of the reaction, have been observed. Bhatia and Perlmutter [15] found zero-activation energy for the carbonation reaction using an atmospheric thermogravimetric analyzer (ATGA) with CO_2 concentrations in the range of 0 to 10 mole%. However, Sun et al. [16] reported activation energies of 29 and 24 kJ/mol for limestone and dolomite, respectively. In our previous study that investigated the effect of biomass presence on the intrinsic rate of the carbonation reaction, the activation energies were found to be 28.3 and 21.6 kJ/mol for calcined limestone with and without biomass, respectively, in the narrow temperature range from 500 to 650°C [17].

With respect to intrinsic carbonation reaction order, Bhatia and Perlmutter [15] and Sun et al. [16] claimed a first-order intrinsic rate changed to zero order, when the CO_2 partial pressure exceeded 0.1 atm; however, Yu and Fan [18] observed a shift in the order of the carbonation reaction from one to zero at CO_2 partial pressures higher than 1 atm. Further studies are, therefore, required to investigate numerous issues with carbonation kinetics.

The present research provides a detailed description of the comprehensive intrinsic kinetics of the carbonation reaction with two commercial limestones, Havelock and Cadomin, using an ATGA and a pressurized thermogravimetric analyzer (PTGA). Different key parameters

were investigated, such as temperature, partial pressure, and total pressure. Moreover, thermodynamic and kinetic modeling were conducted with the Aspen Plus simulator, and the results have been compared with the experimental data. The shift in the pathway of the carbonation reaction with temperature and the shift in the reaction order with total pressure were comprehensively investigated through experiments and simulation.

2.4 Experimental details

2.4.1 Thermogravimetric analyzers

In this study, two thermogravimetric analyzers (TGAs) were used for atmospheric and pressurized conditions. A Perkin-Elmer STA 6000 system ATGA manufactured from USA with a sensitive microbalance, which is capable of detecting weight changes as small as 0.1 μg, was applied to calculate a constant rate and an order of reaction with different CO_2 partial pressures. The THERMAX 500 PTGA manufactured by Thermo Fisher Scientific in Germany, included a Cahn 100 balance with a sensitivity of 1 μg and an Inconel vertical reactor. The total pressure was adjusted with a pressure regulator.

Fig. 2.1 provides schematic diagrams of the ATGA and PTGA. Mass flow meters controlled the gas flow rates, and solenoid valves were applied for switching gases for calcination and carbonation. In all experiments, to achieve complete decomposition, the calcination was carried out by heating samples to 850°C at 40°C/min at atmospheric pressure in a pure nitrogen gas (N_2) flow of 50 ml/min, followed by a 20 min isothermal calcination reaction at 850°C. Following calcination, the predetermined carbonation temperature was approached at the rate of 40°C/min under an N_2 flow of 50 ml/min.

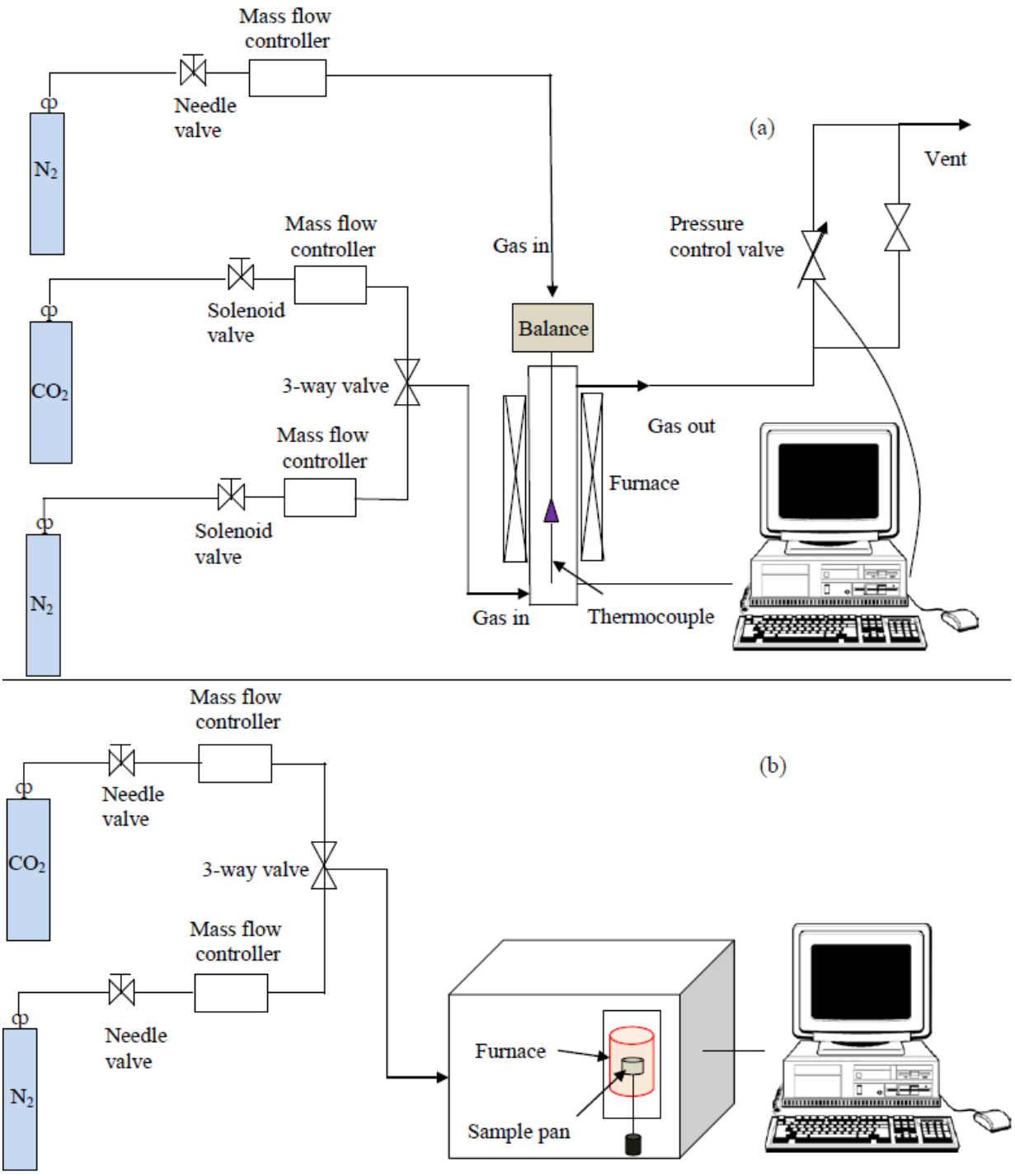

Fig. 2.1 Schematic diagrams of the laboratory setups: (a) PTGA and (b) ATGA

For the PTGA experiments, the desired pressure for carbonation was achieved before beginning carbonation by injecting N_2 from the top of the TGA. The carbonation reaction was then started by switching the gas from N_2 to pure CO_2. The mass samples were chosen as 20 and 200 mg for ATGA and PTGA tests, respectively. The PTGA sample pan is 5 times larger than of the ATGA. External mass transfer resistance, due to formation of gas film around the particles, would be minimized by conducting a high gas flow rate. Therefore, the CO_2 gas flow rate for all carbonation tests was adjusted to 200 and 500 ml/min for the ATGA and PTGA, respectively.

2.5 Simulation assumptions

In this work, the carbonation reactions for two limestones, Havelock and Cadomin, were thermodynamically and kinetically simulated using Aspen Plus software. In the kinetic modeling, comprehensive reaction schemes were considered; whereas in the thermodynamic modeling, the maximum achievable conversion was estimated based on the minimization of the Gibbs free energy. The CO_2 capture process was introduced to the simulator as a reversible gas-solid reaction with experimentally calculated kinetic parameters, such as a rate constant and activation energy, in order to predict the carbonation reaction behavior at different temperatures.

For kinetic and equilibrium simulations of the carbonation reaction, a plug flow reactor (PFR) and a Gibbs reactor (GR) were chosen, respectively. The Gibbs reactor simulated the thermodynamic equilibrium modeling by minimizing the Gibbs free energies of the reactants and products. Fig. 2.2 presents the schematic of the Aspen Plus flow sheet used in this work. Table 2.2 provides an explanation of abbreviations used in Fig. 2.2.

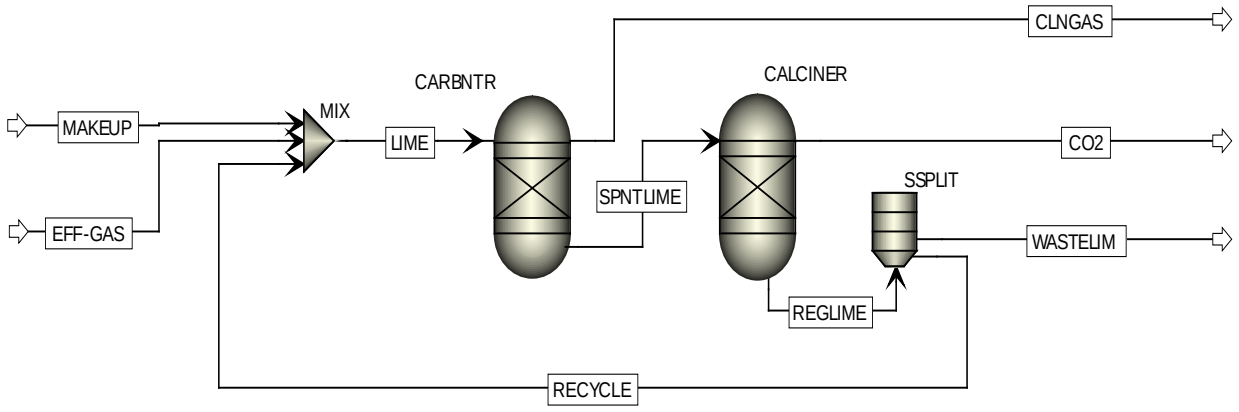

Fig. 2.2 Schematic diagram of Aspen Plus flow sheet

The following assumptions were considered in the modeling:

1- The gas flow rate was sufficiently high and the solid sample was rather small, so the reaction proceeded with no volume change; therefore, a PFR, which considers only the axial variation, was chosen to simulate the behavior of a differential packed-bed reactor.

2- According to low-pressure operating conditions, the ideal equation of state was considered.

3- Calcium oxide (CaO) was defined as a solid inlet stream to the reactors.

4- The carbonation of CaO was the only reaction happening in the PFR.

5- CaO, magnesium oxide (MgO) and other minerals were defined with the relevant fraction for Cadomin in the elemental analysis using energy-dispersive X-ray spectroscopy (EDX, Table 2.1).

Table 2.1 Elemental composition (wt. %)

Sorbent	SiO_2	Al_2O_3	Fe_2O_3	MgO	CaO	Na_2O	K_2O	LOI[a]
Havelock	2.55	1.34	0.71	1.28	49.31	1.09	0.44	43.28
Cadomin	1.71	0.88	1.03	1.06	46.99	0.16	0.44	47.73

[a] LOI: Loss of Ignition

6- Among the components, CO_2, CaO and $CaCO_3$ were the only species that took part in the reaction, according to the prediction by the GR at the process conditions.

7- In the case of the thermodynamic model, a long residence time was considered to reach equilibrium.

Table 2.2 Description of abbreviations used in Schematic diagram of Aspen Plus flow sheet

Stream/Equipment Names	Description
MAKE-UP	The fresh stream of calcined limestone
EFF-GAS	The stream of CO_2 injected to the carbonator
LIME	The total feed stream (CaO) to the carbonator
RECYCLE	The recycle stream of regenerated calcined limestone
SPNTLIME	The stream of used sorbents for carbonation ($CaCO_3$)
REGLIME	The stream of regenerated calcined limestone
CLNGAS	The stream of clean gas contains N_2
CO_2	The stream of CO_2 generated from calcinator
WASTELIM	The stream of waste lime which carries 30% of sorbent out of loop
MIX	Mixer unit
CARBNTR	Carbonator unit modeled with a PFR[a]
CALCINER	Calninator unit
SSPLIT	Solid separator unit which returns 70% of the sorbent to the loop, and the rest out of loop

2.6 Materials

Two different natural limestones, Havelock from eastern Canada and Cadomin from western Canada in size ranges of 500 to1410 μm and 250 to 750 μm, respectively, were used to study the CaO-CO_2 reaction. These limestones were selected in this study, due to their application in the pilot-scale fluidized-bed reactor for investigating the CO_2 capture from combustion flue gases at high temperatures [13]. Chemical analyses of these two sorbents using an EDX analyzer are provided in Table 2.1.

2.7 Results and discussion

2.7.1 Carbonation reaction rate with different partial pressures of CO_2 at a fixed total pressure

The gas-solid reaction between CO_2 and CaO takes places in three consecutive steps: 1) the diffusion of the gaseous reactant through a film surrounding the particle to the surface of the solid; 2) the penetration and diffusion of gas through the product layer; and, 3) the reaction of the gas with the solid at the reaction surface [19]. Therefore, the rate of carbonation reaction as a gas-solid reaction would be highly dependent on the CO_2 partial pressure. Therefore, in this study, the effect of CO_2 partial pressures on the intrinsic rate of the carbonation reaction, which is controlled kinetically, was investigated with a fixed total pressure of 1 atm. Four different CO_2 fractions were used: 20, 35.5, 50, and 100 mole%.

Fig. 2.3 shows CaO conversion versus time for the Havelock and Cadomin calcines at different CO2 partial pressures. The CaO conversion was calculated as follows:

$$\text{CaO Conversion} = \frac{(\text{m(t)} - \text{m(0)})}{44} \Big/ \frac{(\text{m(0)} \times \text{Purity})}{56} \tag{3.1}$$

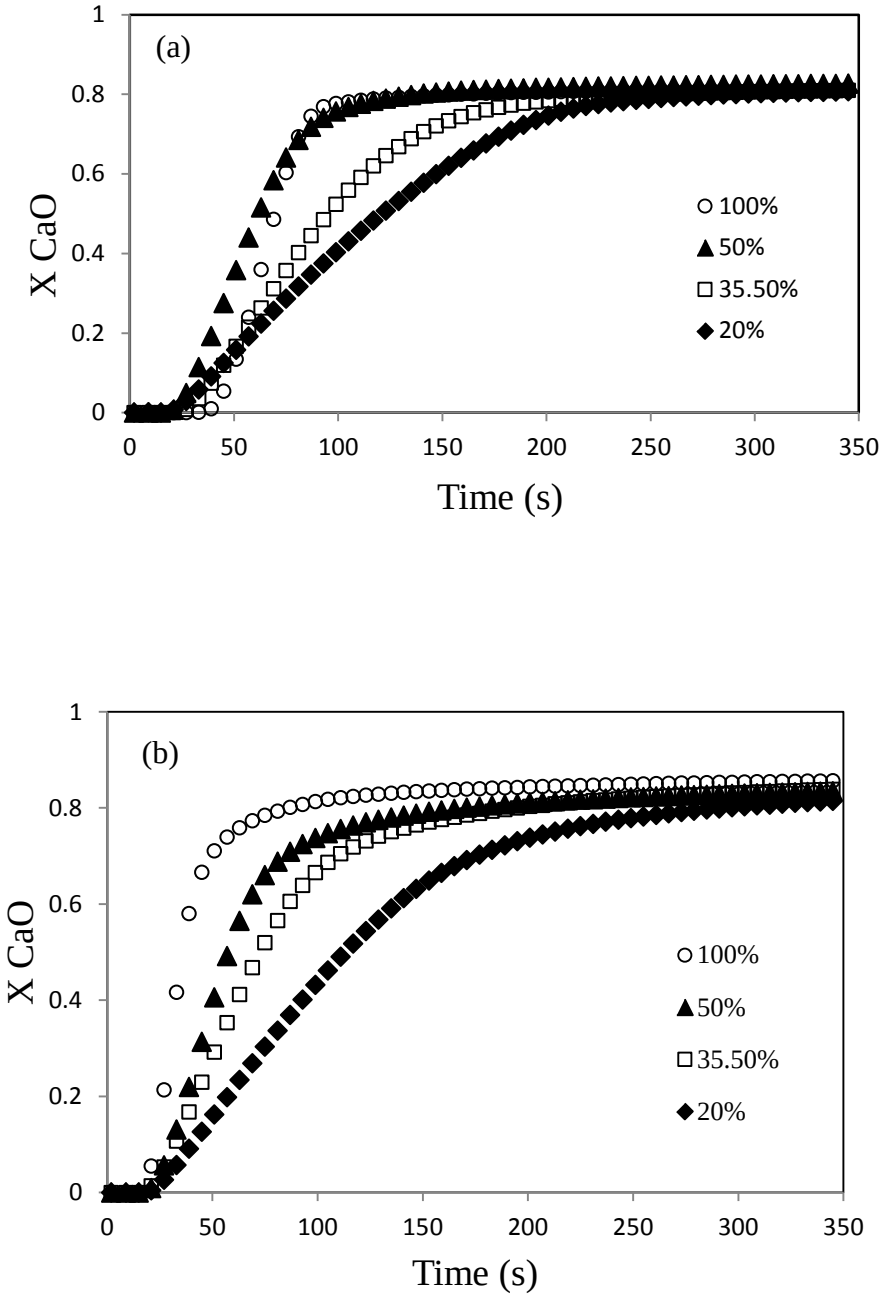

Fig. 2.3 Effect of CO_2 fractions on the carbonation reaction rate with a fixed total system pressure of 1 atm and at 675°C: (a) Havelock limestone and (b) Cadomin limestone.

where 44 and 56 are the CO_2 and CaO molar weights (g/mol). A nucleation period with a low slope is usually observed at several seconds (20 s) after the beginning of a gas-solid reaction.

During the nucleation period, the nuclei of Ca are formed and grow on the surface of the solid particle [5]. Following this step, the chemical reaction plays a significant role and imparts a high linear slope, which was considered as an intrinsic rate in our calculation. However, with the formation of $CaCO_3$, the rate of the reaction decreases (almost zero), due to product layer resistance in accessing CaO by CO_2, leading to an ultimate conversion of less than 100%.

As expected, the intrinsic rate of carbonation was found to increase with an increase in the CO_2 fraction (mole%). According to Fig. 2.3, an increase in the partial pressure of the CO_2 increased the carbonation rate. Based on the LeChâtelier's principle, increasing the CO_2 partial pressure in the system caused a shift in the equilibrium. In complementary fashion, increases in the CO_2 partial pressure increased the mass transfer driving force, due to increased differences between the CO_2 concentration in the gas flow and the equilibrium CO_2 concentration. As can be observed, the highest carbonation reaction rate occurred at a CO_2 fraction of 100% with a 1 atm fixed total pressure for each sorbent.

2.7.2 Intrinsic kinetics analysis of the carbonation reaction using a grain model

A grain model assumes that solid particles consist of several spherical grains of equal size that have a sharp surface to react with the reactant gas. At the beginning of the reaction, the diffusion resistance is negligible and the rate of reaction is high; hence, the chemical kinetics controls the whole reaction (Fig. 2.3). The reversible carbonation reaction between the limestone and CO_2 can be expressed as follows:

$$CaO+CO_2 \leftrightarrow CaCO_3 \tag{2.2}$$

Thus, based on the grain model, the rate of reaction for the reaction in Eq. (2.2) is:

$$r = \frac{dX}{(1-X)dt} = M_{CaO} k_s \left(P_{CO_2} - P_{CO_2,eq}\right)^n S \tag{2.3}$$

For a spherical grain with a uniform CaO concentration, the following expression is valid:

$$X_{CaO} = 1 - \frac{N_{CaO}}{N_{CaO_0}} = 1 - (\frac{r_c}{R})^3 \quad (2.4)$$

Therefore, the initial slope of the conversion curve at the time zero can be written as:

$$\frac{dX}{dt}_{t\to 0} = M_{CaO} k_s \, (P_{CO_2} - P_{CO_2,eq})^n \, S_0 \quad (2.5)$$

In logarithmic form, Eq. (2.5) becomes:

$$ln(\frac{dX}{dt}_{t\to 0}) = ln(M_{CaO} k_s \, S_0) + n \, ln(P_{CO_2} - P_{CO_2,eq}) \quad (2.6)$$

where M_{CaO} is the molar weight of CaO, S_0 is the initial CaO surface area, n is the order of the reaction, and k_s is the intrinsic rate constant, which can be corrected for temperature using the Arrhenus equation:

$$k_s = k_0 \exp\left(-\frac{E}{R_g T}\right) \quad (2.7)$$

The equilibrium partial pressure of CO_2 has been reported to be [20]:

$$log_{10} \, P_{CO_2} \, (atm) = 7.079 - \frac{8308}{T \, (K)} \quad (2.8)$$

Therefore, the slope of the plot of $\ln\left(\frac{dX}{dt}_{t\to 0}\right)$ versus $\ln\left[\left(P_{CO_2} - P_{CO_2,eq}\right)\right]$ can determine the order of the CaO-CO_2 reaction. From Fig. 2.4, it can be seen that the CaO-CO_2 reaction was approximately a first-order reaction for both limestone calcines.

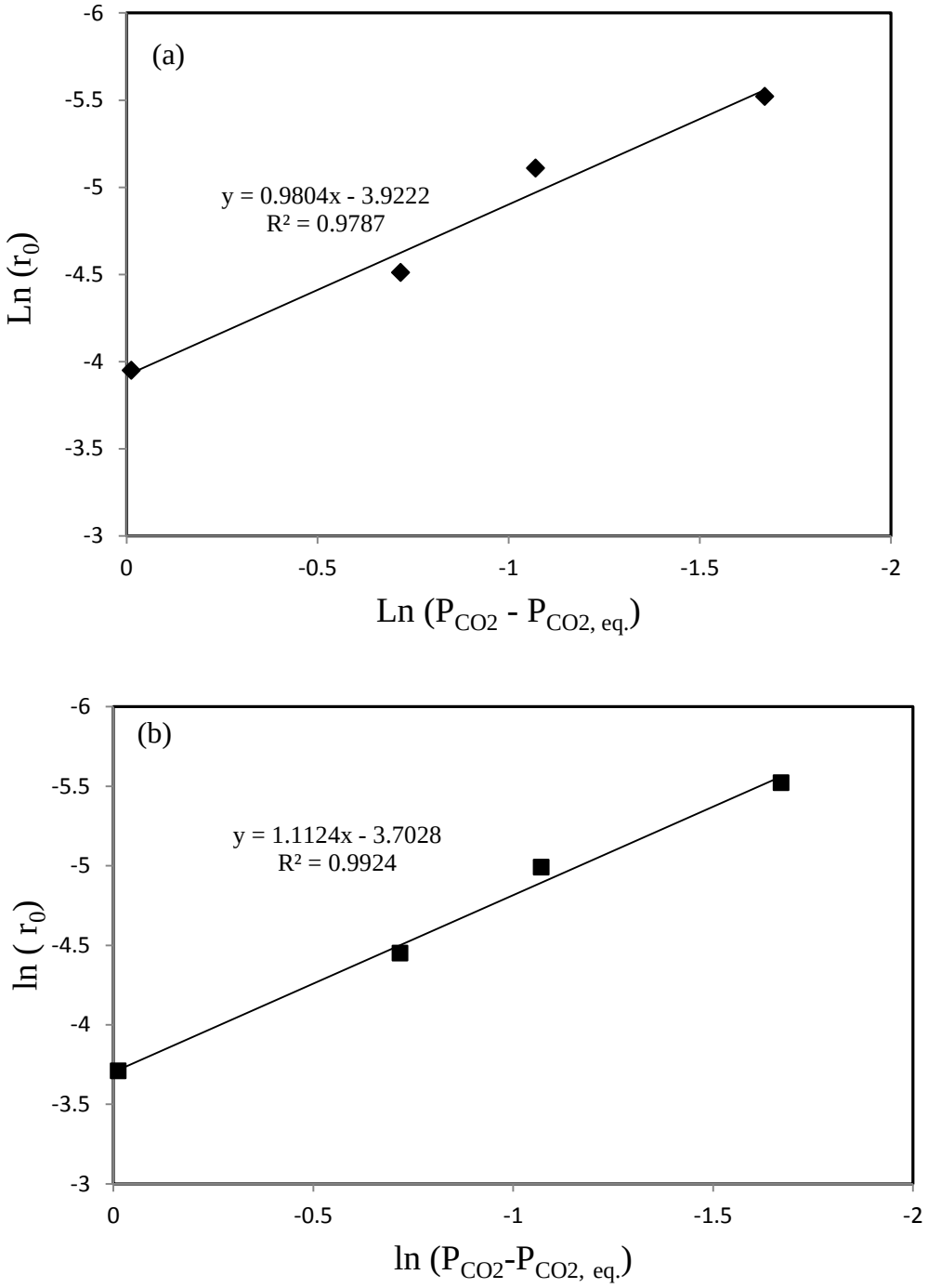

Fig. 2.4 The carbonation reaction rate at different partial pressures of CO_2: (a) Havelock limestone and (b) Cadomin limestone. (Carbonation temperature of 675°C with 100% CO_2 at 1 atm).

2.7.3 Effect of temperature on the carbonation reaction

To explore the effect of temperature on the CaO-CO2 reaction, a series of CO_2 capture experiments were performed at CO_2 partial pressure 1 atm and eight different temperatures in the range of 400 to 800°C using the ATGA. Fig. 2.5(a) and (b) show the effect of temperature on the carbonation reaction rate using both calcined Havelock and Cadomin. The rate of carbonation reaction increased by increasing the temperature up to 675°C and dramatically decreased with further increases.

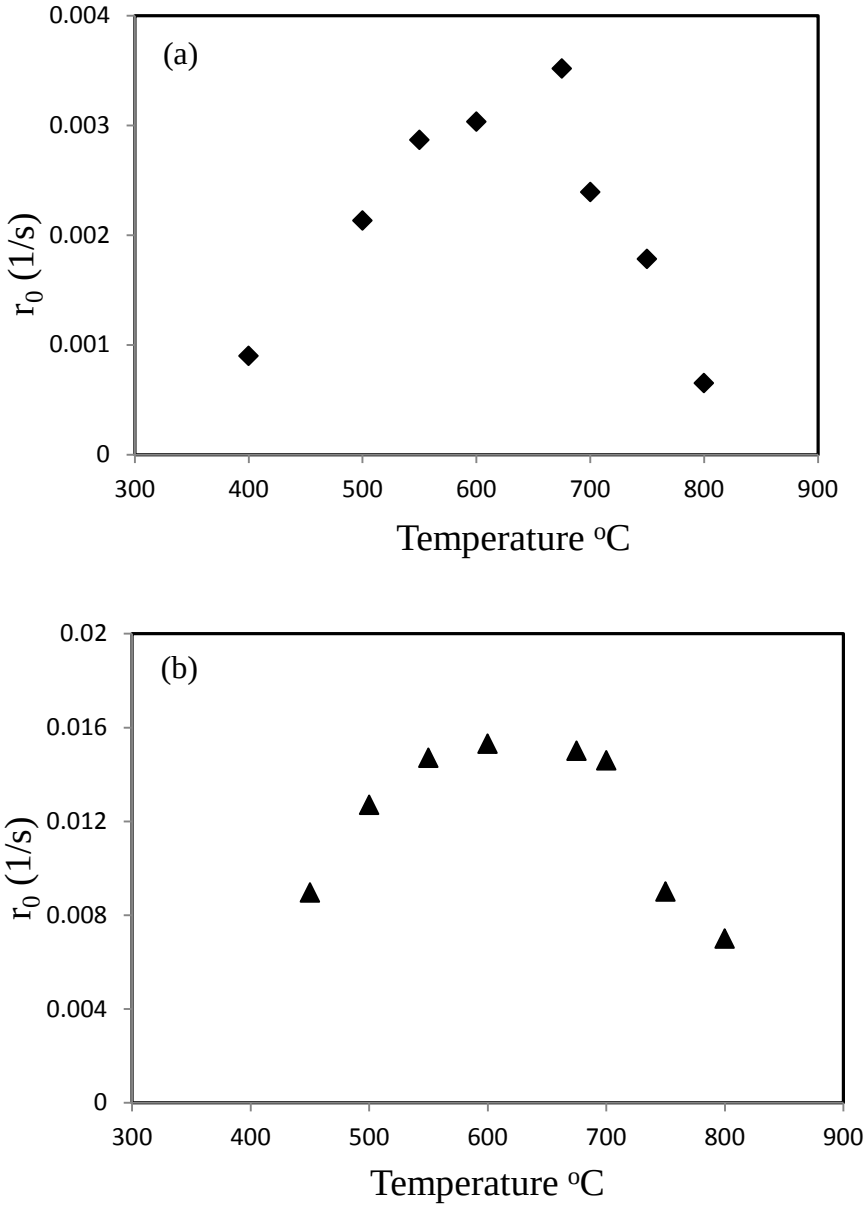

Fig. 2.5 The change of carbonation reaction rate with temperature (400-800°C): (a) Havelock limestone and (b) Cadomin limestone.

The carbonation reaction takes place when the partial pressure of the CO_2 in the flow stream is higher than the equilibrium partial pressure of CO_2 at a certain temperature. According to Eq. (2.8), the equilibrium partial pressure of CO_2 increases with increasing temperatures,

causing a decreasing CO_2 partial pressure driving force ($P_{CO_2} - P_{CO_2,eq}$), which presents the initiation of the reverse reaction (calcination reaction) at a temperature around 700°C.

In order to determine the dependency of the intrinsic rate constant (k_s) on the temperature of the reaction and to calculate the activation energy of the reaction using Eq. (2.7), a certain range of temperatures should be considered. Thus, k_s was determined at the operating temperature range of 450 to 675°C, where the forward reaction would presumably dominate.

Based on the BET (Brunauer, Emmett, Teller) analysis, the calcined Havelock and Cadomin particle surface areas (S_0) were measured to be 16.69 and 13.84 m^2/g, respectively. Fig. 2.6 shows the Arrhenius plot using the fitted parameters' intrinsic rate constant, k_0, and the activation energy, E. The resulting parameters correspond to 95% confidence levels were as follows:

Havelock limestone:

$$k_s = 2.3 \times 10^{-4} \exp\left(\frac{-E}{R_g T}\right) mol/(atm\, m^2 s)$$

$$E = 32.1 \pm 7.0\ kJ/mol \tag{2.9}$$

Cadomin limestone:

$$k_s = 3.0 \times 10^{-4} \exp\left(\frac{-E}{R_g T}\right) mol/(atm\, m^2 s)$$

$$E = 20.3 \pm 3.3\ kJ/mol \tag{2.10}$$

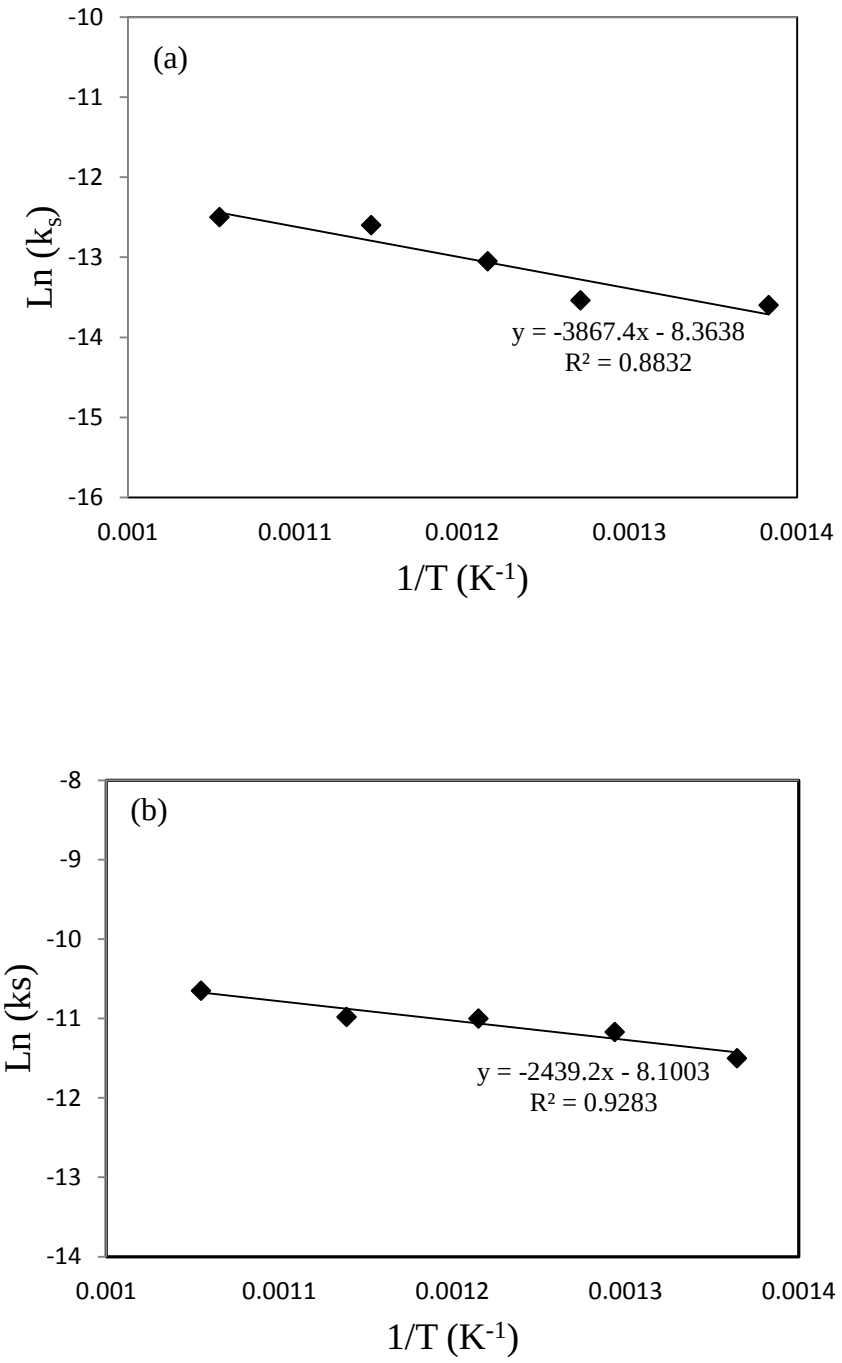

Fig. 2.6 Arrhenius plot for the carbonation reaction for a temperature range of 450-675°C and 100% CO_2 at 1 atm: (a) Havelock limestone and (b) Cadomin limestone.

The difference in the activation energies of the two sorbents may be due to the difference in structural changes during nucleation or solid product formation. Nucleation period would be

different for various particles as during this period, the nucleus is “situated at the regions of disorders such as points of emergence of dislocations, vacancies, interstitial or impurity clusters” [21]. In addition, Young [21] illustrated that the activation energy for gas-solid reactions that produce solid products, such as a carbonation reaction, is not only related to the chemical energy, but also related to the mechanical energy, such as the strain energy among grains in a particle. Therefore, the greater number of impurities in Cadomin limestone may cause lower mechanical energy among grains, leading to lower activation energy than Havelock limestone.

2.7.4 Effect of total pressure on the carbonation reaction at constant temperature and under a gas stream with constant CO_2 mole fraction concentration

To explore the effect of the total pressure on the carbonation reaction, the limestones calcined at 850°C and 1 atm under N_2 were exposed to a constant molar fraction (20%) of CO_2 balanced with N_2 at constant temperature (T=675°C) and total pressures in the range of 1 to 8 atm. Since an increase in the total pressure represents a corresponding increase in the CO_2 partial pressure and its molar concentration, an increase in the carbonation reaction rate would be expected. The carbonation reaction rate increased with increasing total pressure up to 4 atm and then leveled off with further increases for both calcined limestones (Fig. 2.7). With a constant inlet volumetric gas flow rate (500 mL/min), increasing the total pressure caused the reactant gas velocity to decrease, resulting in increased external mass transfer resistance [18].

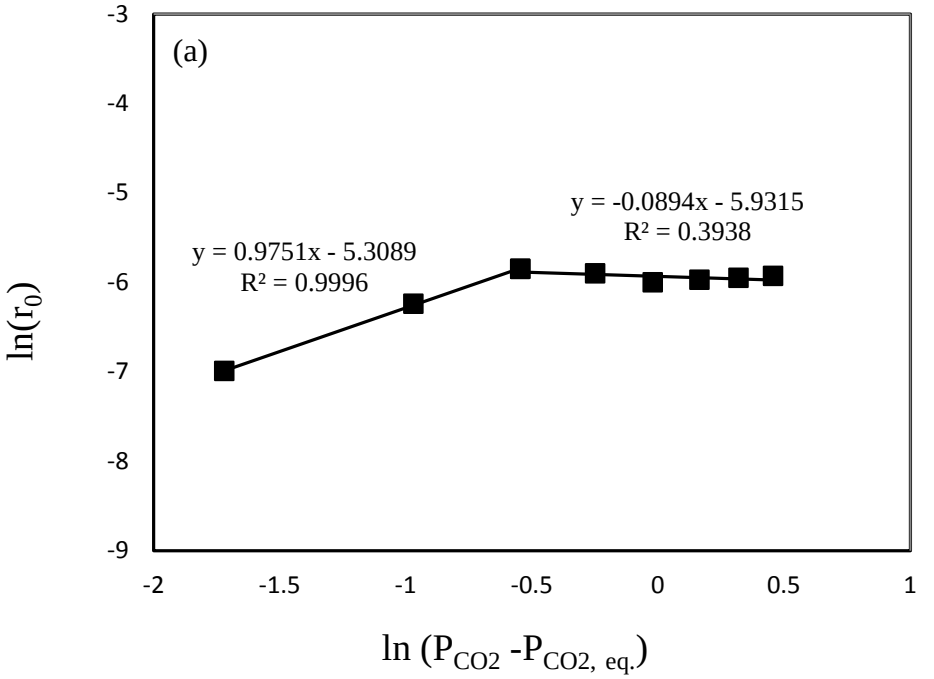

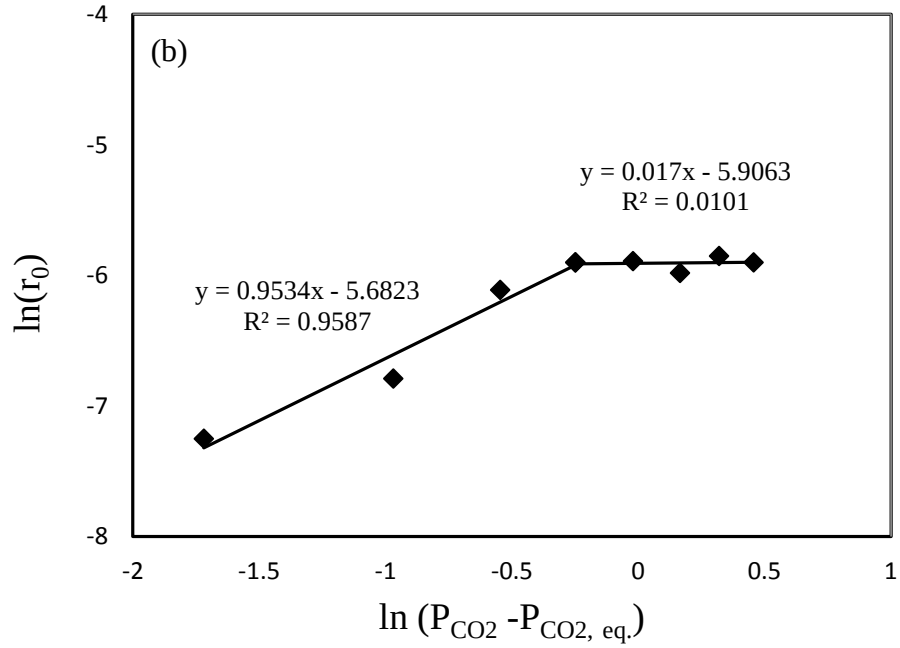

Fig. 2.7 Reaction order plot with varying CO_2 partial pressures corresponding to different total system pressures for fully calcined (a) Havelock limestone and (b) Cadomin limestone.

As shown in Fig. 2.7, an obvious transition of the carbonation reaction order occurred from the first order to the zero order at 675°C and CO_2 partial pressures between 0.6 and 0.8 atm for both calcines, suggesting that the reaction control mechanism changed at $P_{CO_2} \sim 0.7$ atm. The transition of the carbonation reaction order can be explained based on the Langmuir mechanism, by considering two elementary steps for the carbonation reaction:

$CaO + CO_2 \rightleftharpoons CaO.CO_2$ step 1

$CaO.CO_2 \rightarrow CaCO_3$ step 2

where $CaO.CO_2$ is an intermediate complex.

If we assume that step 2 is a rate limiting step, step 1 is at quasi-equilibrium:

$$k_1(1-\theta)\,P_{CO_2} - k_{-1}(\theta) = 0 \tag{2.11}$$

or

$$\theta = \frac{KP_{CO_2}}{KP_{CO_2}+1} \tag{2.12}$$

where $K = \frac{k_1}{k_{-1}}$ is the equilibrium constant for step 1.

The reaction rate can then be expressed as follows:

$$r = k_2(\theta) \tag{2.13}$$

After rearranging Eqs. (2.12) and (2.13), the reaction rate can be written as:

$$r = \frac{Kk_2P_{CO_2}}{KP_{CO_2}+1} \tag{2.14}$$

At $P_{CO_2} < 0.7\ atm$, step 1 is likely to be considered as rate limiting; therefore, $KP_{CO_2} \ll 1$, and the rate of reaction would be first order:

$$r = Kk_2 P_{CO_2} \tag{2.15}$$

On the other hand, at higher CO_2 partial pressures, i.e., $P_{CO_2} > 0.7\ atm$, when step 1 is assumed to be fast, $KP_{CO_2} \gg 1$; and, the order of reaction shifts to zero:

$$r = k_2 \tag{2.16}$$

2.7.5 Effect of particle size on the carbonation reaction

The particle size may play an important role in the rate of carbonation reaction, with smaller sizes minimizing the inter-particle mass transfer resistance. In this study, three different particle size ranges of Havelock limestone were selected: 450-600 μm, 600-850 μm, and 850-1000 μm. Fig. 2.8 presents the carbonation reactions at 675°C for the three different particle size ranges. According to Fig. 2.8, the particle size in the range of 450 to 1000μm did not have a significant effect on the carbonation reaction rate, as the internal mass transfer resistance may have remained constant and the reaction takes place uniformly over the solid sorbent under the conditions studied in this research. Bhatia and Perlmutter [15] have also found a negligible effect of particle size on the carbonation reaction.

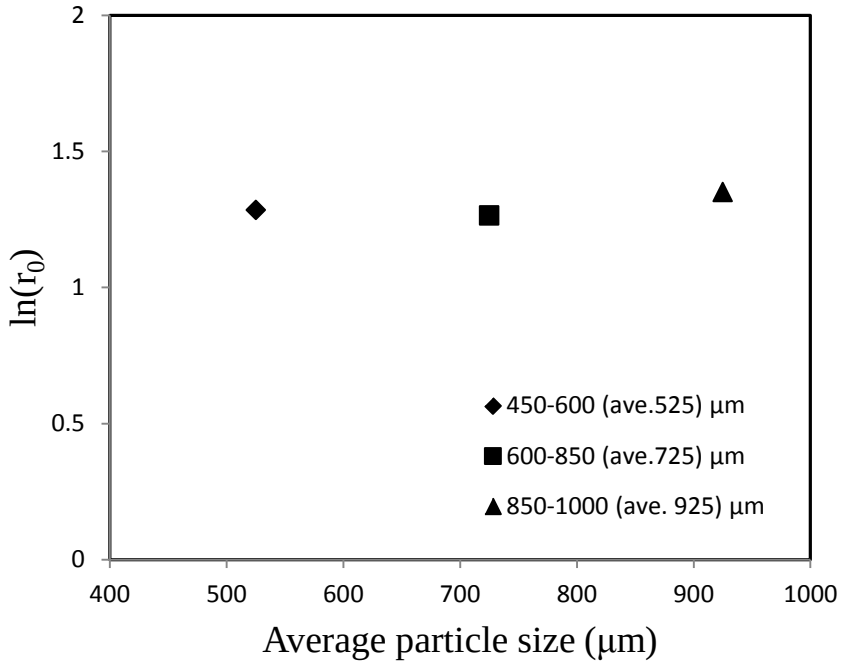

Fig. 2.8 Effect of particle size on the carbonation reaction at 675°C with Havelock limestone.

2.7.6 Predictions of carbonation behavior using Aspen Plus

In this research, the thermodynamic and kinetic simulations of the CO_2 capture process using Cadomin limestone were performed using the Aspen Plus simulator. Table 2.3 presents the value of parameters used in Aspen Plus simulator. Fig. 2.9 shows the sensitivity analysis of the carbonation reaction for Cadomin limestone based on the thermodynamic modeling. According to the result, the carbonation reaction does not proceed at temperatures higher than 800°C, because the reversed reaction (calcination reaction) starts at this temperature or higher.

Table 2.3 Value of parameters used in Aspen Plus simulator

Parameters in Aspen Plus	Units	Value
Equation of State(EOS)	-	PR-BM[b]
Carbonator Temperature	°C	550-750
Carbonator Pressure	bar	1-30
Calciner Temperature	°C	850
Calciner Pressure	bar	0
Loss Percentage	%	20%

[b] PR-BM: Peng-Robinson with Boston-Mathias alpha function

The activation energy and pre-exponential factor (k_0) obtained from the experiment were applied to the kinetic modeling developed using Aspen Plus. Fig. 2.9 presents a distinct optimal temperature (650°C) for the carbonation reaction, which was slightly different from the optimal carbonation temperature obtained from the TGA experiments (675°C). Consequently, due to the reversible and exothermic nature of the carbonation reaction, the rate of carbonation reaction increased until the optimal temperature was achieved and then decreased with further increases in the temperature. The difference between the optimal temperatures obtained from the experiment and modeling is due to the assumptions applied in the Aspen Plus simulator, which are presented in 'Simulation assumptions' section**.**

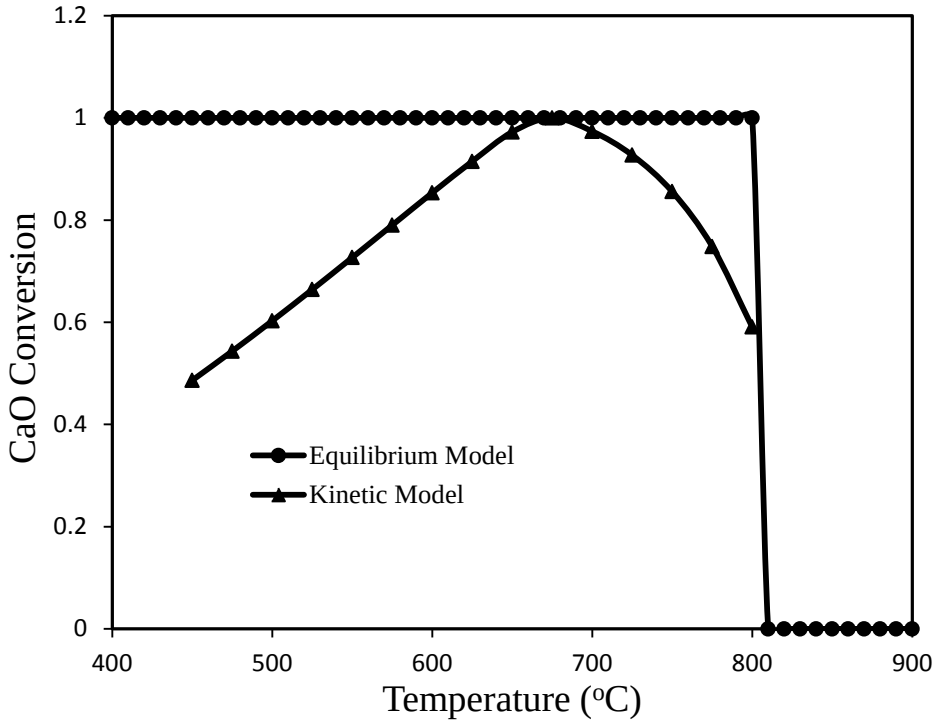

Fig. 2.9 The prediction of final CaO conversion versus temperature for Cadomin limestone in the presence of pure CO_2 using Aspen Plus.

Fig. 2.10 demonstrates a comparison of final CaO conversion after 10 min carbonation for calcined Cadomin limestone between the kinetic model and the experimental data. The model predicted that the maximum conversion occurs at 650°C, which was in very good agreement with the experimental data. The CaO conversion trend predicted by the kinetic model also closely followed the experimental data. This is similar to our previous findings for Dolomite [22], in which the optimal temperature was measured to be 675°C. The subtle difference in the optimal temperatures could be due to the different compositions (i.e., CaO content) and surface structures of these two CaO-based sorbents. The sharp decrease implies the thermodynamically limited nature of the carbonation reaction. This is the point at which the reverse reaction (calcination) began (Fig. 2.9).

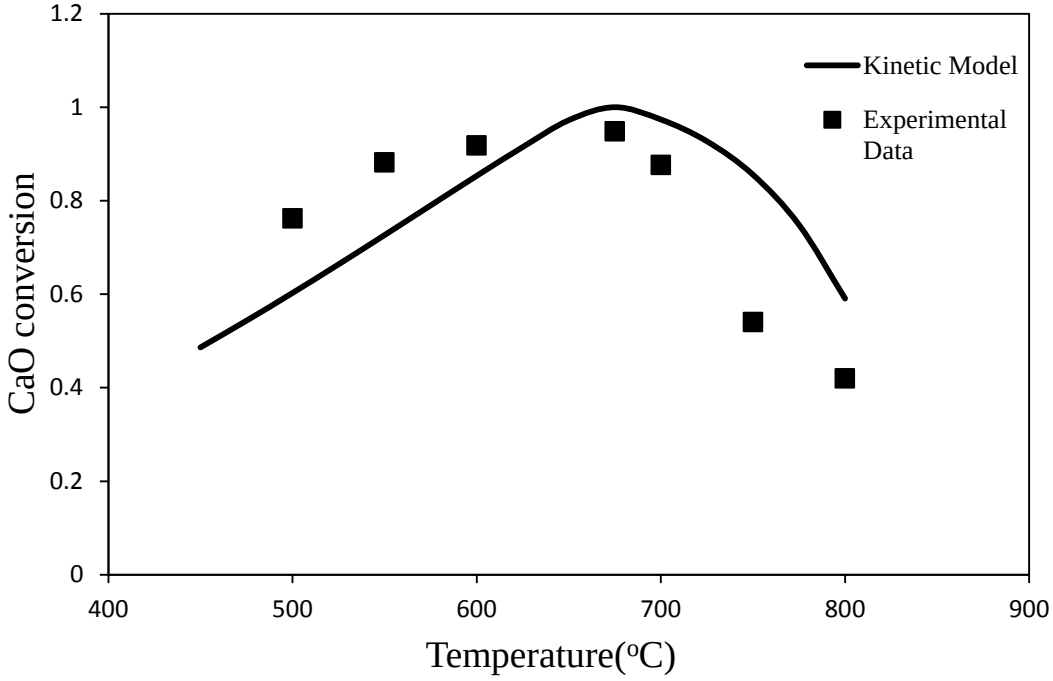

Fig. 2.10 Comparison of the measured final CaO conversion versus temperature for Cadomin limestone in the presence of pure CO_2 using Aspen Plus (Kinetic model).

There were, however, some discrepancies between the model results and the experimental data, due to measurement error and the assumptions included in the modeling. For instance, it is very difficult to measure the reaction rate at the maximum conversion, since the activation energy approaches zero. Moreover, the model assumes an ideal case, where all solid particles are in contact with CO_2 gas and react uniformly with gas.

Fig. 2.11 depicts the effect of CO_2 partial pressure on the CaO conversion over time. This series of graphs resulted from a sensitivity analysis using a base case model for the carbonation reaction of Cadomin with CO_2 using Aspen Plus simulation software, where the CO_2 partial pressure was defined as the parametric value and the temperature as the independent variable. As can be observed, pressure favored the carbonation up to a specific value, which was almost 0.8 atm. The gaps between the series of graphs decreased with increasing pressure. For CO_2 partial

pressures higher than 0.8 atm gauge, the order of reaction approached zero, leading to the elimination of the CO_2 partial pressure effect. This result is in very good agreement with the afore-mentioned discussion for Fig. 2.7 in the previous section (i.e., effect of pressure on the carbonation reaction).

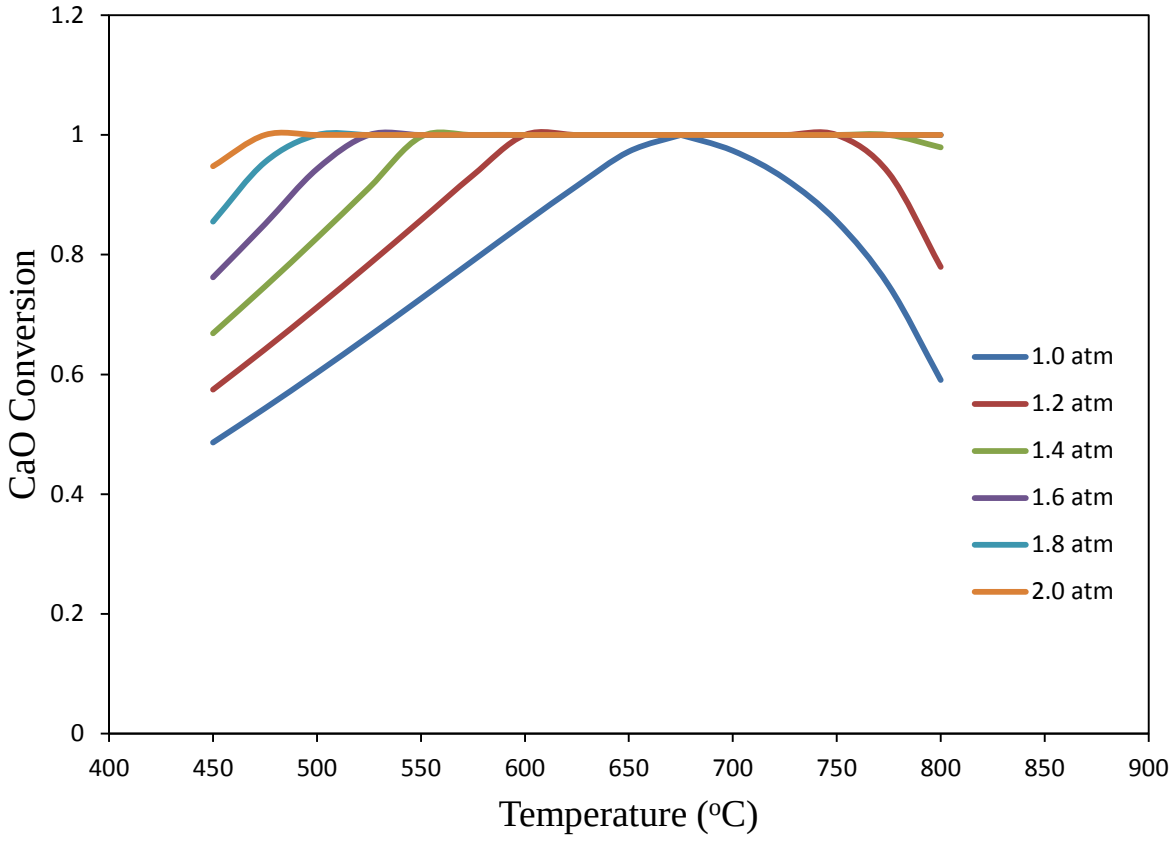

Fig. 2.11 Comparison of the CaO conversion versus temperature for Cadomin limestone for different CO_2 partial pressures using Aspen Plus (kinetic model).

These findings confirmed the fact that the reaction rate was dependent on pressure for lower CO_2 partial pressures (< 0.8 atm gauge), whereas the carbonation reaction appeared to have no dependency on CO_2 partial pressure when the CO_2 partial pressure was higher than this threshold value.

2.8 Conclusion

The intrinsic kinetics of the carbonation reaction for two limestones (Havelock and Cadomin) was studied based on a grain model using an ATGA. The results for both calcined limestones showed linear relations between the rate of carbonation reaction and the CO_2 partial pressure at a constant total pressure of 1 atm. Based on the PTGA test at 675°C, the first-order carbonation reaction rate at a lower total pressure changed to zero order at total pressures higher than 3 and 4 atm for the Havelock and Cadomin calcines, respectively.

The carbonation reaction rate showed an increase with increasing temperature in the range of 450 to 675°C, but decreased with further increases in temperature. The activation energies were found to be 32.1 and 20.3 kJ/mol for the Havelock and Cadomin calcines, respectively. According to the experimental result, no obvious effect of particle size on carbonation reaction was found. A similar dependency of the carbonation rate on temperature was obtained by the thermodynamic and kinetic simulations performed with Aspen Plus software. The trend predicted for the carbonation reaction of the calcined Cadomin limestone by the kinetic model closely followed that of the experimental data, with a sharp decrease in final stage of CaO conversion, showing the thermodynamically limited nature of the carbonation reaction. The discrepancies were mainly due to the assumptions for the simulation and the difficulty of measuring the reaction when the reaction rate is close to zero (i.e., the maximum of conversion versus time).

2.9 References

[1] Herzog, H. J., What future for carbon capture and sequestration?. Environ. Sci. Technol. 35 (2001) 148A–153A.

[2] Rao, A. B., Rubin, E. S., A technical, economic, and environmental assessment of amine-based CO_2 capture technology for power plant greenhouse gas control. Environ. Sci. Technol. (2002) 36**,** 4467–4475.

[3] Figueroa, J.D., Fout, T., Plasynski, S., McIlvried, H., Srivastava, R. D., Advances in CO_2 capture technology—The U.S. department of energy's carbon sequestration program, Int. J. Greenh. Gas Control 2 (2008) 9–20.

[4] Kanniche, M., Gros-Bonnivard, R., Jaud, P., Valle-Marcos, J., Amann, J.M., Bouallou, C., Pre-combustion, post-combustion and oxy-fuel combustion in thermal power plant for CO_2 capture. Appl. Therm. Eng. 30 (2010) 53–62.

[5] Hossain, M. M., de Lasa, H. I., Chemical-looping combustion (CLC) for inherent CO2 separations—a review. Chem. Eng. Sci. 63 (2008) 4433–4451.

[6] Scheffknecht, G., Al-Makhadmeh, L., Schnell, U., Marier, J., Oxy-fuel coal combustion—A review of the current state-of-the-art. Int. J. Greenh. Gas Control 55 (2011) 516-535.

[7] Yang, H., Xu, Z., Fan, M., Gupta, R., Slimane, R. B., Bland. A.E., Wright, I., Progress in carbon dioxide separation and capture: A review. J. Environ. Sci. 20 (2008) 14-27.

[8] Abanades, J. C., Alvarez, D., Anthony, E. J., Lu, D., In situ capture of CO_2 in a fluidized bed combustor, In: Proceedings of the 17th International Fluidized Bed Combustion Conference, ASME, Jacksonville, Florida, USA, pp. 133–135. Paper No.10 (2003).

[9] Silaban, A., Narcida, M., Harrison, D. P., Characteristics of the reversible reaction betweem CO_2 (g) and calcined dolomite. Chem. Eng. Comm. 146 (1996) 149–162.

[10] Lin, S.Y., Suzuki, Y, Atano, H.H., Harada, M., Hydrogen production from hydrocarbon by integration of water-carbon reaction and carbon dioxide removal (HyPr-RING method), Energy Fuels 15 (2001) 339-343.

[11] Lin, S.Y., Harada, M., Suzuki, Y., Hatano, H., Developing an innovative method, HyPr-RING to produce hydrogen from hydrocarbons. Energy Conv. Manag. 43 (2002) 1283–1290.

[12] Lin, S. Y., Process Analysis for Hydrogen Production by Reaction Integrated Novel Gasification (HyPr-RING). Energy Conv. Manag. 46 (2005) 869-880.

[13] Abanades, J. C., Anthony, E. J., Alvarez, D., Lu, D., Salvador, C., Capture of CO_2 from combustion gases in a fluidized bed of CaO. AIChE J. 50 (2004) 1614–1622.

[14] An, H., Song, T., Shen, L., Qin, C., Yin, J., Feng, B., Coal gasification with in situ CO2 capture by the synthetic CaO sorbent in a 1 kWth dual fluidised-bed reactor. Int. Journal of Hydrogen Energy 37 (2012) 14195–14204.

[15] Bhatia, S. K., Perlmutter, D. D., Effect of the product layer on kinetics of the CO_2—lime reaction. AIChE J. 29 (1983) 79–86.

[16] Sun, P., Grace, J. R., Lim, C. J., and Anthony, E. J., Determination of intrinsic rate constants of the CaO-CO_2 reaction. Chem. Eng. Sci. 63 (2008) 47–56.

[17] Sedghkerdar, M.H., Mahinpey, N., Ellis, N., The effect of sawdust on the calcination and the intrinsic rate of the carbonation reaction using a Thermogravimetric Analyzer (TGA). Fuel Proc. Technology (2013) 106, 533–538.

[18] Yu, F. C., Fan, L. S., Kinetic study of high-pressure carbonation reaction of calcium-based sorbents in the calcium looping process (CLP), Ind. Eng. Chem. Res., 50 (2011) 11528–11536.

[19] Szekely, J., Evans, J. W., Sohn, H. Y., Gas Solid Reactions, Academic Press, London (1976)..

[20] Baker, E. H., The calcium oxide-carbon dioxide system in the pressure range 1–300 atmospheres. J. Chem. Soc. (1962) 464–470.

[21] Young, D. A, Decomposition of Solids. Pergamon Press, Oxford (1966).

[22] Mostafavi, E., Sedghkerdar, M. H., and Mahinpey, N., Thermodynamic and kinetic study of CO_2 capture with calcium based sorbents: experimental and modeling. Ind. Eng. Chem.Res. 52 (2013) 4725–4733.

Chapter Three: **A modified grain model in studying the CO_2 capture process with a calcium-based sorbent: a semi-analytical solution**

Ind. Eng. Chem. Res. In press, DOI: 10.1021/ie503989n

3.1 Presentation of the article

This chapter presents an article that describes a global kinetic analysis of a CO_2 capture process with solid calcined Cadomin limestone using the grain model and the changing grain size (CGS) model by applying the intrinsic kinetic parameters obtained from Chapter 2. In the global kinetic analysis, both the kinetic control regime and the diffusion control regime were considered in describing the carbonation reaction mechanism. In addition, the effects of the temperature, particle size, and porosity of the sorbent on the kinetics of the carbonation reaction were investigated using the proposed mathematical models, which are difficult to analyze, experimentally.

The results of the CGS model indicated better agreement with the experimental data than the results obtained using the grain model, because the CGS model considered the physical structure change of the sorbent particle during the reaction. Moreover, the modeling results showed the positive effects of increasing the reaction temperature and particle porosity on the rate of carbonation reaction. However, the rate of carbonation reaction decreased by increasing the sorbent particle size.

This work was performed by Mohammad H. Sedghkerdar under the supervision of Dr. Nader Mahinpey.

A modified grain model in studying the CO_2 capture process with a calcium-based sorbent: a semi-analytical approach

This article is published to Ind. Eng. Chem. Res. journal.

Manuscript ID: ie-2014-03989n

Mohammad Hashem Sedghkerdar, Nader Mahinpey

Department of Chemical and Petroleum Engineering, Schulich School of Engineering, University of Calgary, Calgary, AB, Canada T2N 1N4

3.2 Abstract

In this study, the behavior of the carbonation reaction of the calcined Cadomin limestone used for CO_2 capture is described using the grain model and the changing grain size (CGS) model. To calculate the overall conversion over time, the mathematical modeling was solved semi-analytically. The overall sorbent conversion obtained with the CGS model showed better agreement with the experimental data than the results obtained using the grain model. In the CGS model, the physical structure of the sorbent particle changes during the reaction. The CGS model was modified by considering a variable diffusion coefficient of the gaseous reactant through the development of the product layer. The modeling results showed the positive effects of increasing the reaction temperature and particle porosity on the rate of carbonation reaction. However, the rate of carbonation reaction decreased by increasing the sorbent particle size. Moreover, the modeling results demonstrated an initial kinetic control stage, which was followed by a diffusion control step in the carbonation reaction of the calcined Cadomin limestone.

3.3 Introduction

Heterogeneous catalytic and non-catalytic reactions are numerous and of great importance in industrial applications. The capture of carbon dioxide (CO_2) using a calcium-based sorbent as a heterogeneous non-catalytic gas-solid reaction has been widely proposed for different applications, such as fluidized bed combustors for in situ CO_2 capture [1-2], hydrogen production by reaction-integrated novel gasification (HyPr-Ring) [3-6], and steam reformers [7-9].

A non-catalytic gas-solid reaction with no gaseous product takes places in three steps: first, the external mass transfer of gaseous reactant through the gas film surrounding the solid particle; second, the internal mass transfer of gaseous reactant through the particle and product layer and finally, the reaction at the reaction surface. There are many parameters that affect a non-catalytic gas-solid reaction, such as temperature, solid particle physical structure, and particle size. Therefore, an appropriate mathematical model needs to be developed to show the behavior of the complex interaction between gaseous and solid reactants. The desirable mathematical model should be the closest representation of reality without mathematical complexities.

There are several models proposed for non-catalytic gas-solid reaction in the standard textbooks [10-11]. The un-reacted shrinking core model and the grain model are commonly used for a non-catalytic gas-solid reaction for non-porous and porous solid reactant, respectively. In the un-reacted shrinking core model, the reaction occurs at a sharp interface, separating the product layer from the un-reacted solid's core. As the reaction proceeds, the reaction zone moves into the solid particle but the overall particle size remains constant. The un-reacted shrinking core model has been used by many investigators to interpret their results [12-14].

The grain model, on the other hand, considers a spherical porous solid reactant that consists of numerous small non-porous grains. The reaction occurs at the surfaces of the grains according to the un-reacted shrinking core model. Gibson and Harrison [15] used the grain model to describe the desulfurization reaction using a zinc oxide (ZnO)-based sorbent. Nashtaee and Khoshandam [16] applied the grain model to model a noncatalytic gas-solid reaction in packed bed reactors. The grain model does not consider the change of grain size through the reaction, which occurs in many gas-solid reactions, such as the carbonation reaction (Eq. (3.1)), due to the molar volume differences between the solid reactant (calcium oxide (CaO)) and the solid product (calcium carbonate ($CaCO_3$)). The changing grain size (CGS) model has been developed by Georgakis et al. [17] by taking into account the change in the grain size during the reaction. This model has been used to describe the results of sulfation [18-19], reduction and oxidation [20-21], and CO_2 capture using dolomite [22-24].

$$CaO\ (s) + CO_2\ (g) \leftrightarrow CaCO_3(s) \qquad (3.1)$$

The current work presents a detailed kinetic analysis of a CO_2 capture process with Cadomin limestone was presented using both the grain and the CGS models. The proposed models were solved semi-analytically. In the CGS model, the product layer diffusivity was assumed to be a function of the sorbent conversion which was proposed by Krishnan and Sotirchos [25] for the sulfation of limestone. In addition, the effects of temperature, particle size, and porosity of the sorbent on the kinetics of the carbonation reaction were investigated.

3.4 Experimental details

In this work, the Perkin Elmer TGA 7 Thermogravimetric Analyzer, TGA, was used to study the CO_2 capture process with natural Cadomin limestone from western Canada. A 20 mg Cadomin limestone was subjected to the calcination reaction by heating up to 850°C at 40°C/min

in pure nitrogen (N_2) flow of 50 ml/min, followed by 20 min at 850°C. The physical parameters of the calcined Cadomin limestone are provided in Table 3.1. Table 3.2 presents the elemental composition of the Cadomin limestone.

Table 3.1 Physical parameters of the sorbent

Parameters	Values
Sorbent	Calcined Cadomin limestone
CaO weight fraction (Purity)	94.7%
Surface area (m^2/g)	13.80
Pore size (nm)	34.33
Particle size (μm)	250-750
CaO grain size (nm)	65.9
Initial porosity	0.16

Table 3.2 Chemical composition (wt %) [26]

Sorbent	SiO_2	Al_2O_3	Fe_2O_3	MgO	CaO	Na_2O	K_2O	LOI[a]
Cadomin	1.71	0.88	1.03	1.06	46.99	0.16	0.44	47.73

[a] LOI: Loss of Ignition

Following calcination, the TGA was set to the desired carbonation temperature under a N_2 flow of 50 ml/min. The carbonation reaction was then started by switching the gas flow from N_2 to pure CO_2 balance N_2 at a total flow rate of 200 ml/min. The sample's weight gain during the carbonation reaction was used to calculate the reaction conversion. The conversion of the calcined limestone (CaO) was obtained as follows:

$$\text{Conversion} = \frac{(m(t)-m(0))}{44} \Big/ \frac{(m(0)\times \text{Purity})}{56} \quad (3.2)$$

where 44 and 56 are the CO_2 and CaO molar weights (g/mol), respectively; and, m(0) and m(t) are the sample weights at the beginning and time t of the carbonation reaction, respectively.

3.5 Mathematical Modeling

3.5.1 The grain model

The grain model considers the sorbent as a spherical porous particle and comprised of a large number of non-porous and uniform spherical CaO grains (Fig. 3.1(a)). The carbonation reaction occurs when CO_2 penetrates and diffuses through the porous media in the sorbent particle and reaches the surfaces of the CaO grains [25].

The following assumptions are considered in the grain model:

1- The initial physical structure parameters of the sorbent particle such as porosity and molar density are considered constant throughout the reaction.

2- The product layer diffusivity is sufficiently high within the grains so that the CO_2 can diffuse through the porous product layer to react with the un-reacted core at the reaction surface. It is reasonable to assume that small grains possess shorter diffusion path through the product layer.

3- The particle radius of CaO is considered to remain constant during reaction.

4- The pseudo-steady state assumption is applied to the gas concentration profile in the particle. This assumption is based on the negligible amount of gaseous reactant within the particle compared to the net input and the rate of reaction.

5- The carbonation reaction is considered as a reversible first-order chemical reaction. This assumption was verified in our previous work [26].

6- The gas-film diffusion resistance surrounding the particle is negligible compared to the intra-particle mass transfer and reaction.

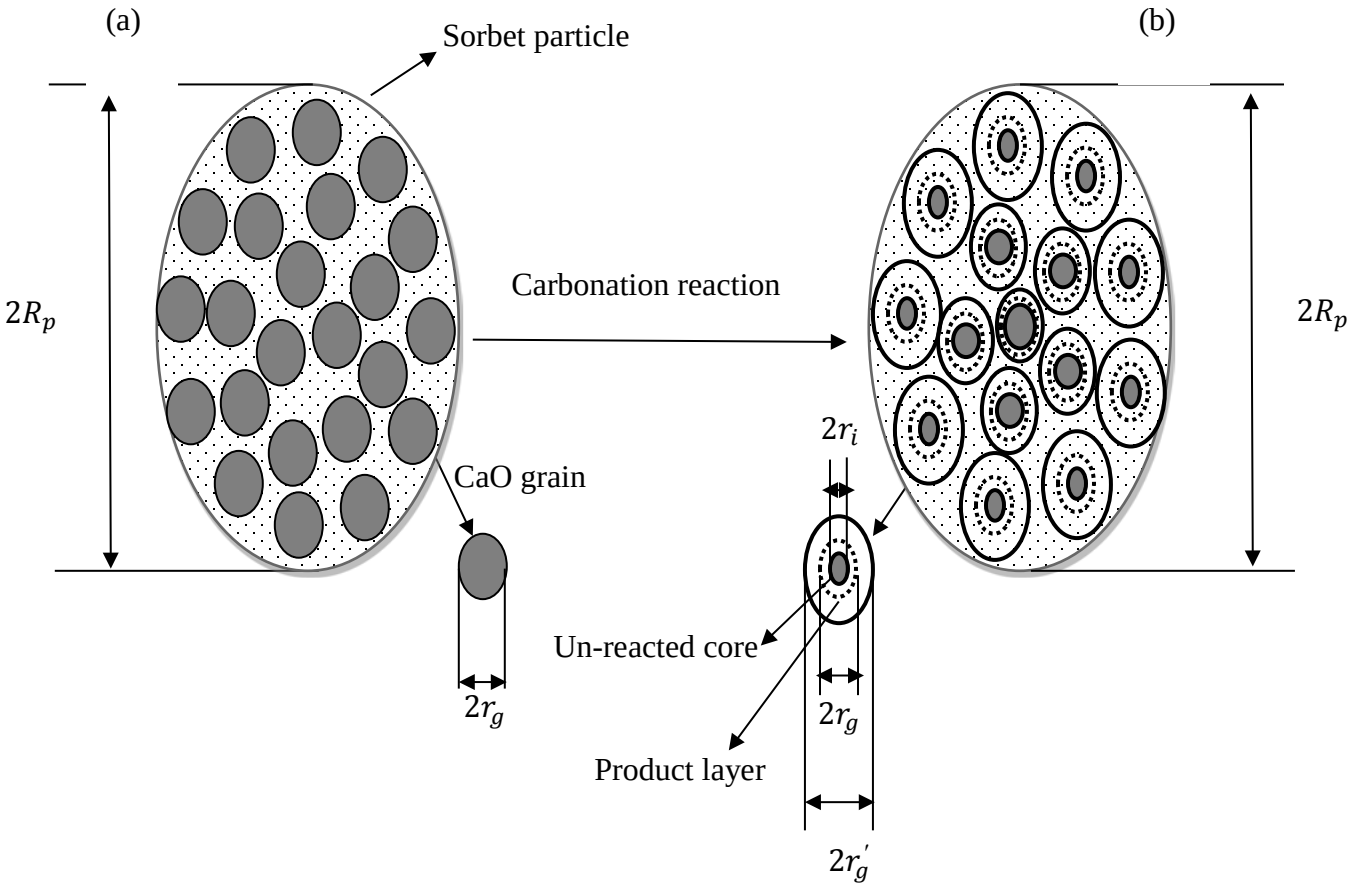

Fig. 3.1 Schematic diagram of the sorbent particle in the CGS model, (a) t=0, (b) t=t.

According to the fourth assumption based on a pseudo-steady state carbonation reaction, the CO_2 concentration profile in the CaO particle was obtained by making a mass balance around the porous particle as follows:

$$\frac{1}{R^2}\frac{\partial}{\partial R}\left(D_e R^2 \frac{\partial C_{CO_2,R}}{\partial R}\right) + r_{CO_2} = 0 \qquad (3.3)$$

The boundary conditions are:

$$\frac{\partial C_{CO_2,R}}{\partial R} = 0 \qquad R = 0 \tag{3.4}$$

$$C_{CO_2,R} = C_b \qquad R = R_p \tag{3.5}$$

In Eq. (3.3), r_{CO_2} expresses the molar rate of disappearance of the CO_2 based on the CaO grain volume. Therefore, the reaction rate at the surface of the CaO grains in the particle is:

$$-r_{CO_2} = \gamma k_s \left(C_{CO_2,R} - C_{CO_2,eq}\right)^n \tag{3.6}$$

In Eq. (3.6) γ presents the ratio of reaction surface to the true volume of the solid particle as follows:

$$\gamma = \frac{3r_i^2}{r_g^3}(1-\varepsilon) \tag{3.7}$$

Regarding to the high product layer diffusivity assumption in the grain model, the CO_2 concentration at the surface interface of grains is identical with that in the particle ($C_{CO_2,R}$) at the same radial coordinate.

The rate constant (k_s) and the order of reaction (n) should be obtained using experimental data. In our previous work, the k_s for the calcined Cadomin limestone has been calculated in the temperature range of 450 to 675°C (Eq. (3.8)), and the order of reaction was also determined using different CO_2 partial pressures for carbonation reaction [28]. According to the results, the carbonation reaction is a first-order reaction (n=1).

$$k_s = (3.0 \times 10^{-8} \times R_g T) \exp\left(-\frac{20.3}{R_g T}\right) \frac{cm}{s} \tag{3.8}$$

In the grain model, the change of the un-reacted CaO radius during the reaction was calculated using Eq. (3.9):

$$\frac{dr_i}{dt} = -\frac{k_s}{\rho_{m,CaO}}\left(C_{CO_2,R} - C_{CO_2,eq}\right) \tag{3.9}$$

The initial conditions are:

$$r_i = r_g \qquad t = 0 \tag{3.10}$$

$$\frac{dr_i}{dt} = 0 \qquad r_i = 0 \tag{3.11}$$

According to the first two assumptions, the grain model will not precisely represent the mechanism of the carbonation reaction. Firstly, in the carbonation reaction the change of grain size occurs through the reaction due to the molar volume differences between solid reactant (CaO) and the solid product ($CaCO_3$). Therefore, the physical structure of the particle such as particle molar density and porosity changes during the reaction. Secondly, the experimental data (solid points in Fig. 3.3) suggest that higher initial reaction rate is followed by the much slower reaction rate at the final conversion (X_f). Therefore, it can be concluded that, the CO_2 diffusion rate through product layer to reach the CaO un-reacted core changes as the reaction proceeds.

Therefore, in this study, a modified grain model, called the changing grain size (CGS) model, proposed by Georgakis et al. [17] was used to model the carbonation reaction and also to compare the obtained results with outcomes from the original grain model. The CGS model and corresponding assumptions are explained the section 3.5.2.

3.5.2 The changing grain size (CGS) model

The same as the grain model, the CGS model also considers a spherical particle of the sorbent, made up of large number of grains of radius, r_g (Fig. 3.1(a)). In the CGS model, the first

two assumptions considered in the grain model (section 3.5.1) are modified to describe the carbonation mechanism more accurate as follows,

1. The grain dimensions change with time due to the differences in the molar volumes of the solid reactant (CaO) and solid product ($CaCO_3$). Therefore the physical properties of the sorbent particle, i.e. porosity and molar density, are change during the reaction. The grains close to the particle surface expand faster and decrease the diffusion rate of the CO_2 through the particle (Fig. 3.1(b)).
2. Within each grain, the CO_2 diffusivity through the product layer (D_{PL}) changes as a function of sorbent conversion during reaction.

In the CGS model and according to the second assumption, the Eq. (3.6) that presents the molar rate of disappearing CO_2 in the grain volume changed to the following equation:

$$-r_{CO_2} = \gamma k_s \left(C_{CO_2,s} - C_{CO_2,eq}\right) \tag{3.12}$$

where $C_{CO_2,s}$ is the CO_2 concentration at the surface interface between the reacted and unreacted portions of a grain. To obtain a relationship between the CO_2 concentration at the surface interface of grains ($C_{CO_2,s}$) and that of in the particle ($C_{CO_2,R}$), a second mass balance was performed around the individual grains:

$$D_{PL}\left[\frac{1}{r}\frac{\partial}{\partial r}\left(r^2\,\frac{\partial C_{CO_2,g}}{\partial r}\right)\right] = 0 \tag{3.13}$$

where the D_{PL} is not a function of radial position.

The boundary conditions are:

$$C_{CO_2,g} = C_{CO_2,R} \qquad\qquad r = r_g' \tag{3.14}$$

$$-D_{PL}\frac{\partial C_{CO_2,g}}{\partial r} = k_s\left(C_{CO_2,s} - C_{CO_2,eq}\right) \qquad r = r_i \tag{3.15}$$

After solving Eq. (3.13) and applying the boundary conditions:

$$C_{CO_2,s} = \frac{D_{PL}C_{CO_2,R} - k_s r_i\left(1-\frac{r_i}{r_g'}\right)C_{CO_2,eq}}{D_{PL} - k_s r_i\left(1-\frac{r_i}{r_g'}\right)} \tag{3.16}$$

After substituting Eq. (3.16) in Eq. (3.12), the reaction rate in the particle can be calculated as:

$$-r_{CO_2} = \beta k_s\left(C_{CO_2,R} - C_{CO_2,eq}\right) \tag{3.17}$$

where,

$$\beta = \frac{\gamma}{\left[1+\frac{k_s}{D_{PL}}r_i\left(1-\frac{r_i}{r_g'}\right)\right]} \tag{3.18}$$

In addition, Eq. (3.9), which was used in the grain model to calculate the changes of the un-reacted CaO radius during the reaction, reformed to the Eq. (3.19) in the CGS model with the same initial conditions:

$$\frac{dr_i}{dt} = -\frac{k_s}{\rho_{m,CaO}}\left[\frac{\left(C_{CO_2,R}-C_{CO_2,eq}\right)}{1+\frac{k_s}{D_{PL}}r_i\left(1-\frac{r_i}{r_g'}\right)}\right] \tag{3.19}$$

According to the first assumption in the CGS model, the expanded CaO grain radius can be obtained as:

$$r_g'^3 = Zr_g^3 + (1-Z)r_i^3 \tag{3.20}$$

where

$$Z = \frac{\nu_{m,CaCO_3}}{\nu_{m,CaO}} \tag{3.21}$$

The change in the particle porosity due to grain expansion during the reaction as a function of the initial porosity can be calculated through following equation:

$$\varepsilon = \varepsilon_0 - (1-\varepsilon_0)(Z-1)X \tag{3.22}$$

The equations used to calculate the effective diffusivity and the molecular gas diffusivity are expressed in the appendices.

The local and overall conversion of CaO as a function of time and particle radius (R) are calculated using following equations, respectively:

$$X(R,t) = 1 - \left(\frac{r_i(R,t)}{r_g}\right)^3 \tag{3.23}$$

$$X_o(t) = \frac{\int_0^{Rp} 4\pi R^2 X(R,t) dR}{\frac{4}{3}\pi R_p^3} \tag{3.24}$$

Therefore, based on the second assumption for the CGS model, the product layer diffusivity, D_{PL}, was considered as a function of the overall CaO conversion proposed by Krishnan and Sotirchos [25]:

$$D_{PL}(X) = D_{PL0} \exp(-a.X_o) \tag{3.25}$$

where D_{PL0} (the initial product layer diffusivity), and a are fitting parameters determined using the Simplex-Nelder-Mead optimization method [27]. The regressed parameters were obtained by minimizing the following objective function:

$$OF = \sum_{i=1}^{NP} (X_o^{exp} - X_o^{calc})^2 \tag{3.26}$$

where NP is the number of experimental data points and superscripts “exp” and “calc” denote the experimental and calculated values respectively.

3.5.3 Semi-analytical Approach

In this work, the CO_2 concentration profile through the particle, i.e., Eq. (3.3) was solved analytically, while Eqs. (3.9) and (3.19) were solved numerically using the Runge-Kutta method to obtain the grain un-reacted core radius (r_i), resulting in the calculation of the local and overall particle conversion using Eqs. (3.23) and (3.24) respectively, for the grain and the CGS models. A time step of 0.002 min was chosen to satisfy the pseudo steady state assumption of the CO_2 concentration profile through the particle. Fig. 3.2 presents the flowchart of the algorithm in the MATLAB software.

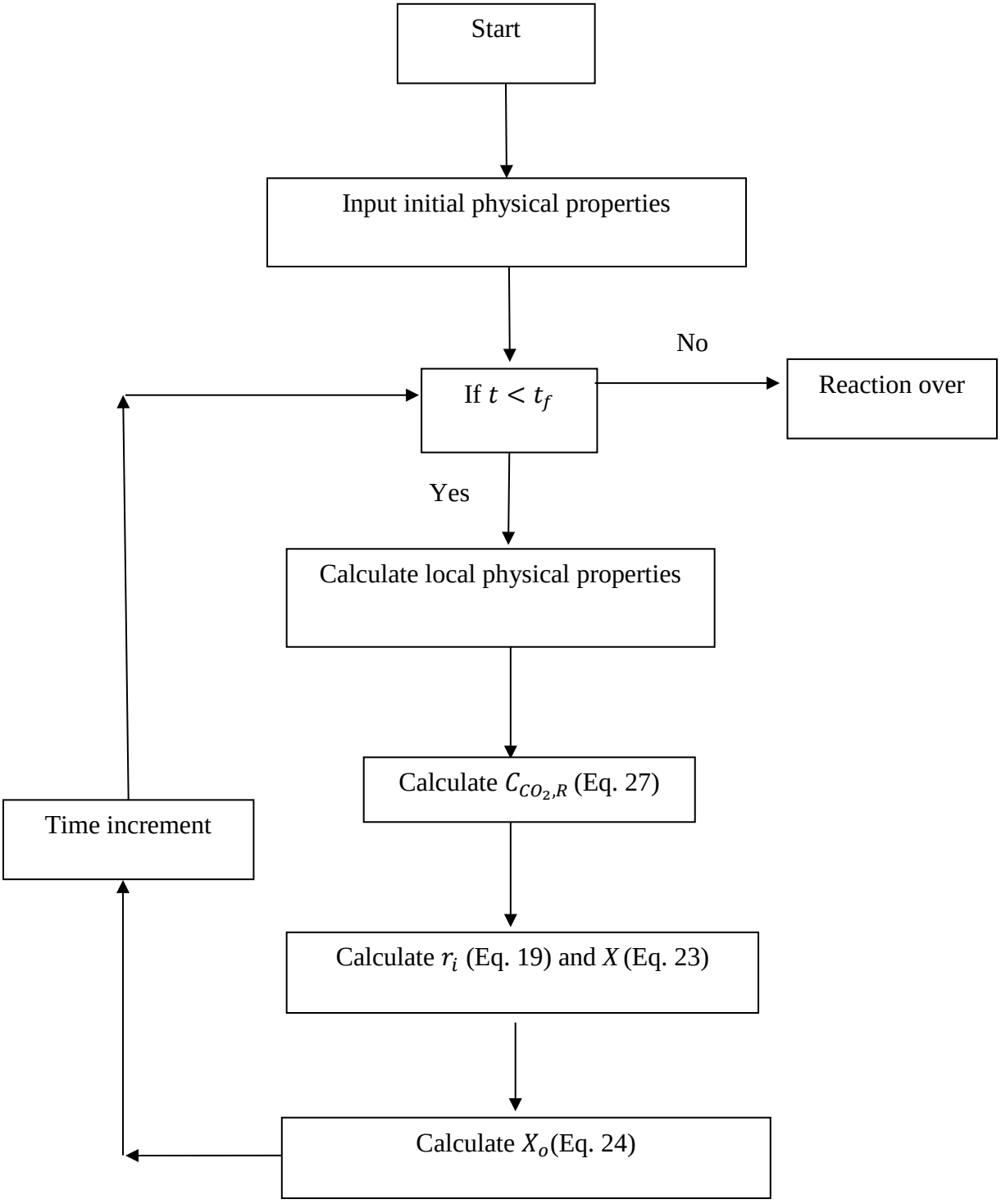

Fig. 3.2 Flowchart of the algorithm used in MATLAB software.

The analytical solution of Eq. (3.3) in terms of hyperbolic functions and after applying the boundary conditions (Eqs. (3.4) and (3.5)), provides:

$$\frac{C_{CO_2,R}-C_{CO_2,eq}}{C_b-C_{CO_2,eq}} = \frac{R_p}{R}\,\frac{sinh\left[\sqrt{\frac{\omega k_s}{D_e}}R\right]}{sinh\left[\sqrt{\frac{\omega k_s}{D_e}}_{R_p}\right]} \tag{3.27}$$

where for the grain model $\omega = \gamma$ (Eq. (3.7)) and for the CGS model $\omega = \beta$ (Eq. (3.18)). In eq (27), $\varphi = \sqrt{\frac{\omega k_s}{D_e}}R_p$ is the local Thiele modulus. The overall Thiele modulus through the particle is calculated as follows:

$$\varphi_o = \frac{\int_0^{R_p} 4\pi R^2 \varphi\, dR}{\frac{4}{3}\pi R_p^3} \tag{3.28}$$

The main steps of the analytical solution of eq (3) can be found elsewhere [30]. The molar mass transfer flow of CO_2, W_{CO_2}, at the surface of particle ($R = R_p$) :

$$W_{CO_2} = 4\pi R_p D_e (C_b - C_{CO_2,eq})(1 - \varphi\, coth\varphi) \tag{3.29}$$

The effectiveness factor, η, presents the ratio of actual CO_2 molar rate (W_{CO_2}) (Eq. (3.29)) to the CO_2 molar rate when the CO_2 diffusion resistance through pores is negligible (Eq. (3.30)) at the surface of particle. Eq. (3.31) defines the equation of effectiveness factor for the spherical particle.

$$W_{CO_2,0} = -\frac{4}{3}\pi R_p^3 \omega k_s (C_b - C_{CO_2,eq}) \tag{3.30}$$

$$\eta = \frac{3}{{\varphi_o}^2}(\varphi_o\, coth\varphi_o - 1) \tag{3.31}$$

3.6 Results and discussion

3.6.1 Model validation

In order to validate the modeling results, the overall conversion of CaO was calculated using both the grain and the CGS models and compared with experimental data points obtained at 650 and 550 °C and atmospheric pressure during carbonation reaction. The solid points in Fig. 3.3 show the experimental data. More details in experimental work could be found in our previous work [26].

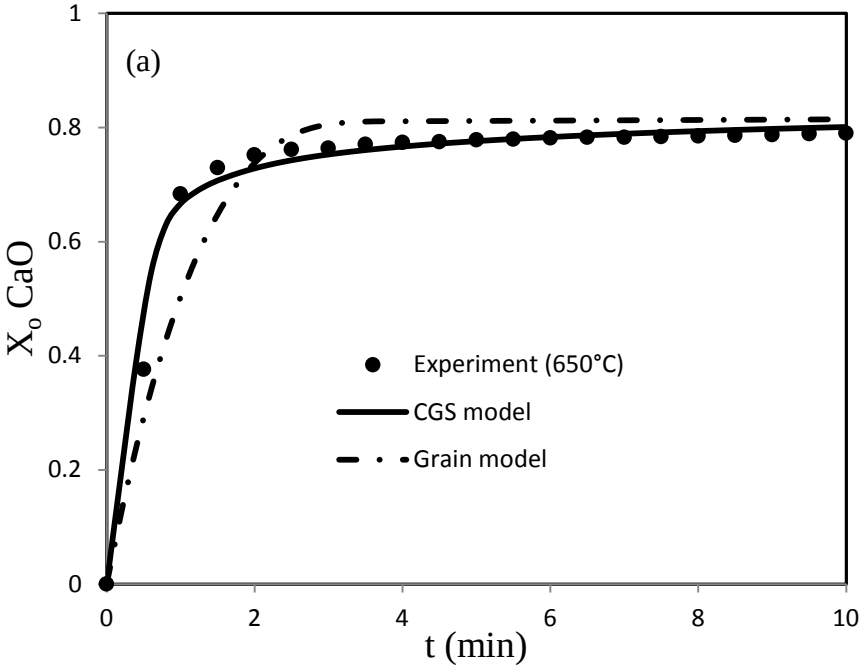

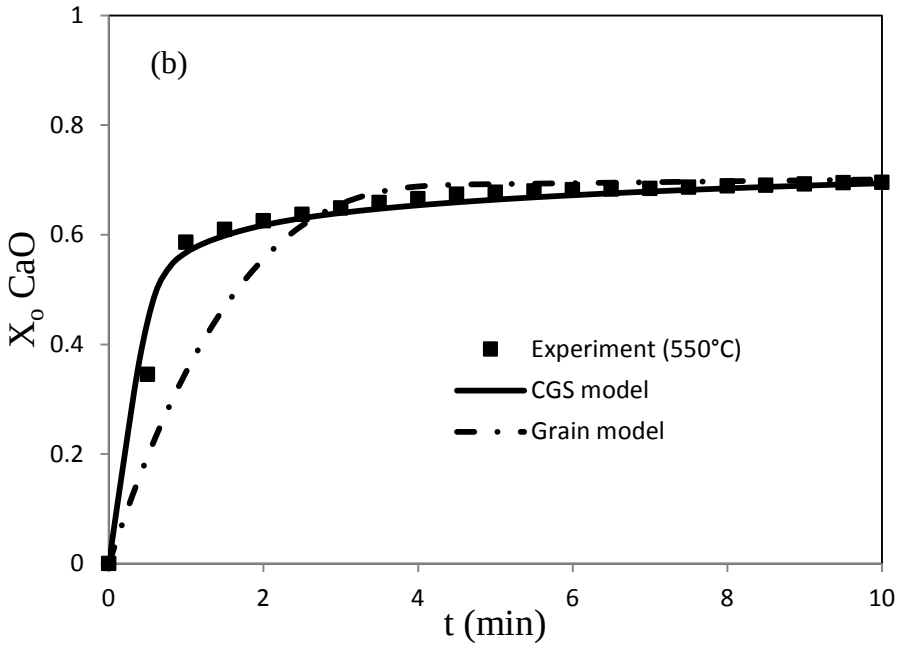

Fig. 3.3 Comparison between modeling results and experimental data during carbonation reaction at 1 atm and (a) 650°C, and (b) 550°C

Table 3.3 presents the model parameters for calculation of product layer diffusion in Eq. (3.25). D_{PL0} represents the initial product layer diffusivity, which is a function of temperature. The result of the fitted parameters shows that by increasing the temperature, the D_{PL0} increases resulting in an initial higher reaction rate at higher temperatures than at lower temperature. Therefore, a higher initial product layer diffusivity indicates a higher permeable (porous) product layer. On the other hand, according to the results obtained for "a", it may be inferred that the smaller value of "a" at higher temperature shows a lower tendency to agglomerate for the product layer at higher temperature, which causes a higher CO_2 diffusivity.

Table 3.3 Product layer diffusion model parameters in Eq. (3.25)

Temperature	D_{PL0}	a
T=650 °C	4.3×10^{-10}	8.2
T=550 °C	2.5×10^{-11}	10.6

A comparison of the experimental data with modeling results at 650 and 550°C are presented in Fig. 3.3(a) and (b), respectively. As seen, the modeling results obtained using the CGS model (solid line) agrees with the experimental data better than those obtained from the grain model (dash point). Therefore, the CGS model which considers the continuous change of particle's physical structure during the reaction due to molar volume difference between the solid reactant and the solid product is closer to reality than the grain model.

The initial fast stage of the reaction occurs due to the presence of fresh CaO surfaces for CO_2. The reaction is then followed by a much slower reaction, due to product layer formation, creating more resistance to the access of the CaO by the CO_2. In the first stage, the reaction is controlled kinetically and after formation of product layer, the diffusion controls the whole reaction.

3.6.2 Effect of temperature on the carbonation reaction

Fig. 3.4 illustrates that the rate of the carbonation reaction improves slightly by increasing the temperature from 550 to 650°C. According to Eq. (3A.6) in the appendices, the CO_2 molecular diffusivity increases with increasing temperature resulting in increased carbonation reaction rate. However, due to the increase in the equilibrium partial pressure of the CO_2 with temperature and the nature of the exothermic and reversible of carbonation reaction at higher temperatures (>700°C), the reversible reaction would presumably dominate [28].

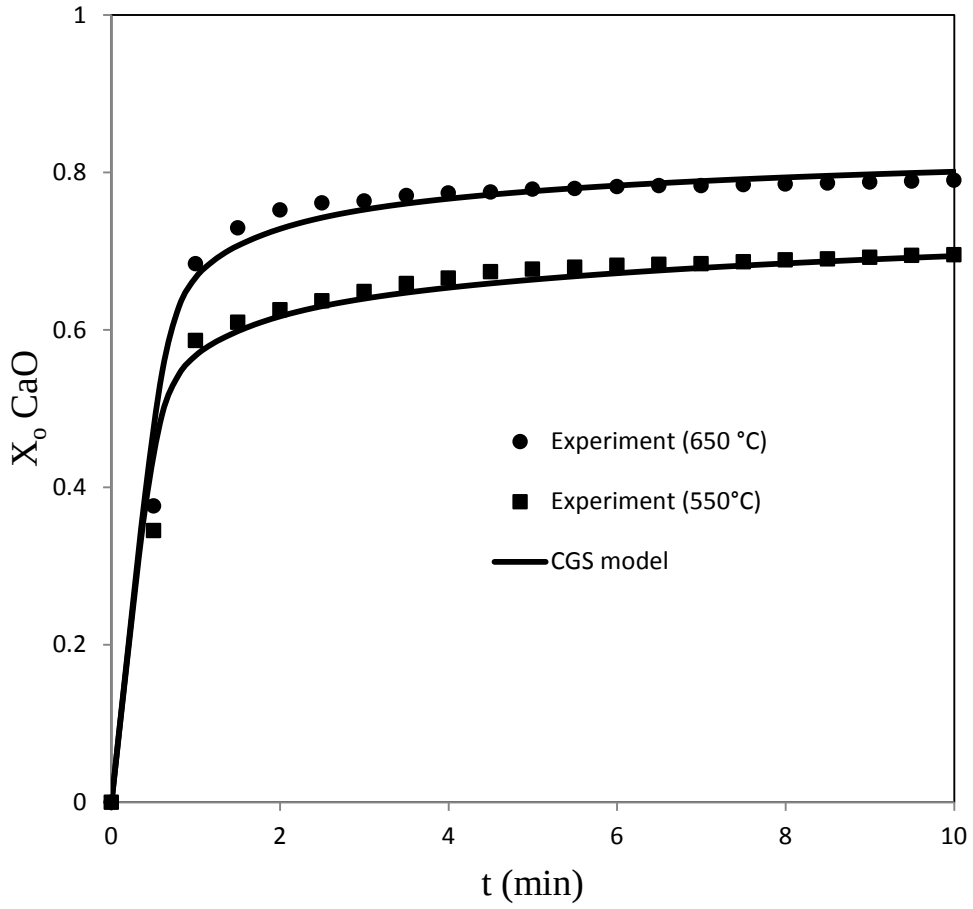

Fig. 3.4 Effect of temperature on the carbonation reaction at 1 atm

3.7 Modeling results:

3.7.1 CO_2 concentration profile in the sorbent particle

Fig. 3.5 presents the modeling output of the CO_2 concentration profile within the particle at different times. As seen, the CO_2 concentration profile at t = 0.2 min shows the fast stage of the reaction at the surface of the particle which shows a rapid CO_2 concentration reduction in the particle. However, by increasing the time of the reaction, the CO_2 concentration difference within the particle decreases, exhibiting the effect of product layer formation at the outside of the grains.

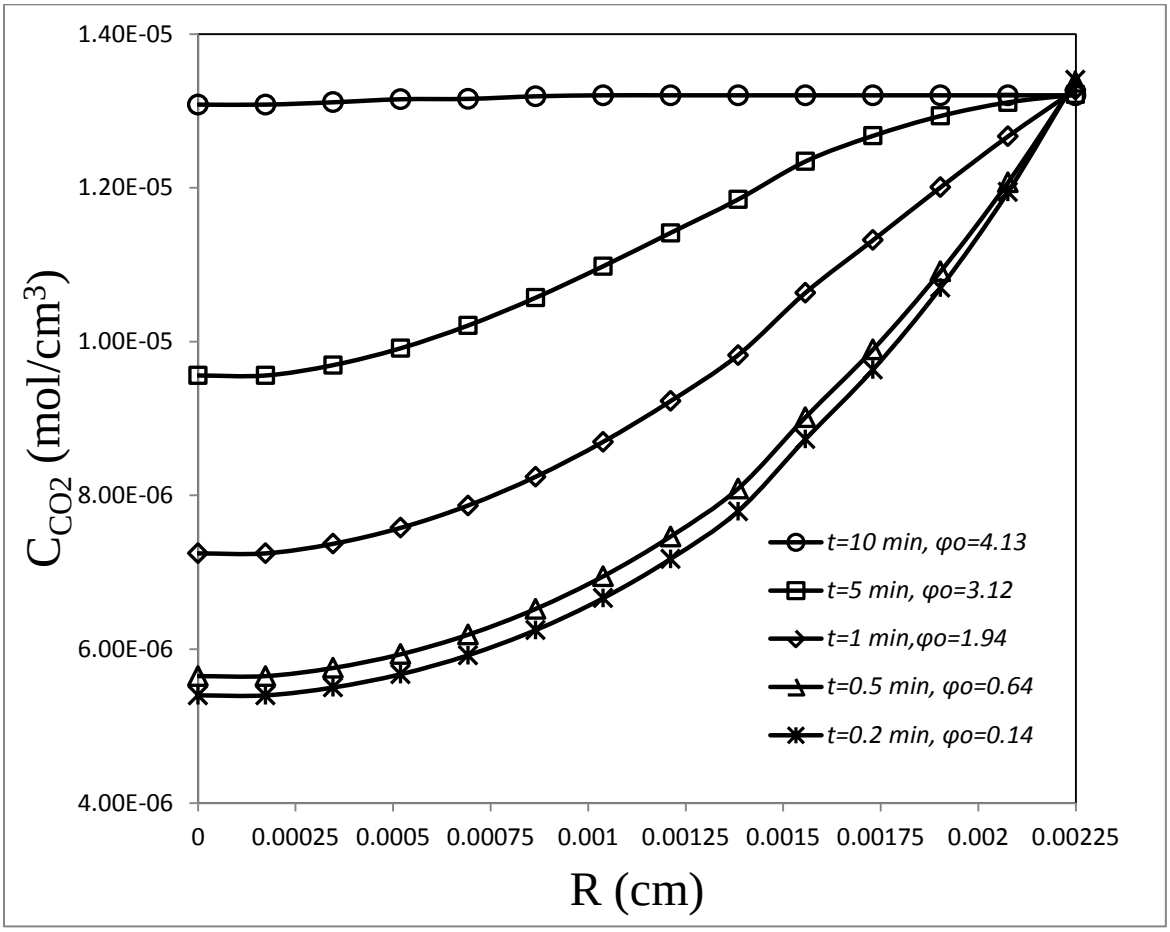

Fig. 3.5 CO_2 concentration profile in the particle during the carbonation reaction at 650°C and 1 atm

The Thiele modulus and effectiveness factor are calculated based on the grain model formulas. By increasing the reaction time, the overall Thiele modulus (φ_o) is also increased which confirms that the carbonation reaction is initially under kinetic control followed by the diffusion control stage where the rate of the carbonation reaction is slow and the CO_2 concentration profile within the particle becomes flat. The effectiveness factor (η) is plotted as functions of the overall Thiele modulus (φ_o) in Fig. 3.6. This figure shows the inverse relation between the effectiveness factor and the overall Thiele modulus ($\eta \propto \frac{1}{\varphi_o}$). As seen, at low values

for the overall Thiele modulus, the effectiveness is high which means the reaction is controlled chemically. However, by increasing the overall Thiele modulus, the effectiveness factor decreases resulting in the important role of diffusion in control of the reaction.

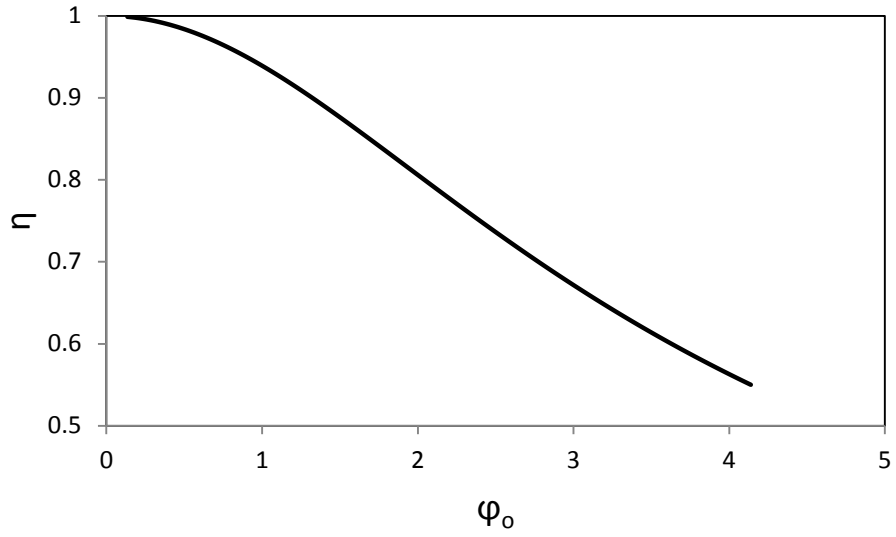

Fig. 3.6 Effectiveness factor profile versus the overall Thiele modulus

3.7.2 Porosity profile in the sorbent particle

Parameters of physical structure, such as porosity, were considered constant throughout the carbonation reaction in the grain model; however, in the CGS modeling, the porosity change during the reaction was viewed as a function of the CaO conversion. Fig. 3.7 indicates the CGS modeling results of the porosity profile within the particle through the carbonation reaction. According to Fig. 3.7, the particle porosity decreases dramatically at the beginning of the reaction (in the first 1 min of the reaction) due to the fast reaction and is followed by a slight change in the particle porosity, which is representative of the diffusion control stage of the reaction.

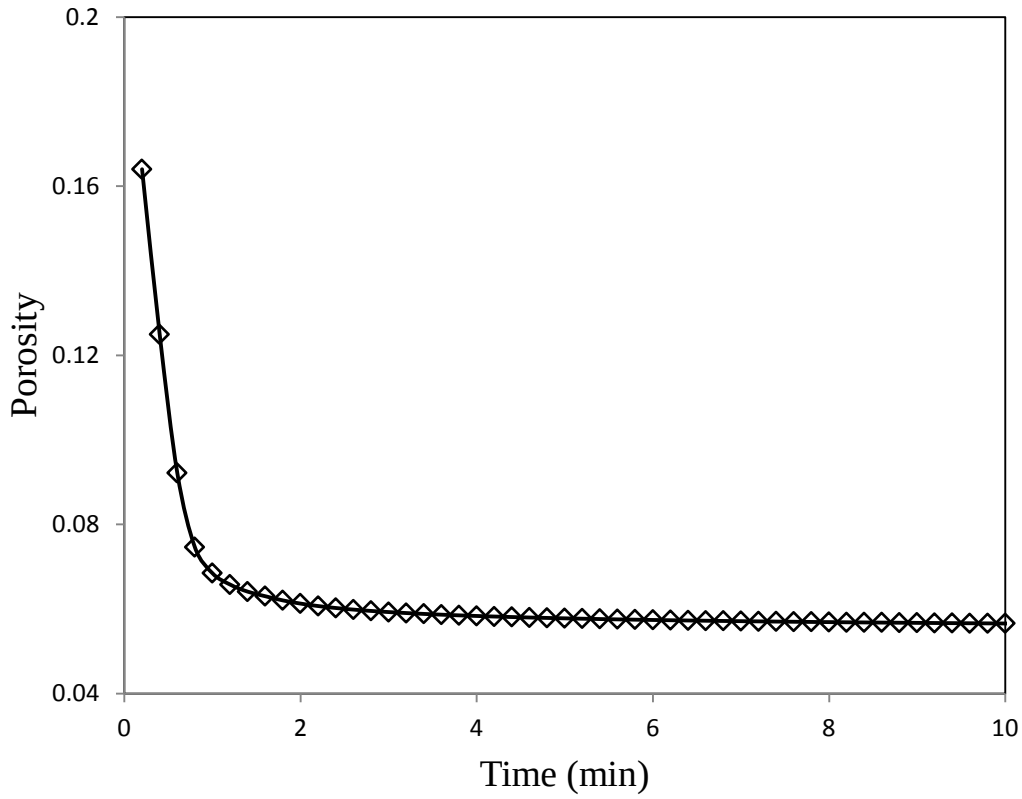

Fig. 3.7 Porosity profile in the sorbent particle during the carbonation reaction at 650°C and 1 atm

3.7.3 Product layer diffusivity profile

Fig. 3.8 presents the change of product layer diffusivity during the carbonation reaction with respect to the overall CaO conversion. As observed, at the beginning of the reaction the product layer diffusivity is high; however, as the reaction proceeds, the product layer diffusivity decreases exponentially (Eq. (3.25)). It is clear that due to the initial high product layer diffusivity, the carbonation reaction rate is fast. As the reaction proceeds, CO_2 permeability through the product layer decreases which causes a reduction in the carbonation reaction rate. Therefore, the carbonation reaction includes an initial kinetic control stage follow by the diffusion control stage.

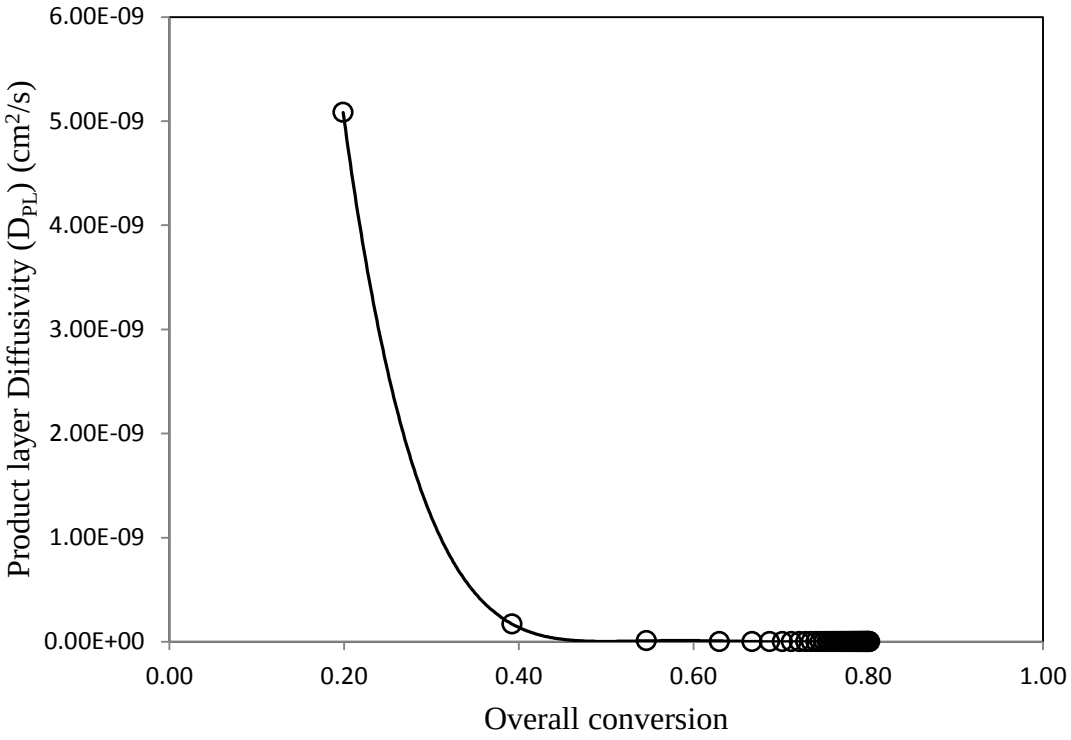

Fig. 3.8 Product layer diffusivity profile during the carbonation reaction at 650°C and 1 atm

3.7.4 Effect of particle porosity on the carbonation reaction:

Sorbent particle porosity plays an important rate in the gas-solid reaction. Sorbents with high porosity allows the reactant gas to achieve active sites, leading to a higher rate of reaction and overall conversion in a specific residence time, compared to a sorbent with low porosity. Fig. 3.9 presents the CGS modeling results of the effect of sorbent porosity on the carbonation reaction. As expected, a sorbent with a porosity of 0.2 generates a higher rate of reaction and higher overall conversion (0.68), which is 63% higher than the sorbent with a porosity of 0.1.

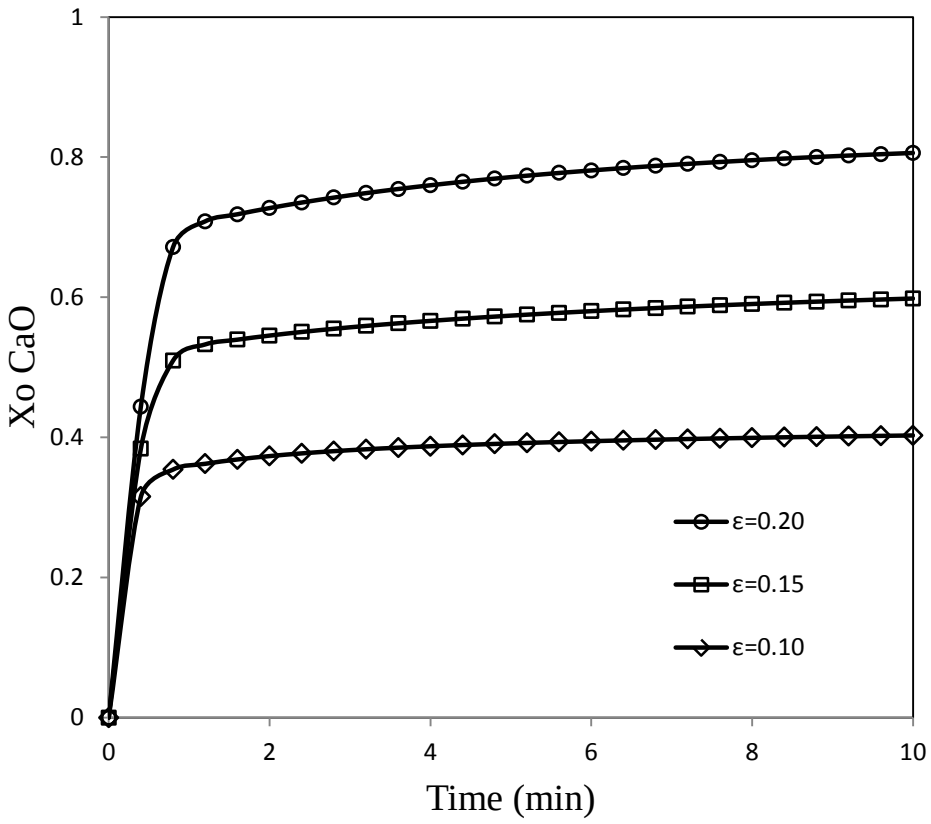

Fig. 3.9 Effect of particle porosity on the carbonation reaction at 650°C and 1 atm

3.7.5 Effect of particle size on the carbonation reaction:

Fig. 3.10 presents the CGS modeling results of the effect of the sorbent particle size in the range of 400-800 μm on the carbonation reaction. The particle size affects the carbonation reaction through the intra-mass transfer of CO_2 within the sorbent. As seen in Fig. 3.10, decreasing the diameter of the sorbent particle increases the initial reaction rate and the overall CaO conversion due to decreased intra-mass transfer resistance. Bhatia and Perlmutter [31] and our previous study [26]; found no significant effect of the particle size (450-1000 μm) on the

carbonation reaction. This phenomenon may have been due to a uniform reaction through the solid sorbent in the tested conditions which were not considered in the modeling work.

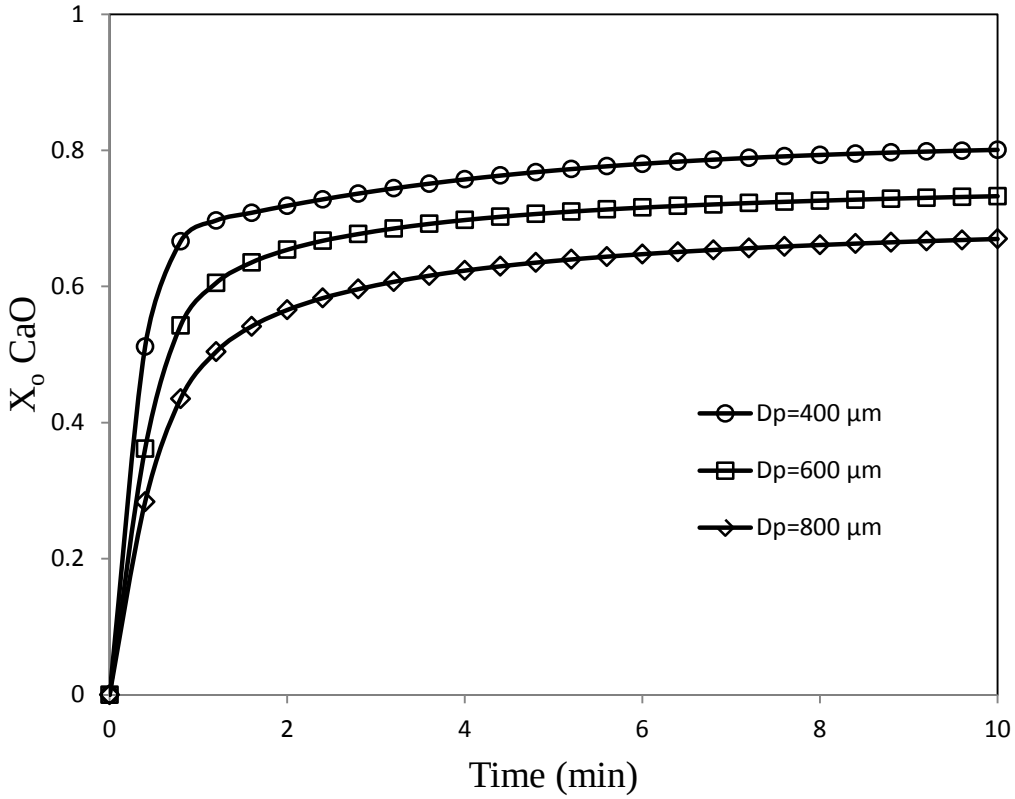

Fig. 3.10 Effect of particle size on the carbonation reaction at 650°C.

3.8 Conclusion

The grain and the CGS models were used to describe the carbonation reaction with Cadomin limestone. The mathematical modeling was solved semi-analytically to obtain the overall CaO conversion over time. According to the modeling results, the CGS model coupled with the variable product layer diffusivity as a function of the overall CaO conversion showed better agreement with the experimental data than the results obtained by the grain model.

The effects of different parameters, such as temperature, sorbent particle size, and sorbent particle porosity on the carbonation reaction were also investigated using the CGS modeling. As expected, the modeling results show an improvement in the carbonation reaction rate by increasing the temperature and particle porosity and decreasing the sorbent particle size. The CO_2 concentration sorbent particle porosity and product layer diffusivity profiles inside the sorbent particle during the carbonation reaction time were predicted. The comparison between the modeling and experimental results show that the CGS model was able to predict the behavior of the carbonation reaction more accurately that the grain model. The modeling results confirmed that the carbonation reaction consists of two stages; the kinetic controlled stage at the beginning followed by the diffusion control stage.

3.9 Appendix A

The effective diffusivity, D_e, for CO_2 diffusion within the porous CaO particle is estimated as a function of the particle porosity:

$$D_e = D_g \varepsilon^2 \tag{3A.1}$$

The gas diffusivity through the particle pores as a stagnant medium to reach the reaction interface of the grains within the particle is considered as a combination of the molecular diffusivity and Knudsen diffusivity as follows:

$$D_g = \left[\frac{1}{D_{CO_2}} + \frac{1}{D_K}\right]^{-1} \tag{3A.2}$$

The Knudsen diffusivity, D_K, which represents the collision of the gas molecules with the pore wall is calculated by:

$$D_K = \frac{4}{3}\left(\frac{8R_gT}{\pi MW_{CO_2}}\right)^{\frac{1}{2}} K_0 \tag{3A.3}$$

where the proportionality factor is:

$$K_0 = \left(\frac{128}{9} n_d r_g'^2 (1 + \frac{\pi}{8})\right)^{-1} \quad \text{(3A.4)}$$

And the number of solid grains per unit volume of porous particle, n_d, is calculated by:

$$n_d = \frac{3(1-\varepsilon)}{4\pi r_g'^3} \quad \text{(3A.5)}$$

The CO_2 molecular diffusivity, D_{CO_2}, is calculated using the equation developed by Fuller et al. [32]:

$$D_{CO_2} = \frac{10^{-3} T^{1.75} \left(\sum_{i=1}^{k} \frac{1}{MW_i}\right)^{0.5}}{P \sum_{i=1}^{k} \left((v_i)^{\frac{1}{3}}\right)^2} \quad \text{(3A.6)}$$

3.10 References

[1] Abanades, J. C., Anthony, E. J., Alvarez, D., Lu, D., Salvador, C., Capture of CO_2 from combustion gases in a fluidized bed of CaO. AIChE J. 50 (2004) 1614–1622.

[2] An, H., Song, T., Shen, L., Qin, C., Yin, J., Feng, B., Coal gasification with in situ CO2 capture by the synthetic CaO sorbent in a 1 kWth dual fluidised-bed reactor. Int. J. Hydrogen Energy 37 (2012) 14195–14204.

[3] Lin, S. Y., Suzuki, Y, Atano, H. H., Harada, M., Hydrogen production from hydrocarbon by integration of water-carbon reaction and carbon dioxide removal (HyPr-RING Method). Energy Fuels 15 (2001) 339-343.

[4] Lin, S. Y., Harada, M., Suzuki, Y., Hatano, H., Developing an innovative method, HyPr-RING to produce hydrogen from hydrocarbons. Energy Conv. Manag. 43 (2002) 1283–1290.

[5] Lin, S. Y., Process analysis for hydrogen production by reaction integrated novel gasification (HyPr-RING). Energy Conv. Manag. 46 (2005) 869-880.

[6] Sedghkerdar, M. H., Mostafavi, E., Mahinpey, N., Sorbent Enhanced Hydrogen Production from Steam Gasification of Coal Integrated with CO_2 Capture. Int. J. Hydrogen Energy 39 (2014) 17001-17008.

[7] Balasubramanian, B., Ortiz, A. L., Kaytakoglu, S., Harrison, D. P., Hydrogen from methane in a single-step process. Chem. Eng. Sci. 54 (1999) 3543–3552.

[8] Ortiz, A. L., Harrison, D. P., Hydrogen production using sorption-enhanced reaction. Ind. Eng. Chem. Res. 40 (2001) 5102–5109.

[9] Johnsen, K., Ryu, H. T., Grace, J. R., Lim, C. J., Sorption-enhanced steam reforming of methanes in a fluidized bed reactor with dolomite as CO_2-acceptor. Chem. Eng, Sci. 61 (2006) 1195–1202.

[10] Levenspiel, O., Chemical reaction engineering. Third ed. Wiley, New York (1972).

[11] Szekely, J., Evans, J. W., Sohn, H. Y., Gas-solid reactions. Academic Press, New York (1976).

[12] Ishida, M., Wen, C.Y., Comparison of zone-reaction model and unreacted-core shrinking model in solid–gas reactions—I Isothermal analysis. Chem. Eng. Sci. 26 (1971) 1031–1041.

[13] Ishida, M.,Wen, C. Y., Shirai, T., Comparison of zone-reaction model and unreacted-core shrinking model in solid–gas reactions—II Nonisothermal analysis. Chem. Eng. Sci. 26 (1971) 1043–1048.

[14] Nikulshina, V., Galvez, M. E., Steinfeld, A., Kinetic analysis of the carbonation reactions for the capture of CO_2 from air via the $Ca(OH)_2$-$CaCO_3$-CaO solar thermochemical cycle. Chem. Eng. J. 129 (2007) 75-83.

[15] Gibson, J. B., Harrison, D. P., The reaction between hydrogen sulfide and spherical pellets of zinc oxide. Ind. Eng. Chem. Pro. Des. 19 (1980) 231-237.

[16] Sha'ban Nashtaee, P., Khoshandam, B., Noncatalytic Gas-Solid Reactions in Packed-Bed Reactors: A Comparison Between Numerical and Approximate Solution Techniques, Chem. Eng. Comm. 201 (2014**)** 120-152.

[17] Georgakis, C., Chang, C.W., Szekely, J., A changing grain size model for gas-solid reactions. Chem. Eng. Sci. 34 (1979) 1072-1075.

[18] Hajaligol, M. R., Longwell, J. P., Sarofim, A. F., Analysis and modeling of direct sulfating of $CaCO_3$. Ind. Eng. Chem. Res. 27 (1988) 2203-2210.

[19] Shih, S. M., Hung, J. T., Wang, T. Y., Lin, R. B., Kinetic of the reaction of sulfur dioxide with calcium oxide powder. J. Chin. Ins.Chem. Eng. 35 (2004) 447-454.

[20] Davidson, M. L., Harrison, D. P., Evaluation of the changing grain size model. Chem. Eng. Comm. 25 (1984) 213-228.

[21] Garcia-Labiano, F., Diego, L. F., Adanez, J., Abed, A., Gayan, P., Temperature variations in the oxygen carrier particles during their reduction and oxidation in a chemical-looping combustion system. Chem. Eng. Sci. 60 (2005) 851-862.

[22] Hassanzadeh, A., Abbasian, J., Regenerable MgO-based sorbents for high temperature CO_2 removal from syngas: 1. Sorbent development, evaluation, and reaction modeling. Fuel 89 (2010)1287-1297.

[23] Yu, Y. S., Liu, W. Q., An, H., Yang, F. S., Wang, G. X., Feng, B., Zhang, Z. X., Rudolph, V., Modeling of the carbonation behavior of calcium based sorbent for CO_2 capture. Int. J. Greenh. Gas Control 10 (2012) 510-519.

[24] Stendardo, S., Foscolo, P. U., Carbon dioxide capture with dolomite: a model for gas-solid reaction within the grains of a particulate sorbent. Chem. Eng. Sci. 64 (2009) 2343-2352.

[25] Krishnan, S. V., Sotirchos, V., A variable diffusivity shrinking-core model and its application to the direct sulfation of limestone. Canad. J. Chem. Eng. 71 (1993) 734-745.

[26] Sedghkerdar, M. H., Mahinpey, N., Sun, Z., Kaliaguine, S. Novel synthetic sol-gel CaO based pellets using porous mesostructured silica in cyclic CO_2 capture processes. Fuel 127 (2014) 101-108.

[27] Szekely, J., Evan, J.W., Studies in gas-solid reactions: part I. A structural model for the reaction of porous oxides with a reducing gas. Metall. Trans. 2 (1971) 1691-1698.

[28] Sedghkerdar, M. H., Mostafavi, E., Mahinpey, N., Investigation of the kinetics of carbonation reaction with CaO-based sorbents using experiments and Aspen Plus simulation,

Chem. Eng. Comm. In press, available online July 1, (2014). DOI: 0.1080/00986445.2013.871709

[29] Lagarias, J. C., Reeds, J. A., Wright M. H., and Wright, P. E., Convergence properties of the Nelder−Mead simplex method in low dimensions. SIAM J. Optim. 9 (1998) 112−147.

[30] Kreyszig, E., Advanced engineering mathematics. John Wiley and Sons: New York (2011).

[31] Bhatia, S. K., Perlmutter, D. D. Effect of the product layer on kinetics of the CO_2—lime reaction, AIChE J. 29 (1983) 79–86.

[32] Fuller, E. N., Ensley, K., Giddings, J. C., Moreno, A., Calcium carbonate thermal decomposition in white-body wall tile during firing. 1. Kinetic study. J. Eur. Ceram. Soc. 30 (2010)1989-2001.

Chapter Four: **The effect of sawdust on the calcination and the intrinsic rate of the carbonation reaction using a thermogravimetric analyzer (TGA)**

Fuel Proc. Technology 106 (2013) 533-538

4.1 Presentation of article

The sintering of calcium-based sorbents as CO_2 carriers during high temperature calcination step causes much of the loss in the sorbent reactivity which is a significant issue in the calcium-looing cycle process. Sintering decreases both the porosity and surface area of the sorbent. The paper presented in this chapter focuses on the effects of sawdust as a biomass during high temperature calcination on the calcium-based sorbent and consequently, on the carbonation kinetics. The results of the above study indicated the positive effect of the presence of sawdust during calcination by enhancement of the CaO surface area, which led to a significant increase in the initial rate of the carbonation reaction.

The majority of this work was performed by Mohammad H. Sedghkerdar; Dr. Naoko Ellis assisted with the interpretation of some results; and, Dr. Nader Mahinpey supervised the project.

The effect of sawdust on the calcination and the intrinsic rate of the carbonation reaction using a thermogravimetric analyzer (TGA)

This article has been published in Fuel Proc. Technology journal, 106 (2013) 533-538.

Mohammad Hashem Sedghkerdar[a] *, Nader Mahinpey* [*], *Naoko Ellis* [b]

[a]Department of Chemical and Petroleum Engineering, Schulich School of Engineering,The University of Calgary, Calgary, Canada, AB T2N 1N4

[b]Department of Chemical and Biological Engineering, University of British Columbia, 2216 Main Mall, Vancouver, BC, Canada V6T 1Z4

4.2 Abstract

The effect of sawdust on the rate of limestone carbonation/calcination reactions was studied in a thermogravimetric analyzer applying a grain model for calcium-based sorbent, namely Havelock limestone (0.50-1.41 mm). Two samples were employed for calcination under N_2 at 850^{o}C: one containing limestone and the other a mixture containing limestone and sawdust. The resulting limestone samples were observed under a scanning electron microscope (SEM), while the quantitative influence of calcination conditions was examined by BET surface areas. The presence of sawdust during calcination caused a significant increase in the initial rate of carbonation, which has been attributed to the enhancement of CaO surface area. The presence of H_2 which is emitted from sawdust pyrolysis was assumed to be responsible for reduction of limestone sintering.

4.3 Introduction

The anthropogenic increase of CO_2 concentration in the atmosphere has been identified as a major contributor to global warming [1-2]. The concentration of carbon_dioxide (CO_2) in Earth's_atmosphere is approximately 390 ppm (parts per million) by volume as of 2010, rising steadily by 1.9 ppm/yr from 2000–2009, in comparison to 0.9 ppm/yr 40 years earlier [3].

In order to prevent further increases in CO_2 levels, there are several CO_2 capture processes involving absorption, adsorption, and membrane separation currently being tested [4-5]. It is assumed that commercial fossil fuel fired power-plants will use post combustion CO_2 capture based on chemical absorption with amine solutions [6]. However, the main disadvantages of this approach are the high operating costs including high steam requirement of solvent regeneration [2]. Therefore, new energy efficient and cost effective approaches are being urgently explored. Among them, calcium-based materials have attracted significant attention as sorbents for capturing CO_2 due to their natural abundance, relatively low cost and regeneration potential [7-9]. Possible applications of calcium-based sorbents for CO_2 adsorption include conventional pulverized fuel fired boiler fluidized bed boilers, steam reformers, and gasifiers [6, 9-12].

To date, extensive research has been devoted on the effect of various gases on the reaction kinetics of calcination and carbonation of limestone. Symond et al. [13] showed that the presence of syngas increases the initial rate of carbonation of limestone by increasing the local CO_2 concentration due to water-gas shift reaction. Wang and Thompson [14] observed that steam accelerates the rate of calcite decomposition by decreasing the strength of the bond between CaO and CO_2. Manovic et al. [15] concluded that calcination under pure CO_2 stream causes significant loss of sorbent activity. However, no work is reported on the influence of biomass

during calcination and on the carbonation kinetics. Today, thermochemical processes for biomass such as pyrolysis and gasification are becoming more attractive for the use of biomass as a source of energy. Thus, this paper focuses on the effect of sawdust as biomass on the calcination and carbonation kinetics of CaO-CO_2 reaction using a grain model [16].

4.4 Experimental details

4.4.1 Thermogravimetric analyzer (TGA)

The Perkin Elmer TGA 7 Thermogravimetric Analyzer, TGA, (sensitivity 0.1 μg) with a platinum basket as sample holder and a sensitive microbalance which capable of detecting weight changes as small as 0.1 μg (11 mm diameter, 4 mm height) operated at atmospheric pressure was used in this study. A schematic diagram of the apparatus used for the TGA studies is shown in Fig. 4.1.

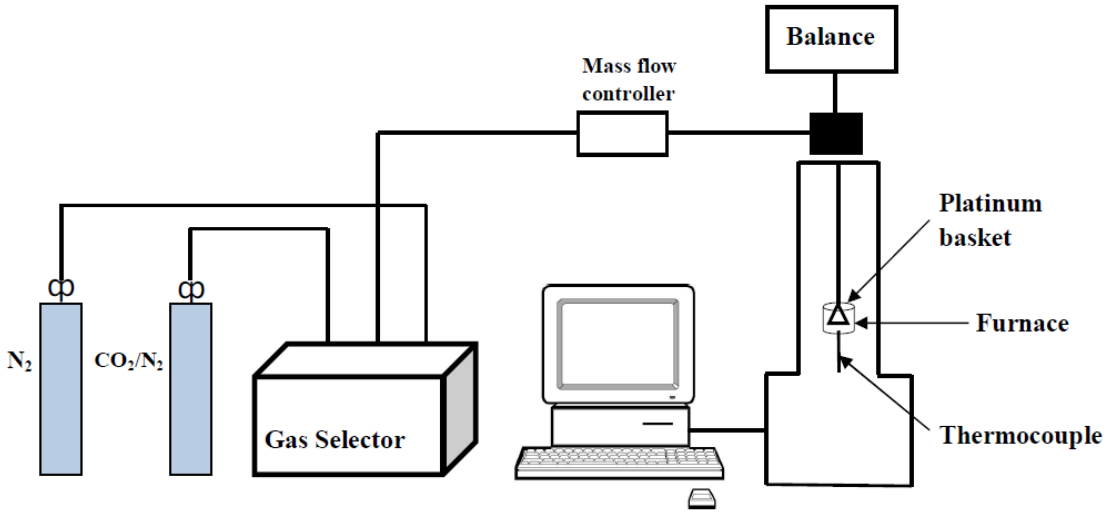

Fig. 4.1 Schematic diagram of a laboratory TGA set-up.

4.4.2 Materials

The Havelock limestone from CANMET energy technology centre in Ottawa, in the size range of 0.50-1.41 mm was used to capture CO_2. The sawdust samples were employed in this work was obtained from a waste wood recycling company in Calgary. Sawdust of 100-230 μm in size was added to the limestone in order to investigate its influence on calcination and carbonation reactions. Chemical analysis of the sawdust and the sorbent using CHNS and Energy Dispersive X-ray (EDX) analyzers, are provided in Tables 4.1 and 4.2, respectively. The ash content of sawdust is in the range of 1-10% depending on the particle size of biomass [17].

Table 4.1. Chemical analysis (in wt.%) of Havelock limestone.

Sorbent	SiO_2	Al_2O_3	Fe_2O_3	MgO	CaO	Na_2O	K_2O	LOI
Havelock	2.55	1.34	0.71	1.28	49.31	1.09	0.44	43.28

Table 4.2 Chemical analysis (in wt.%) of sawdust.

Biomass	carbon	hydrogen	nitrogen	sulfur	Oxygen[a]
sawdust	46.1	6.13	2.31	1.47	43.99

[a] Oxygen percentage obtained by difference.

4.4.3 Experiment

In this work, two samples: one containing 30 mg Havelock limestone, and the other a mixture containing 30 mg Havelock limestone and 10 mg sawdust (3:1 w/w) have been subjected to the calcination condition of heating up to 850^{o}C at 20^{o}C/min in pure N_2 flow of 30 ml/min followed by a 20 min hold at 850^{o}C for calcination in a TGA. After completion of calcination of the second mixture sample, the sawdust pyrolysis product was separated from the calcined

limestone, owing to the difference in density between char and limestone. Degassing procedure using BET was applied to remove all the char from the sorbent. During this procedure the sample was put in the sample tube of BET and then connected to nitrogen under vacuum condition less than 0.1 mmHg at temperature 120^{o}C for 2 hours.

EDX analysis has been performed to detect the calcium (Ca) content of char produced from sawdust pyrolysis at 850^{o}C under N_2 flow which is presented in Table 4.3. The result shows 11.63% Ca present in the char. Although the Calcium content of the char is not high and negligible and it was tried to remove all the char from the sorbent surface after calcination, however, to find the separation efficiency of char from sorbent, EDX analysis has been performed for calcined sorbent with and without sorbent after separation of char from the sorbent which is presented in Table 4.4.

Table 4.3 Elemental analysis (wt.%) of char produced from sawdust pyrolysis

Samples	C	O	Na	Al	Si	Ca	Fe	K
char	69.13	3.25	0.79	1.32	2.28	11.63	1.82	9.79

Table 4.4 Chemical analysis (wt.%) of calcined Haveklock limestone with and without sawdust.

Calcinations Samples[a]	SiO_2	Al_2O_3	Fe_2O_3	CaO	Na_2O	K_2O
HV + sawdust	1.43	0.72	0.52	96.14	0.61	0.93
HV	2.01	0.70	1.20	94.80	0.36	0.88

[a] HV- Havelock limestone

Following calcination, the TGA was set to a pre-determined carbonation temperature (500, 550, 600, and 650^{o}C) under N_2 flow of 30 ml/min. The carbonation reaction was then

initiated by switching the gas flow from N_2 to a gas stream containing 50% CO_2 balance N_2 at the total flow rate 100 ml/min. The weight gain during the carbonation reaction was used to provide adequate kinetic data required to determine the activation energy. A grain model with kinetic control was used to study the intrinsic carbonation reaction kinetics of carbonation reaction.

4.5 Result and discussion:

4.5.1 Carbonation reaction kinetics-grain model

The gas-solid reaction between CO_2 and CaO takes places in three consecutive steps: first, diffusion of gaseous reactant through a film surrounding the particle to the surface of solid; second, the penetration and diffusion of gas through the product layer; and third, reaction of gas with solid at the reaction surface [16]. At the beginning of the process, the chemical reaction plays a significant role. However, by forming $CaCO_3$ as a product, the rate of reaction decreases due to product layer resistance in accessing the CaO by CO_2.

A grain model assumes that solid particles consist of spherical grains that have a sharp surface to react with reactant gas. As for most calcined limestones and dolomite, the grains are almost spherical, so using grain model with kinetic control for determining the intrinsic surface chemical rate constant and activation energy is appropriate [18]. The grain model under kinetically controlled regime is [16]:

$$\frac{dX}{dt(1-X)^{2/3}} = 3r \tag{4.1}$$

where r is the reaction rate and X is CaO conversion.

After integrating Eq. (4.1),

$$[1-(1-X)^{\frac{1}{3}}] = r \times t \tag{4.2}$$

According to Eq. (4.2), by plotting $[1-(1-X)^{\frac{1}{3}}]$ versus $[t]$, a straight line of slope r should be obtained.

From Fig. 4.2, a short induction period followed by a mass breakthrough led to a nearly linear stage which identifies the kinetically controlled region with the slope representing the intrinsic surface reaction rate r. Following the kinetically controlled region, the rate of the reaction slows down, gradually, which shows that the reaction is controlled by both kinetic and product layer diffusion. As carbonation reaction proceeds further, diffusion through the product layer becomes a significant resistance which causes the rate of the reaction to diminish.

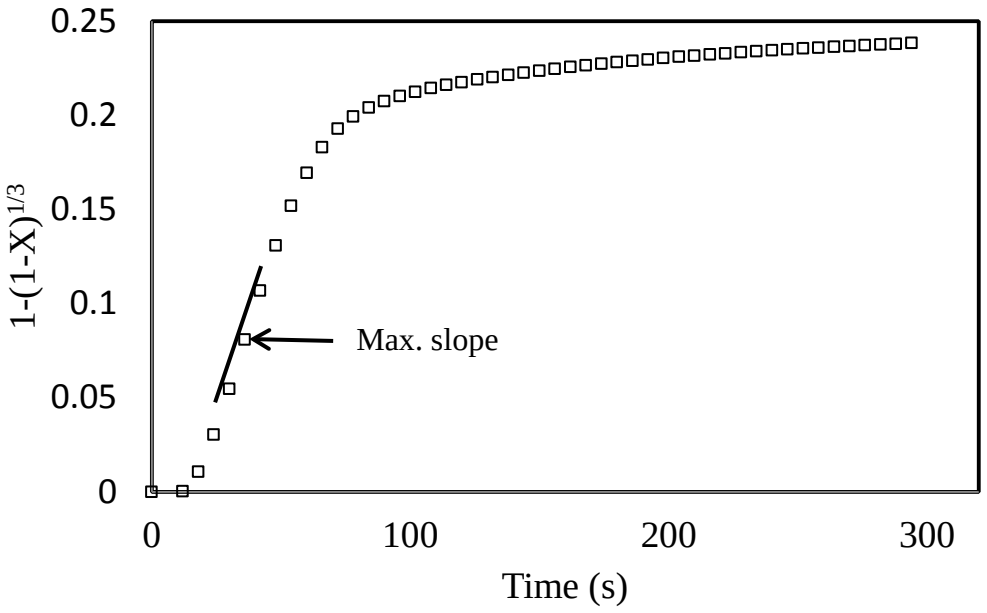

Fig. 4.2 Slope extraction using grain model during initial steps of carbonation for 0.50-1.41 mm Havelock limestone particles at 600^{o}C with 50% CO_2 and 50% N_2.

The induction period with lower slope should belong to the kinetically controlled regime. Thus, the slope of r obtained from the maximum slope in the kinetically controlled region could be extrapolated to represent the true rate at t=0 and X=0,

$$r_0 = r \tag{4.3}$$

Usually, when the gas solid reaction is controlled kinetically, the reaction rate is expressed by a specific rate R,

$$R = \frac{dX}{dt(1-X)} \tag{4.4}$$

In the kinetically control region, the specific rate can be also expressed in power law form of the difference between partial pressure of CO_2 and the equilibrium pressure of CO_2 at the specific temperature,

$$R = \frac{dX}{dt(1-X)} = 56k_s(P_{CO_2} - P_{CO_{2.}eq})^n S \tag{4.5}$$

where 56 is the molar weight of CaO, k_s is the intrinsic rate constant, *S* is the CaO surface area, and *n* is the order of the reaction.

By combining Eqs. (4.2) and (4.5) in terms of specific reaction rate,

$$\frac{dX}{dt(1-X)} = 3r(1-X)^{-1/3} = 56k_s(P_{CO_2} - P_{CO_{2.}eq})^n S \tag{4.6}$$

At *t=0*, *X=0* and the surface area $S=S_0$, Eq. (4.6) becomes,

$$\frac{dX}{dt}|t = 0 = 3r_0 = 56k_s(P_{CO_2} - P_{CO_{2.}eq})^n S_0 \tag{4.7}$$

The initial sorbent surface area (S_0) was measured using BET (Table 4.6). Sun et al. [18] showed that the order of carbonation reaction, *n*, is zero when the CO_2 partial pressure is in the range of 0-10 kPa; while it is one when the partial pressure of CO_2 is higher than 10 kPa. This result was confirmed using the results obtained by Bhatia and Perlmutter [19]. Therefore, for 50% CO_2 concentration at atmospheric pressure, the order of reaction was set to zero, leading to,

$$r_0 = \frac{56k_sS_0}{3} \tag{4.8}$$

Thus, using the Arrhenius equation ($k_s = k_0 \exp(-\frac{E}{R_g T})$), n=0 and taking a logarithm of Eq. (4.8),

$$ln r_0 = ln \frac{56 k_0 S_0}{3} - \frac{E}{R_g T} \quad (4.9)$$

The pre-exponential factor, k_0, and activation energy, E, were obtained using linear fitting the Arrhenius equation with experimental data.

[a] HV- Havelock limestone

4.5.2 Effect of sawdust during calcination

Table 4.5 indicates the intrinsic rate of CaO-CO_2 reaction at 600^{o}C for two different samples in calcination. A significant increase in the rate of carbonation reaction is noted when the Havelock limestone is calcined in the presence of sawdust. Fig. 4.3 shows a plot of the grain model for Havelock limestone calcined with and without sawdust and carbonated with 50% CO_2. It is observed that diffusion controlled region of carbonation reaction for calcined Havelock limestone with sawdust occurs at around 200s earlier due to the higher reaction rate.

Table 4.5 Intrinsic rate constants for 0.50-1.41 mm Havelock limestone particles carbonated at 600℃ and 1 atm for two different calcination conditions.

Calcinations condition[a]	r_0 (1/s)
HV sawdust- cal	0.0037
HV-cal	0.0013

[a] HV- Havelock limestone, cal- calcination

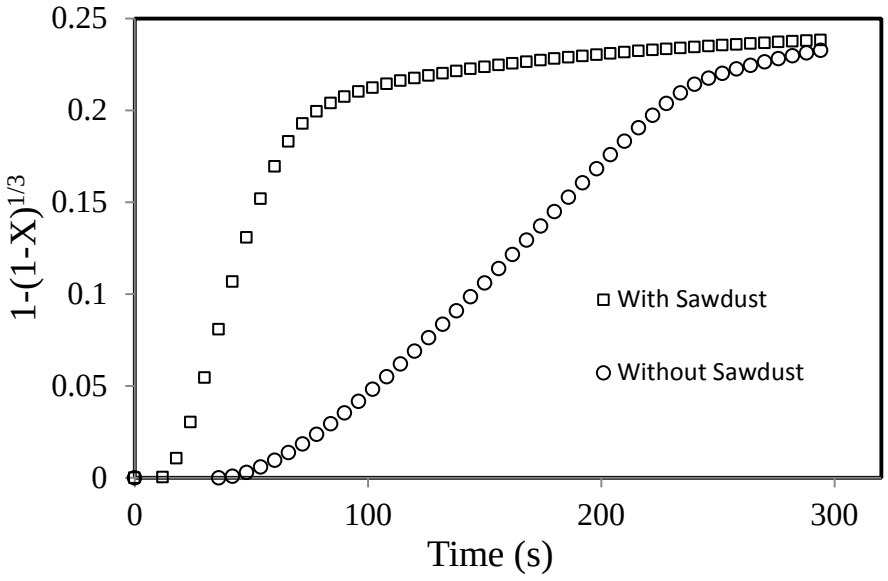

Fig. 4.3 Grain model plot for 0.50-1.41 mm Havelock limestone particle calcined with and without sawdust at 850^{o}C with N_2 and carbonated at 600^{o}C under 50% CO_2.

In this work, since the partial pressure of CO_2 is higher than 10kPa, the order of the reaction is assumed to be zero. Therefore, the difference in the rate of carbonation reaction must be related primarily to the surface area of the calcined limestones.

As shown in Fig. 4.4, sawdust alone under N_2 begins to decompose from temperature around 300^{o}C. According to Sun et al. [20], CO and H_2 are the two main gases that are emitted from sawdust pyrolysis under N_2 flow at temperatures around 700-1000^{o}C. Due to strong bond between C and O in CO, the lesser effect is expected from CO than H_2 on the surface morphology and subsequent increase in intrinsic rate of carbonation reaction. Scanning electron microscope (SEM) images and BET/BJH analysis were used to investigate the surface morphology, surface area, and pore size of limestone samples obtained from calcination with and without sawdust.

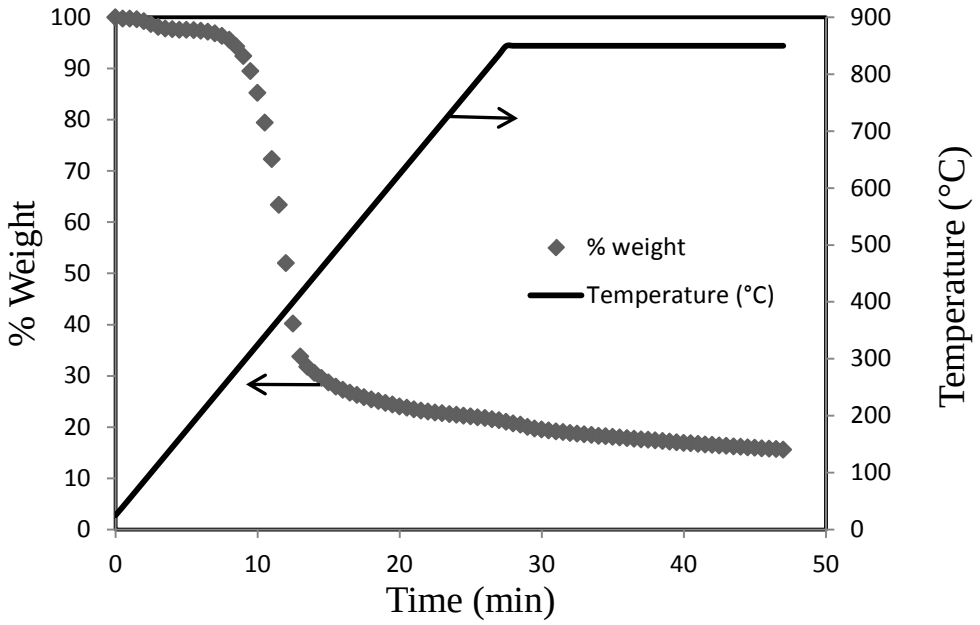

Fig. 4.4 Weight loss of the sawdust by increasing temperature.

SEM images in Fig. 4.5 are shown at two different magnifications (100 and 10μm scales) for calcined Havelock limestone with and without sawdust. Although Fig. 4.5(a) and (b) depict a similar surface texture of calcined Havelock with and without sawdust, Fig. 4.5(c) and (d) at higher magnification show the surface morphology of the Havelock particles calcined in the presence of sawdust is more developed with increase in small sub-grains. Therefore, the difference between SEM images in Fig. 4.5(c) and 5(d) show the lower level of sintering of Havelock particles calcined with sawdust.

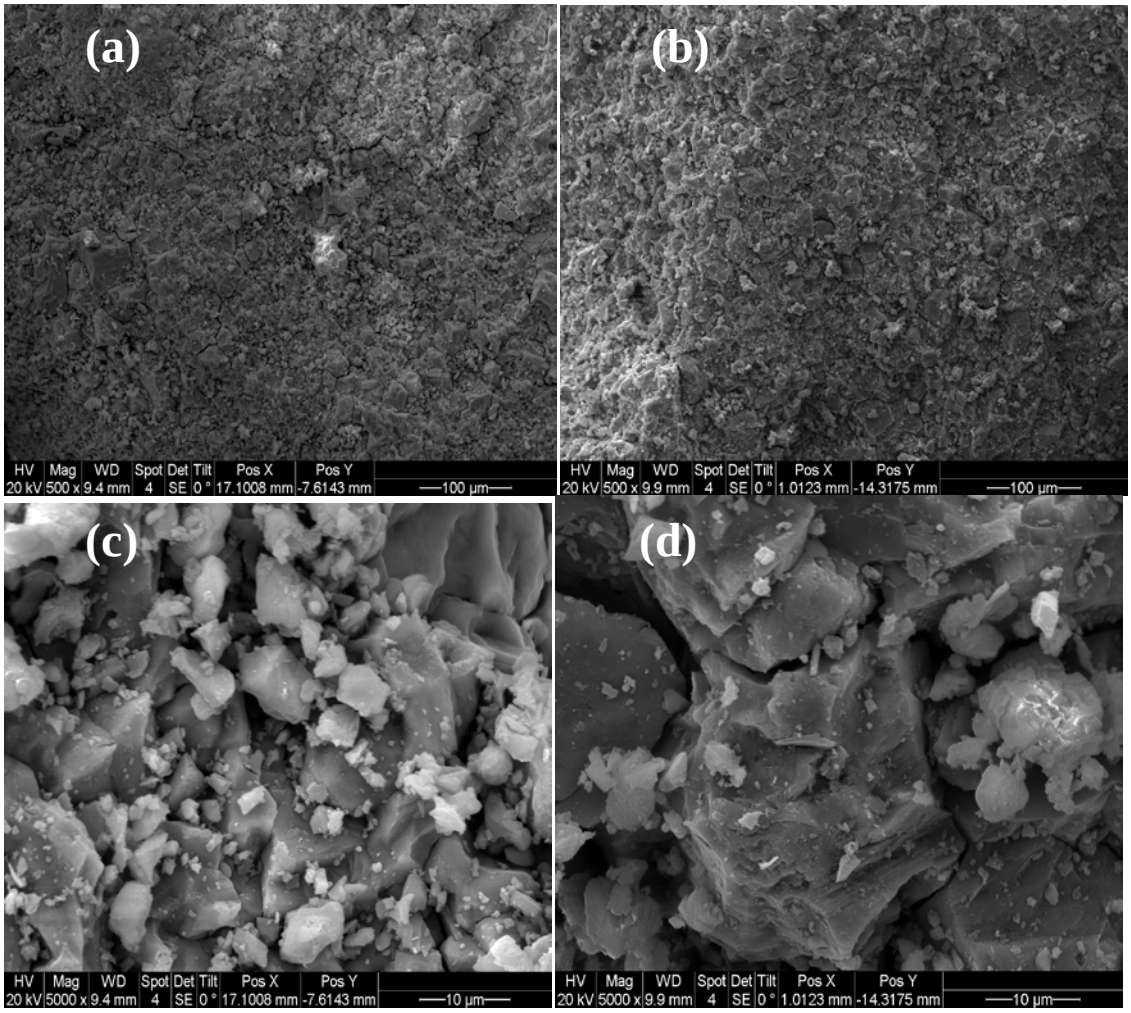

Fig. 4.5 SEM image of Havelock limestone particle calcined at 850^{o}C under N_2 (a) with sawdust (in 100 µm scale), (b) without sawdust (in 100 µm scale), (c) with sawdust (in 10 µm scale), (d) without sawdust (in 10 µm scale).

The samples were further analyzed through BET/BJH analysis, which confirmed the trend of less sintering. According to Table 4.6, the BET surface area for Havelock samples which is calcined in presence of sawdust is greater than calcined Havelock sample alone. In addition, BJH analysis shows that sawdust affects the surface morphology of limestone particles with decreasing the pore diameter and increasing the pore volume. Therefore, calcination with sawdust causes an increasing in surface area on the calcined Havelock limestone, which

improves the carbonation reaction. Furthermore assumption would be the presence of biomass char between the grains of sorbents may contribute to some extent in decreasing the sintering effects.

Table 4.6 Result of nitrogen adsorption/desorption tests.

Sample no.	Designation[a]	BET surface area (m^2/g)	BJH cumulative pore volume (cm^3/g)	BJH desorption average pore diameter (nm)
1	HV+ sawdust- cal	17.28	0.139	19.2
2	HV- cal	15.84	0.129	22.3

[a] HV- Havelock limestone, cal- calcination

Fig. 4.6 shows Arrhenius plot using the fitted parameters intrinsic rate constant, k_0, and the activation energy, E. The resulting parameters correspond to 95% confidence levels are:

For Havelock calcined without sawdust,

$$k_s = 2.22 \times 10^{-4} \exp\left(\frac{-E}{RT}\right) mol/m^2 s$$

$$E = 28.3 \pm 9.1\ kJ/mol \quad (4.10)$$

For Havelock calcined with sawdust

$$k_s = 2.06 \times 10^{-4} \exp\left(\frac{-E}{RT}\right) mol/m^2 s$$

$$E = 21.6 \pm 6.1\ kJ/mol \quad (4.11)$$

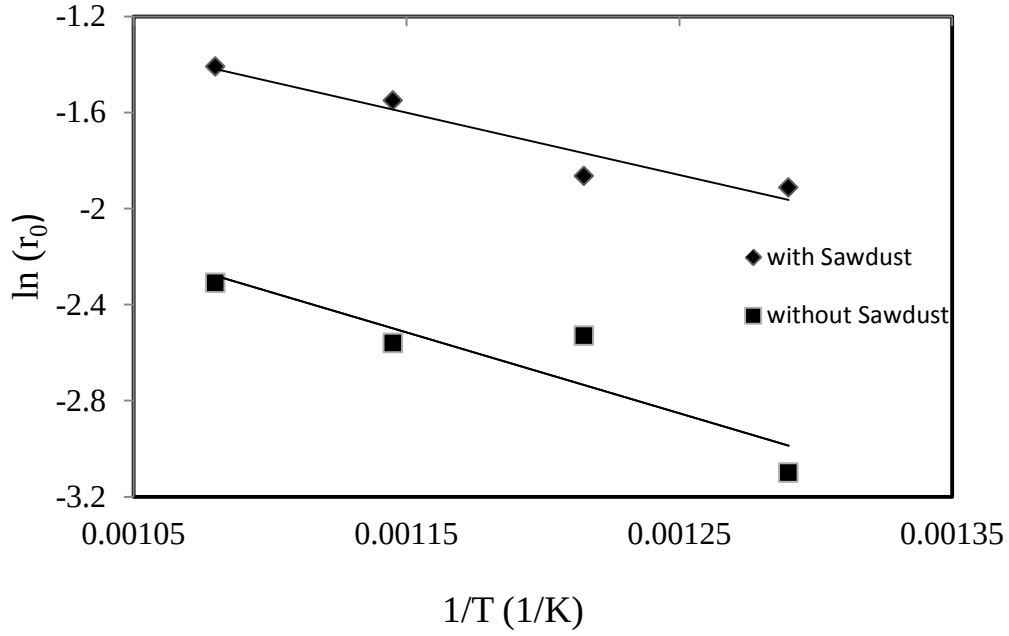

Fig. 4.6 Arrhenius plot for carbonation reaction with 0.50-1.41 mm Havelock limestone particles calcined at 850^{o}C under N_2 with and without sawdust.

The activation energy determined for limestone calcined without sawdust is in good agreement with the value 29±4 kJ/mol obtained by Sun et al. [18] for 38-45 μm Strassburg limestone sample.

4.6 Future work

The work reported here is only the beginning to the effort of using biomass on the clacination and the intrinsic rate of the carbonation reaction. This study confirms that the present of biomass and gases emitted from biomass pyrolysis during calcination could improve the surface morphology of the sorbent which cause an improvement in the reaction rate of the carbonation reaction. To confirm the hypothesis, a few calcination tests will be conducted in the streams of N_2/H_2, N_2/CO, and one set of experiments with $N_2/CO/H_2$ to explore the actual effect of H_2, CO, and mixture of them on the surface morphology of the sorbent.

In this study, atmospheric pressure and temperature range of 500-650^{o}C were considered for kinetic analysis of carbonation reaction. Further study will be carried out in the extended range of temperatures and pressures to understand the behaviour of the carbonation reaction rate in various conditions.

As limestone is a natural product with considerable variations, further experiments will be conducted with limestones other than Havelock to comprehend the effect of biomass on the CO_2 adsorption to confirm on the hypothesis to a variety of sorbents.

Several studies have been showed the negative effect of presence of alkalis materials such as calcium, magnesium, and sodium on volatile yields from coal pyrolysis [21-23]. Therefore, further investigation could be guided to see the effect of alkalis material on biomass pyrolysis and volatile yields.

The current work is, to our knowledge, the first application of the effects of biomass on the calcinations and adsorption of CO_2 on the sorbents. There is obvious room for much further efforts and refinement.

4.7 Conclusion

This study investigated the intrinsic rate of carbonation reaction using grain model for calcined Havelock limestone particles which were calcined with or without sawdust under N_2 environment. The experiments conducted in a thermogravimetric analyzer (TGA) under atmospheric pressure revealed that the presence of sawdust during calcination increased the initial carbonation rate significantly, where the reaction is kinetically controlled. SEM tests and BET analysis showed that the presence of sawdust improves the surface morphology based on smaller pore size and higher surface area. Gases such as H_2 produced from sawdust pyrolysis under N_2 environment were assumed to be responsible for improving the surface morphology of

the Havelock limestone. Activation energies for limestone carbonation reaction calcined with and without biomass were found to be 21.6 kJ/mol and 28.3 kJ/mol, respectively.

4.8 Reference

[1] Herzog, H. J., What future for carbon capture and sequestration?. Environ. Sci. Technol. 35 (2001) 148A-153A.

[2] Rao, A. B., and Rubin, E. S., A technical, economic, and environmental assessment of amine-based CO_2 capture technology for power plant greenhouse gas control. Environ. Sci. Technol. 36 (2002) 4467–4475.

[3] Tans, Pieter, Trends in carbon dioxide. NOAA/ESRL. Retrieved (2009) 12-11.

[4] Reimer, P., Audus H., and Smith, A., Carbon dioxide capture from power stations. IEA greenhouse R&D programme, Cheltenham, UK (2001).

[5] Kikkinides, E. S., Yang, R. T., and Cho, S. H., Concentration and recovery of CO_2 from flue gas by pressure swing adsorption. Ind. Eng. Chem. Res. 32 (1993) 2714–2720.

[6] Abanades, J. C., Anthony, E. J., Alvarez, D., Lu, D., and Salvador, C., Capture of CO_2 from combustion gases in a fluidized bed of CaO. A.I.Ch.E. J. 50 (2004) 1614–1622.

[7] Silaban, A., Harrison, P., High temperature capture of carbon dioxide: characteristics of the reversible reaction between CaO(s) and CO_2(g). Chem. Eng. Comm. 137 (1995) 177–190.

[8] Silaban, A., Narcida, M., and Harrison, D.P., Characteristics of the reversible reaction between CO_2(g) and calcined dolomite. Chem. Eng. Comm. 146 (1996) 149–162.

[9] Shimizu, T., Hirama, T., Hosoda, H., Kitano, K., Inagaki M., and Tejima, K., A twin fluid-bed reactor for removal of CO_2 from combustion processes. Trans IChemE. 77 (part A) (1999) 62–68.

[10] Ortiz, A. L., Harrison, D. P., Hydrogen production using sorption-enhanced reaction. Ind. Eng. Chem. Res. 40 (2001) 5102–5109.

[11] Johnsen, K., Ryu, H. T., Grace, J. R., Lim, C. J., Sorption-enhanced steam reforming of methane in a fluidized bed reactor with dolomite as CO_2-acceptor. Chem. Eng. Sci. 61 (2006) 1195–1202.

[12] Lin, S. Y., Suzuki, Y., Hatano, H., Harada, M., Hydrogen production from hydrocarbon by integration of water–carbon reaction and carbon dioxide removal (HyPr-RING method). Energy Fuels 15 (2001) 339–343.

[13] Symonds, R. T., Lu, D. Y., Macchi, A., Hughes, R. W., Anthony, E. J., CO_2 capture from syngas via cyclic carbonation/calcination for a naturally occurring limestone: Modeling and bench-scale testing. Chem. Eng. Sci. 64 (2009) 3536–3543.

[14] Wang, Y., and Thomson, W. J., The effect of steam and carbon dioxide on calcite decomposition using dynamic x-ray diffraction. Chem. Eng. Sci. 50 (1995) 1373–1382.

[15] Manovic, V., Charland, J. P., Blamey, J., Fennell, P. S., Lu, D. Y., Anthony, E. J., Influence of calcination conditions on carrying capacity of CaO-based sorbent in CO_2 looping cycles. Fuel 88 (2009) 1893-1900.

[16] Szekely, J., Evans J. W., Sohn, H. Y., Gas solid reactions, Academic Press, London (1976).

[17] Aqsha, A., Mahinpey, N., Mani, T., Salak, F., Murugan, P., Study of sawdust pyrolysis and its devolatilisation kinetics. Canad. J. Chem. Eng. 89 (2011) 1451-1457.

[18] Sun, P., Grace, J. R., Lim, C. J., and Anthony, E. J., Determination of intrinsic rate constants of the CaO-CO_2 reaction. Chem. Eng. Sci. 63 (2008) 47-56.

[19] Bhatia, S. K., Perlmutter, D. D., Effect of the product layer on kinetics of the CO_2-lime reaction. AIChE J. 29 (1) (1983) 79–86.

[20] Sun, S., Tian, H., Zhao, Y., Sun, R., Zhou, H., Experimental and numerical study of biomass flash pyrolysis in an entrained flow reactor. Bioresour. Technol. 101 (2010) 3678–3684.

[21] Royce, A. J., Miyawaki, S., Piskorz, J., Scott, D. S., Fouda, S., The influence on inorganic matter on the pyrolysis of Canadian. Fuel Proc. Technology 25 (1990) 201-214.

[22] Sathe, C., Pang, Y., Li, C. Z. Effect of heating rate and ion-exchanging cations on the parolysis yields from a Victorian brown coal. Energy Fuels 13 (1999) 748-755.

[23] Tyler, R. J., Schafer, H. N. S., Flash pyrolysis of coals: influence of cations on the devolatization behavior of brown coals. Fuel 59 (1980) 487-494.

Chapter Five: **Novel synthetic sol-gel CaO based pellets using porous mesostructured silica in cyclic CO_2 capture processes**

Fuel 127 (2014) 101-108

5.1 Presentation of the article

This chapter presents an article that investigated calcium-looping cycles through 31 carbonation–calcination cycles using several calcium-based sorbents. To decrease the negative effects of sorbent sintering in the calcium-looping cycles, a natural calcium-based sorbent was modified using different methods and materials. A novel CO_2 carrier is fabricated as a core/shell sorbent using an external layer of mesostructured silica as a protective shell. In addition, two pelletized Cadomin sorbents were synthesized using different additives, such as calcium aluminate cement (CA-14) and silica-sol (HS-40). The surface morphology and porosity of the sorbents were observed with a scanning electron microscope (SEM) and quantified by BET (Brunauer-Emmett-Teller) / BJH (Barrett-Joyner-Halenda) model.

The results of the study concluded that, the pelletized sorbent using calcium aluminate cement exhibited a slower decay in sorbent activity with increased numbers of cycles due to the presence of the Mayenite phase ($Ca_{12}Al_{14}O_{33}$). Moreover, the core/shell pellets provided the best performance in the retention of CO_2 uptake activity over 31 cycles.

This study was performed as a collaborative work of the University of Calgary, Université Laval, and CanmetEnergy, Natural Resources Canada. The main part of this work, included conducting the experiments and analyzing the results were completed by Mohammad H. Sedghkerdar. Mr. Zhenkun Sun provided the core/shell pellet (CD-CS) from Université Laval and CanmetEnergy supplied the calcium aluminate pellets (CD-CZ-14). Dr. Serge Kaliaguine assisted with results interpretation, and Dr. Nader Mahinpey supervised the whole project.

Novel synthetic sol-gel CaO based pellets using porous mesostructured silica in cyclic CO_2 capture processes

This article has been published in Fuel journal, 127 (2014) 101-108

Mohammad Hashem Sedghkerdar[a], Nader Mahinpey[a], Zhenkun Sun[b], Serge Kaliaguine[b]

[a] Department of Chemical & Petroleum Engineering, University of Calgary, Calgary, Canada T2N 1N4

[b] Department of Chemical Engineering, Université Laval, Ste-Foy, Qué., Canada G1V 0A6

5.2 Abstract

In this study, four CO_2 carriers were examined through 31 carbonation–calcination cycles. The carriers included one natural limestone (Cadomin) and three modified calcium oxide-based sorbents, Cadomin-calcium aluminate cement pellets (CD-CA-14), Cadomin-silica-sol pellets (CD-Si), and Cadomin-mesostructred silica core/ shell pellets (CD-CS). The modified sorbents were not only prepared using two different binders (calcium aluminate cement, CA-14, and silica-sol, HS-40), but the CD-CS sample was provided with a protective porous shell (using a mesoporous silica layer). Natural Cadomin limestone was the base common to the modified sorbents. The surface morphology and porosity of these sorbents before and after different cycles were investigated by scanning electron microscopy (SEM) and nitrogen physisorption (BET/BJH). X-ray diffraction (XRD) was also used to identify the crystal phase composition of the sorbents before and after calcination. The results showed that the presence of the Mayenite phase ($Ca_{12}Al_{14}O_{33}$) in the CD-CA-14 pellets led to slower decay in sorbent activity with increased numbers of cycles. Although the CD-CS pellets showed the best performance in the retention of CO_2 uptake activity over 31 cycles, with an activity loss of only 46%, the pellet shells experienced severe disintegration during the first few cycles.

5.3 Introduction

It is widely accepted that the increasing content of carbon dioxide (CO_2) in the atmosphere contributes to man-made global warming. Fossil fuel power plants represent a major contributor to anthropogenic CO_2 emissions. One possible approach to decrease CO_2 emissions is CO_2 capture and sequestration (CCS) from flue gases produced from the combustion or gasification of fossil fuels [1-2]. In CCS, the capture of CO_2 is the most challenging step and has the highest energy cost. Many efforts have, therefore, been made to improve the CO_2 capture [3]. Regenerable calcium oxide (CaO)-based sorbents have attracted attention as potential inexpensive and efficient sorbents for cyclic CO_2 capture processes [4-5]. Fluidized-bed combustion is certainly a potentially optimal technology for CO_2 looping cycles that use calcium-based solids [4]. This process can be used for post-combustion CO_2 capture in fossil fuel power plants. According to recent studies [6-8], CO_2 looping cycling using CaO-based sorbents showed a lower cost than CO_2 scrubbing by amine solutions. In addition, this process can be applied to other technologies, such as hydrogen production by reaction-integrated novel gasification (HyPr-Ring) and lime-enhanced gasification of solid fuels (LEGS) processes [9-10].

The cyclic CO_2 capture process is based on the reversible carbonation–calcination chemical reaction:

$$CaO\ (s) + CO_2\ (g) \leftrightarrow CaCO_3(s) \qquad (5.1)$$

The advantages of cyclic CO_2 capture using CaO-based sorbent include producing a pure CO_2 stream suitable for sequestration [11], overall energy cost and efficiency and environmental benefits [12-13]. However, considerable challenges remain. The loss of sorbent activity, due to sintering and attrition, with the increasing number of cycles is the most important issue [13-14]. The actual rate and extent of sintering depend on many factors, including the nature of the metal

oxide, the initial crystallite size and size distribution, the presence of additives that control sintering, and the environment. The vital variable is temperature, and operation at low temperatures greatly reduces the sintering rate. The reaction atmosphere also affects sintering. Water vapor and possibly CO_2 may accelerate crystallization and structural changes in the metal oxide. The presence of specific additives is also known to reduce the solid sintering. For example, barium oxide (BaO), cerium oxide (CeO_2), lanthanum oxide (La_2O_3), silica (SiO_2) and zirconium oxide (ZrO_2) improve the stability of alumina and decreases sintering, whereas sodium oxide (Na_2O) increases the sintering [15-19].

Some methods that have been investigated to counteract the negative effects of sorbent sintering include thermal pretreatment of the sorbent [20] and steam hydration [21]. Improving the physical strength of the sorbent using different binders such as alumina is another promising method to improve sorbent reactivity during cyclic CO_2 capture [22-24]. Manovic et al. [25] investigated different binders, such as sodium and calcium bentonites, and concluded that these binders increase sintering due to formation of calcium-silica (spurrite, $Ca_5(SiO_4)_2CO_3$). Liu et al. [26] developed a mesoscopic hollow sphere sorbent containing $CaO/Ca_{12}Al_{14}O_{33}$, using sulfonated polystyrene as a hard template over 30 cycles. The results showed stable adsorption capacity and durability during the cycles. Karami and Mahinpey [27] synthesized a calcium (Ca) based sorbent using the precipitation of solutions containing nitrate NO_3^-, and chloride Cl^- by various alkaline precipitants under certain conditions. This showed an improvement in the sorbent capacity and stability upon cyclic carbonation–calcination reactions.

The main objective of this study was to synthesize new sorbents prepared by various procedures, and to investigate their CO_2 capture activity and cyclic stability through 31 carbonation–calcination cycles. Natural Cadomin limestone was used as the base of the sorbents.

A novel CO_2 carrier was fabricated as a core/shell sorbent using an external layer of mesostructured silica as a protective shell. In addition, two pelletized Cadomin sorbents were synthesized using different additives, such as calcium aluminate cement (CA-14) and silica-sol (HS-40).

5.4 Experimental

5.4.1 Materials

In this study, Cadomin limestone (CD) was used as the base material to prepare the various examined sorbents. The CD sample had a particle size range of 250-750 μm. Its chemical composition is given in Table 5.1. Two samples were also prepared with Cadomin limestone, but mixed with a binder, either CA-14 or HS-40. The fourth sample was a core/shell material obtained by coating Cadomin particles with a shell of porous mesostructured silica.

Table 5.1 Elemental composition (wt.%)

Sorbent	SiO_2	Al_2O_3	Fe_2O_3	MgO	CaO	Na_2O	K_2O	LOI[a]
Cadomin (CD)	1.71	0.88	1.03	1.06	46.99	0.16	0.44	47.73

[a] LOI: Loss Of Ignition

5.4.1.1 Cadomin-calcium aluminate cement pellets

Cadomin-calcium aluminate cement (CD-CA-14) pellets was prepared at CanmetEnergy, Natural Resources Canada in Ottawa. Its particle size range was 500-1410 μm. These pellets were prepared by mixing the limestone and CA-14 (71% aluminum oxide (Al_2O_3) and 28% CaO) as a binder. The limestone was first calcined at 850°C for 120 min. The calcined limestone (lime) and cement were then mixed at a ratio of 9:1 by weight. Water was slowly added to the mixture to obtain a gel. The gel was extruded and then air dried for one day. The pellet preparation

method is given in detail elsewhere [28]. Another set of Cadomin limestone pellets, in the size range of 700-1000 μm, was prepared by the same procedure, but without any binder addition, using just hydrated lime. It was designated as a blank pellet. These were used as the core for the synthesis of core/shell pellets described later.

5.4.1.2 Cadomin-silica-sol pellets

Cadomin-silica-sol (CD-Si) pellets were made by crushing Cadomin limestone, which was sieved to achieve a particle size < 45 μm. The powdered Cadomin limestone to LUDOX HS-40 colloidal silica (40 wt. % suspension in H_2O) ratio was 9:1 by weight. Due to the exothermic nature of the hydration process, water was added slowly to minimize the effect of heat generation. The formed gel was extruded and then air dried for 24 h. The final pellets had diameters of around 1500-2400 μm.

5.4.1.3 Core/shell pellets

The core/shell (CD-CS) pellets used in this work were synthesized at Université Laval in the size range of 720-1200 μm. These core/shell calcium-based pellets with mesoporous silica shells were prepared by a simple wet coating process combined with conventional evaporation-induced self-assembly (EISA) sol–gel process [29] using Pluronic P123 as the mesoporous structure-directing agent and tetraethylorthosilicate (TEOS) as the silica source [30]. In a typical preparation, 1 g of blank pellets was immersed in a homogeneous silicate precursor solution obtained by mixing TEOS (2.08 g), water (H_2O, 0.9 g), 2.0 M hydrochloric acid (HCl, 0.1 g), P123 (1.0 g) and ethanol (15 g) for 1 h. After impregnation and ethanol evaporation for 48 h at room temperature, the composite pellets were heated to 40 °C and left for another 4 h, so that any remnants of ethanol were completely evaporated. Finally, the impregnated pellets were calcined in air at 550°C for 6 h at a heating rate of 1°C/min to remove the P123 template, resulting in the

core/shell pellets with mesoporous silica shells. Fig. 5.1shows the SEM images of the CD-CS pellets before and after silica coating. Before coating, the out surface of the pristine pellet is rough due to the aggregation of CaCO3 crystalline. However, after silica coating, the out surface becomes much more smooth and uniform indicating the successfully coating of the silica shell which exhibits porous feature. Fig. 5.2 presents the cut-edge of the CD-CS pellet. The denser layer should be the mesoporous silica shell which is 4.8 μm in thickness.

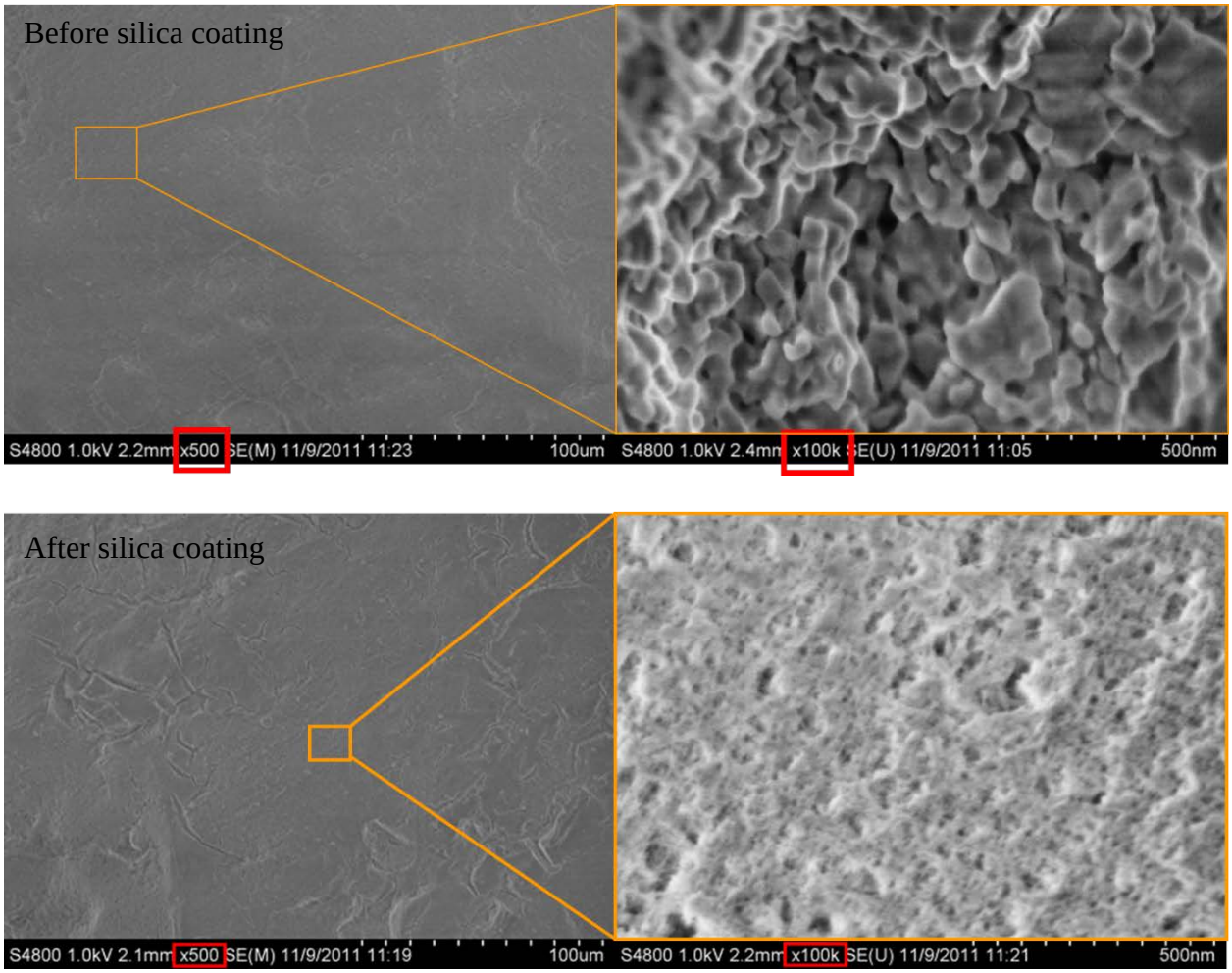

Fig. 5.1 SEM images of CD-CS pellets before and after silica coating.

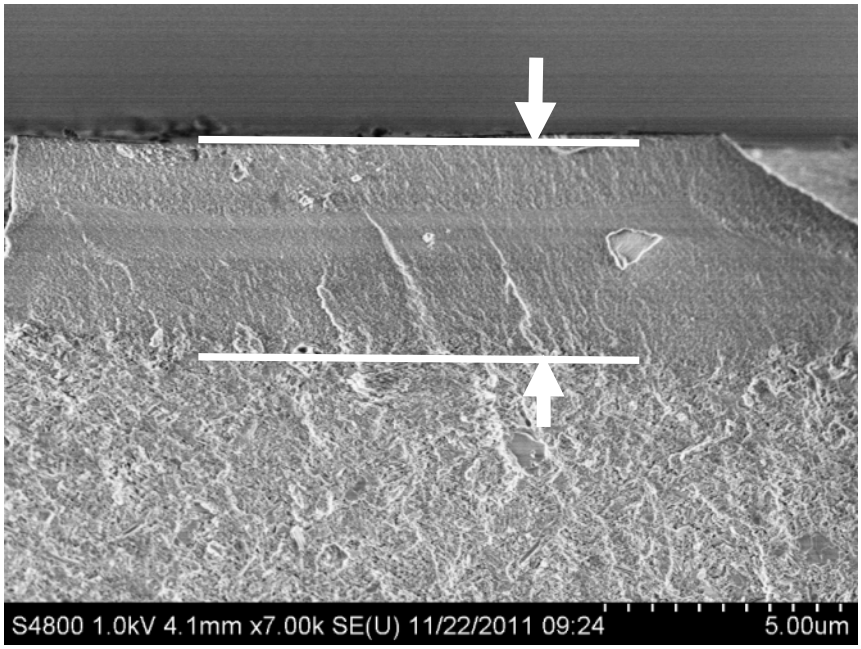

Fig. 5.2 SEM image of the cut-edge of the CD-CS.

5.4.2 Cyclic CO_2 capture

A Perkin-Elmer Pyris-STA6000 thermogravimertric analyzer (TGA), which includes a microbalance with a sensitivity of 0.1 μg, was used for the carbonation–calcination experiments. Pyris software was used to control the temperature and gas flow rate. A Perkin-Elmer thermal analysis gas station (TFGS) with four gas channels allowed for automatic switching of the gas for the carbonation and calcination reactions. About 20 mg of a sample were introduced to the ceramic sample pan of the thermobalance and heated to 850°C at a ramp rate of 40°C/min under a nitrogen (N_2) flow of 50 ml/min, followed by a 10 min hold at 850°C for calcination. After completion, the sample was cooled to 675°C. After the temperature reached 675°C, the gas was switched from pure N_2 to pure CO_2 for a 20 min carbonation period. The CO_2 was then replaced by N_2, and the sample was heated up to 850°C. This procedure was then repeated for 31 carbonation–calcination cycles. According to previous studies [31-32], higher calcination

temperatures and CO_2 partial pressures increase sintering and cause decay in the sorbent activity. Therefore, to decrease the sorbent sintering, the calcination time was set at a short time of 10 min under pure N_2. During the process, the sorbent weight and temperature were monitored using Pyris software.

5.4.3 Characterization of the sorbents

An energy-dispersive X-ray (EDX) analyzer was used for the elemental analysis of the samples. The changes in sorbent morphology over different numbers of cycles were observed by scanning electron microscopy (SEM). The calcined samples were coated with a thin layer of gold-platinum before SEM examination. The EDX analyzer attached to the scanning electron microscope allowed for the determination of the elemental composition at any point of interest on the sorbent surface. The surface area and pore size distribution of the sorbents were quantified by N_2 adsorption/ desorption isotherms (Brunauer-Emmett-Teller, BET, and Barrett-Joyner-Halenda, BJH) using a Micromeritics 2020 volumetric adsorption analyzer. XRD patterns (Siemens D500 diffractometer) were collected over the angular range of 10-50° (2θ) and used to characterize the crystal structure of the sorbent. The Jade 7 XRD MDI library was used to identify the XRD patterns.

5.5 Results and discussion

Fig. 5.3 represents typical TGA results of the Cadomin limestone weight change with temperature through 31 carbonation–calcination cycles. Fig. 5.4 shows the CO_2 uptake capacity and the stability of the four different sorbents over 31 carbonation–calcination cycles under the same conditions. The sorbent CO_2 uptake and conversion were calculated as follows:

$$CO_2 \text{ uptake} = \frac{(m(t)-m(0))}{44} \Big/ \frac{(m(0)\times X_{CaO})}{1000} \quad (5.2)$$

$$\text{Conversion} = \frac{(m(t)-m(0))}{44} \Big/ \frac{(m(0)\times X_{CaO})}{56} \quad (5.3)$$

where 44 and 56 are the CO_2 and CaO molar weights (g/mol), X_{CaO} is the weight percent of the active CaO in the sorbent, and m(0) and m(t) are the sample weights at the beginning and time t of the carbonation reaction, respectively. X_{CaO} is the weight percent of the active CaO in the calcined sorbent and is determined from the elemental analysis of the calcined sorbents using an EDX analyzer. According to the carbonation reaction stoichiometry, the complete conversion of 1 kg of CaO can adsorb 17.85 moles of CO_2. In this study, 20 min was chosen for the carbonation time, in order to represent a reasonable reactor size throughput.

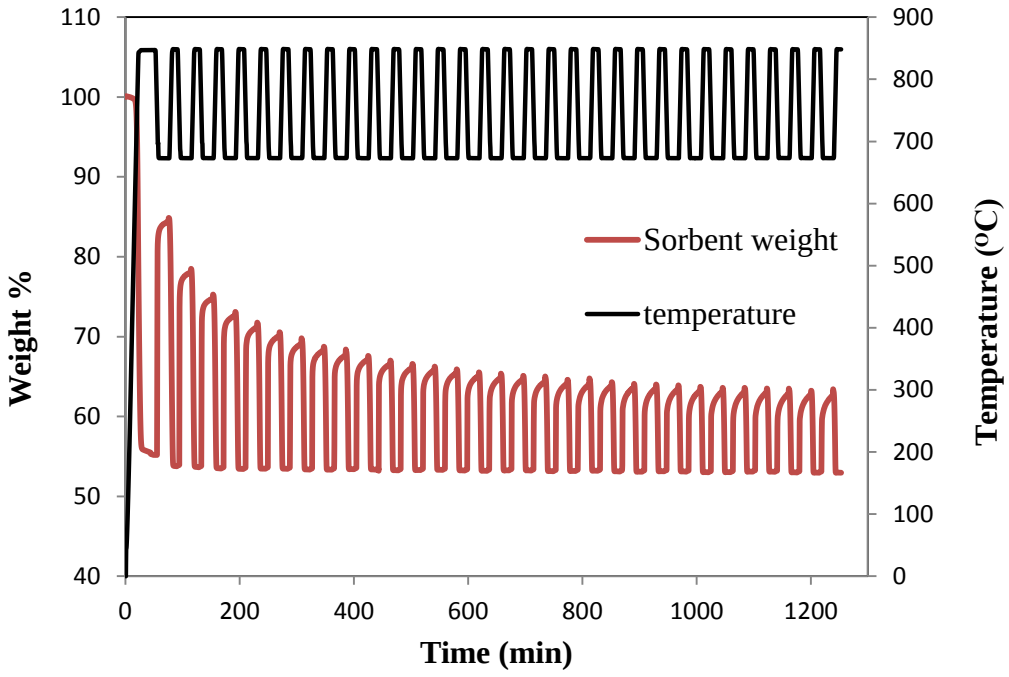

Fig. 5.3 Weight change of the CD during 31 carbonation-calcination cycles; calcination, 10 min under 100% N_2 at 850°C; and carbonation, 20 min under 100% CO_2 at 675°C.

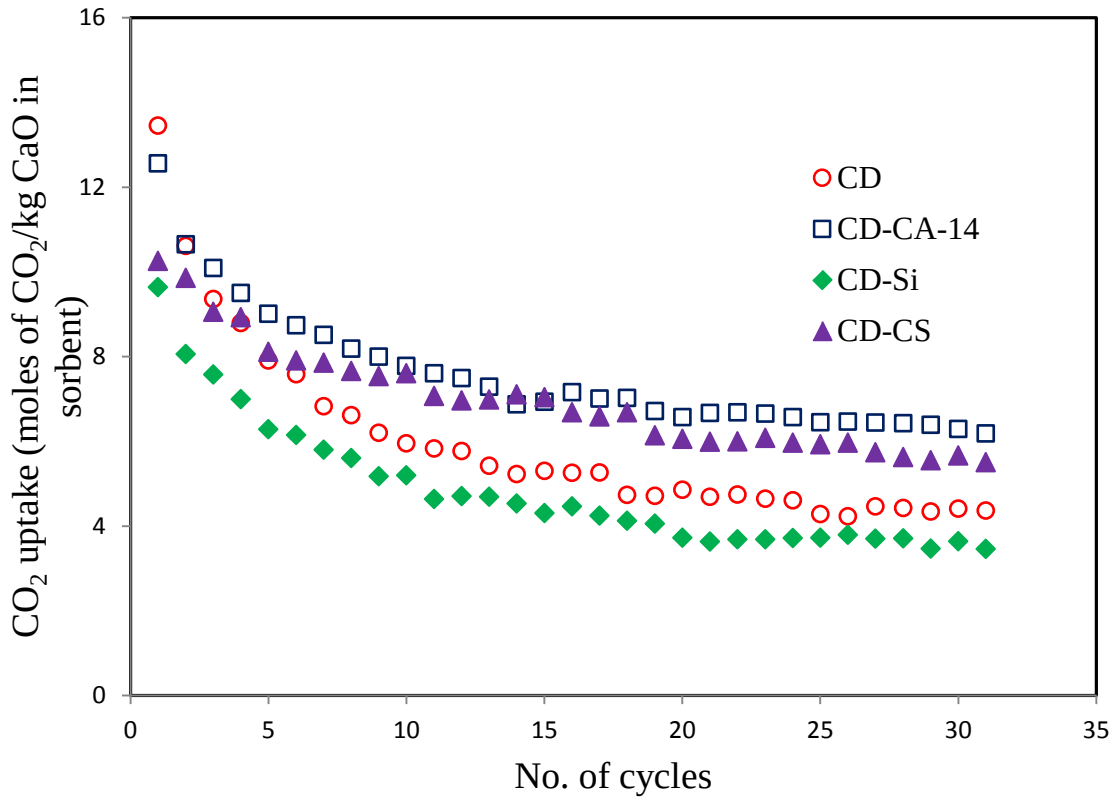

Fig. 5.4 Comparison of ultimate CO_2 uptake capacity of the sorbents (calcination, 10 min under 100% N_2 at 850°C; and carbonation, 20 min under 100% CO_2 at 675°C).

Fig. 5.5 shows the rapid loss of activity of the Cadomin limestone (CD), resulting in the CO_2 uptake dropping from 12.7 to 4.1 moles of CO_2/kg calcined sorbent after 31 cycles. The presence of the calcium aluminate cement in the CD-CA-14 sample increased the dispersion of the Ca (II) active phase, resulting in a higher CO_2 uptake after a few cycles. From Fig. 5.5, CD-CS also showed a similar increase, indicating that the low uptakes recorded per unit mass were mostly due to the large weight fraction of the silica shell, which caused high diffusion mass transfer resistance to CO_2 reaching the core of the pellet. Therefore, refining of the shell coating to produce a thinner shell will enhance the performance of the CD-CS, due to the reduction in the CO_2 mass transfer limitation.

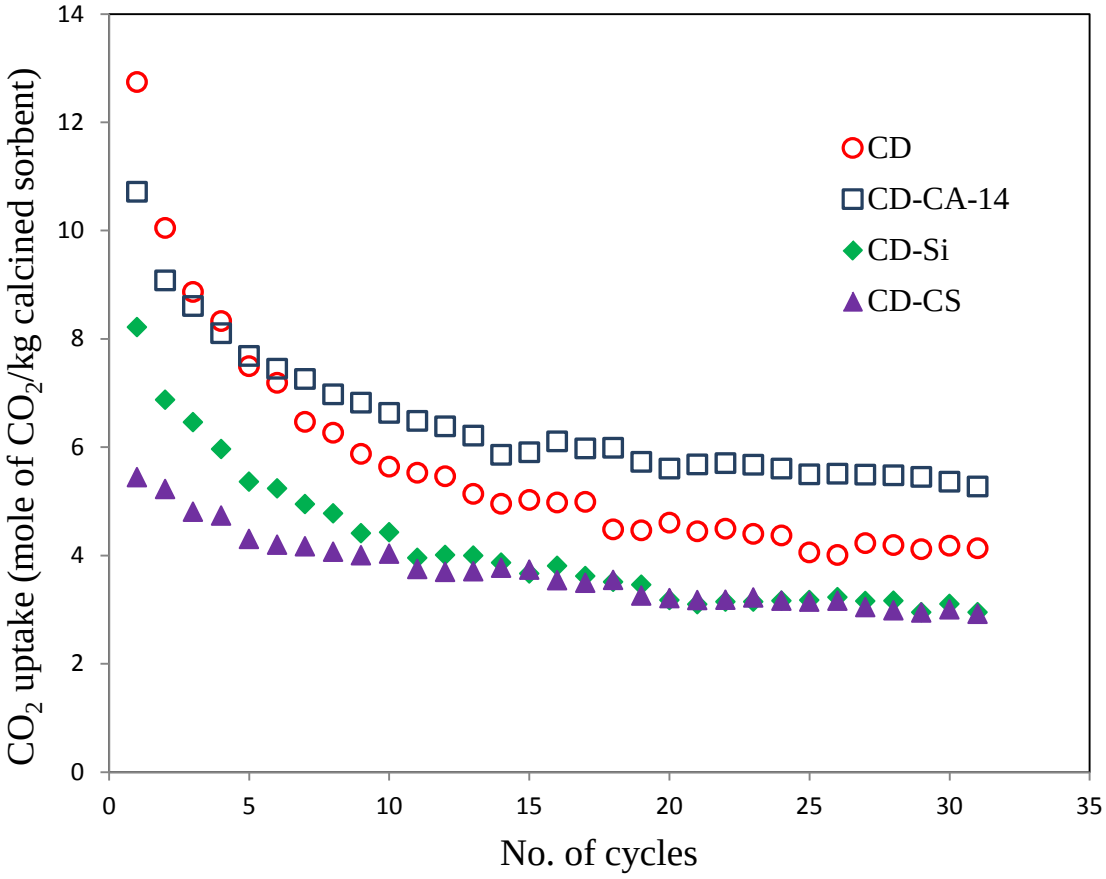

Fig. 5.5 Comparison of ultimate CO_2 uptake capacity of the sorbents in mole of CO_2/kg calcined sorbent (calcination, 10 min under 100% N_2 at 850°C; and carbonation, 20 min under 100% CO_2 at 675°C).

The main loss of activity for all four samples occurred over the first 10 cycles with different rates and continued slowly during the next 21 cycles. Table 5.2 presents the maximum CO_2 uptake of the four sorbents in the first and last cycles and the activity loss of sorbents after 31 looping cycles. The activity loss of the sorbents was calculated as follows:

Sorbent activity loss = [1 - (conversion at 31st cycle / conversion at 1st cycle)] × 100 (5.4)

Table 5.2 Maximum CO_2 uptakes, conversion, and loss of activity after 1st and 31st carbonation-calcination cycle.

Sorbent	CO_2 uptake at 1st cycle moles CO_2 /kg CaO in the calcined sorbent	CO_2 uptake at 31st cycle moles CO_2 /kg CaO in the calcined sorbent	conversion % at 1st cycle	conversion % at 31st cycle	Activity loss %
CD	13.4	4.4	75.6	24.5	67.6
CD-CA-14	12.6	6.2	70.6	34.7	50.8
CD-Si	9.6	3.5	54.1	19.4	64.0
CD-CS	10.2	5.5	57.6	30.9	46.3

From Table 5.2, the CD and CD-CS samples showed the highest and lowest sorbent activity loss in CO_2 uptake after 31 cycles, respectively. High sorbent activity over numerous cycles and high sorbent CO_2 uptake are important for the cyclic CO_2 capture process. Although the CD sorbent had the highest uptake at the first cycle, it also displayed the highest sorbent activity loss. By contrast, the core/shell material (CD-CS) had the lowest activity loss with a rather low CO_2 uptake. These differences reflect the various ways that differences in morphology and in morphology evolution with the number of cycles affected the carbonation reaction rate.

The carbonation reaction rate depended on the chemical nature of the Ca containing phase, its surface area and the surface area changes from the carbonation and calcination processes. From Fig. 5.4, the nature of the binder affects the behavior of Cadomin limestone in

different ways, with the calcium aluminate cement in CD-CA-14 increasing the CO_2 uptake of CaO after 5 cycles; whereas the silica-sol in CD-Si decreased the uptake at any number of cycles. Interestingly, the mesoporous silica shell also increased the calcium oxide CO_2 uptake after 5 cycles. Fig. 5.5 and Table 5.3 present the CO_2 uptake of sorbents based on the total mass of the calcined sorbent, which may be used in up-scaling the process. According to Table 5.3, it takes twice as many CD-CS pellets than the other sorbents for the same mole CO_2 uptake. However, the CD-CS showed the lowest activity loss of the sorbents.

Table 5.3 Maximum CO_2 uptake the sorbents studied based on total mass

Sorbents	Active CaO, wt%	CO_2 uptake at 1st cycle moles CO_2 /kg calcined sorbent	CO_2 uptake a 31st cycle moles CO_2 /kg calcined sorbent
CD	94.7	12.7	4.1
CD-CA-14	85.3	10.7	5.3
CD-Si	85.3	8.2	2.9
CD-CS	53.1	5.4	2.9

Fig. 5.6 presents SEM images of the calcined fresh, after 10th and 31st cycles for all four samples. The cause of activity loss of the CaO-based sorbents after numerous carbonation–calcination cycles is apparent from Fig. 5.4. The left column of the SEM images shows the calcined fresh sorbents, while the middle and the right columns present the calcined samples after 10 and 31 cycles, respectively. A significant progressive change of the initial porous sorbents to a less porous, denser morphology after 10 and 31 cycles can be observed. Similar

sintering has been reported by several researchers [33-34]. Sintering occurs as a result of the diffusion of atoms through the microstructure of solids, which is faster at higher temperatures, and leads to densification and grain growth. Sintering decreases the pore openings and eventually blocks the pores, making the active species inaccessible to the reactants.

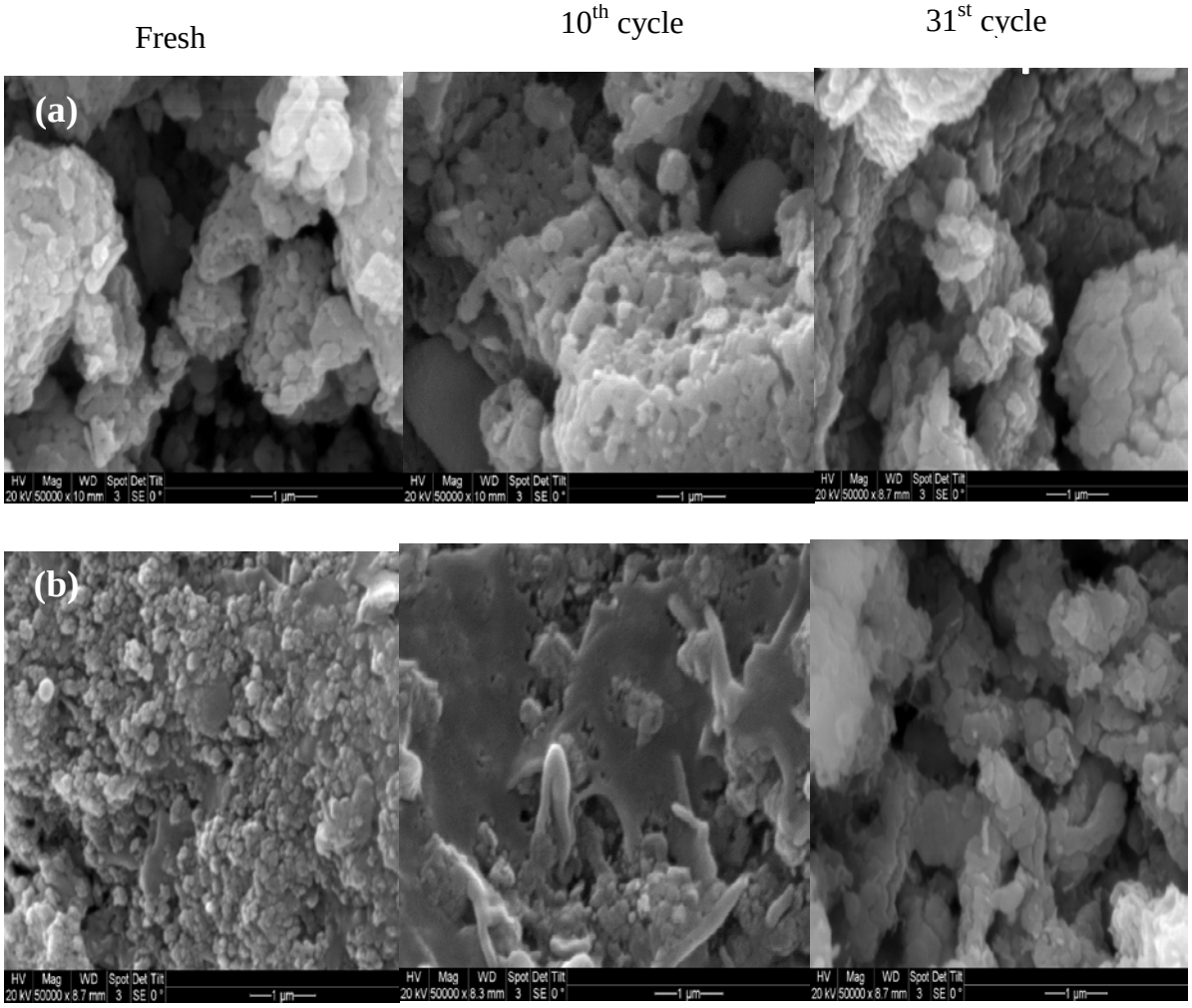

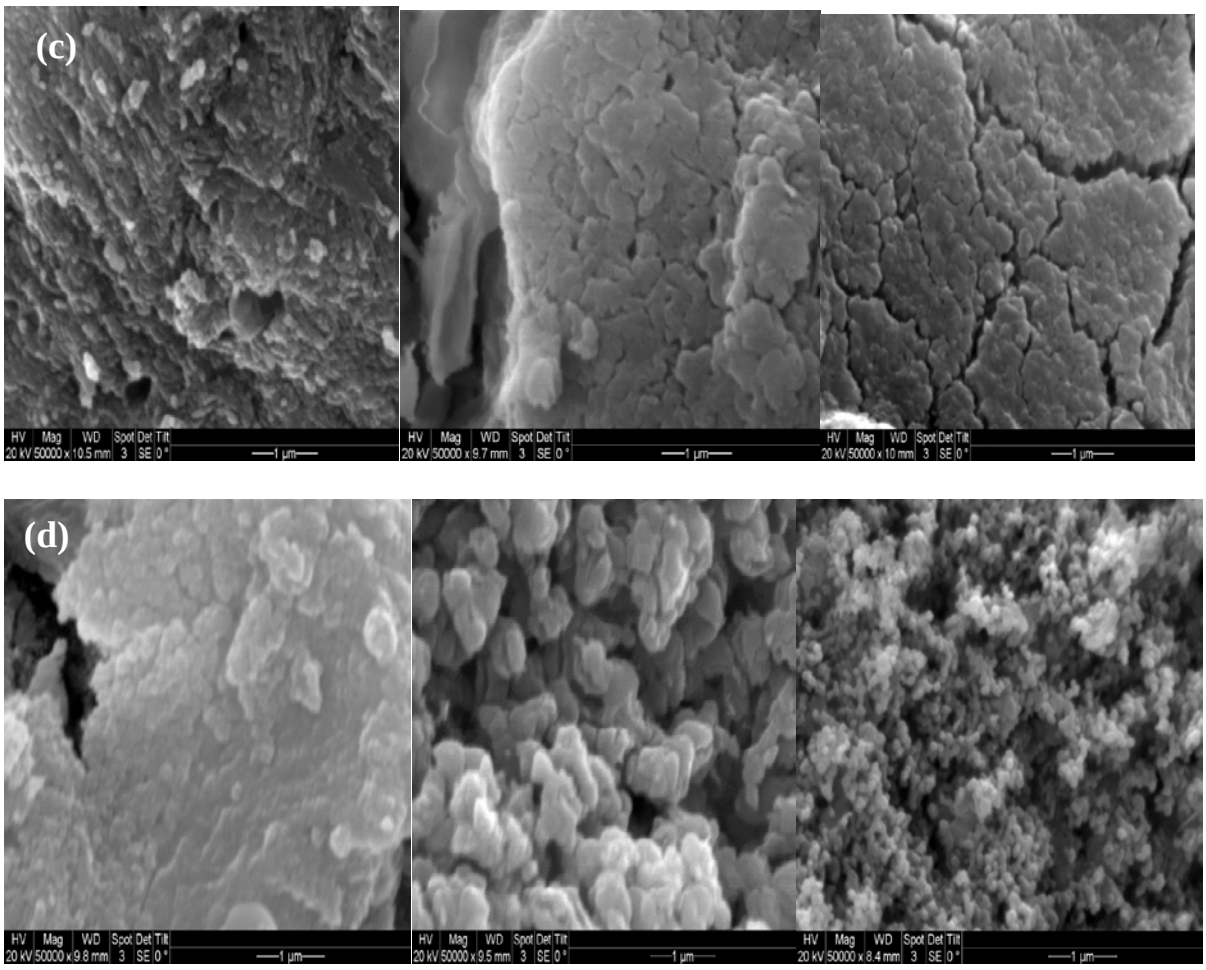

Fig. 5.6 SEM images of the calcined fresh, after 10th, and 31st cycles for the samples: (a) CD, (b) CD-CA-14, (c) CD-Si, (d) CD-CS.

The changes in pore diameter distribution of the sorbent samples after the 31st calcination are shown in Fig. 5.7. Table 5.4 presents the BET surface area, pore diameter, and pore volume of all the sorbents before and after the first calcination at 850°C. The nonporous Cadomin limestone converted to porous material with a BET surface area (S_{BET}) of 13.8 m^2/g and macropores with an average pore diameter of 34.3 nm (Fig. 5.6(a)). According to Table 5.4, introducing calcium aluminate (CA-14) and silica-sol (HS-40) as binders increased the sorbent surface area.

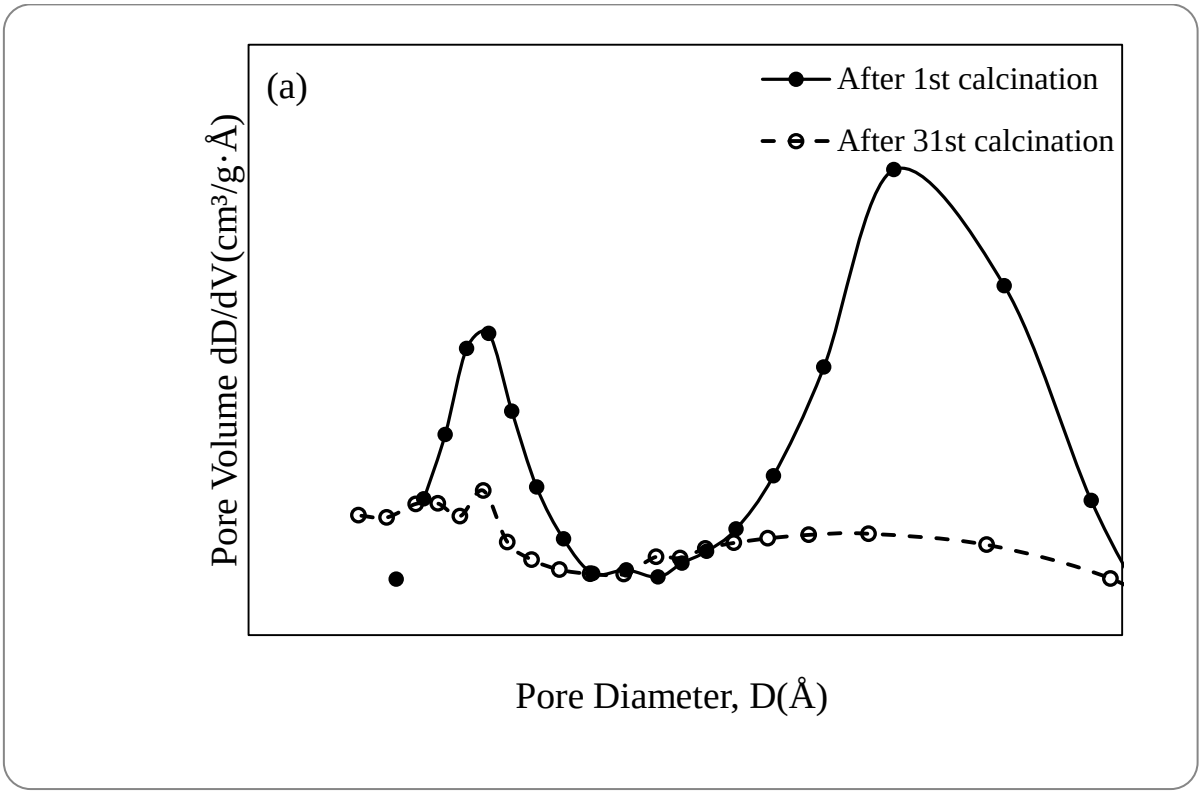
(a)
After 1st calcination
After 31st calcination
Pore Volume dD/dV(cm³/g·Å)
Pore Diameter, D(Å)

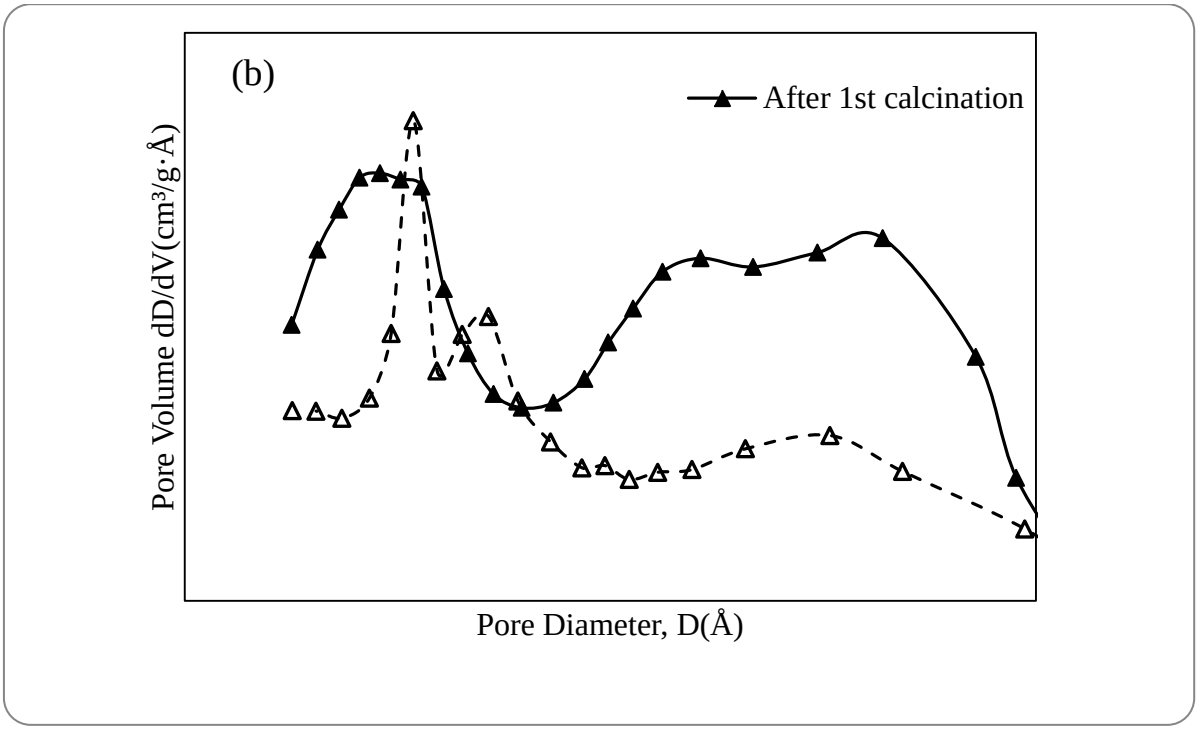
(b)
After 1st calcination
Pore Volume dD/dV(cm³/g·Å)
Pore Diameter, D(Å)

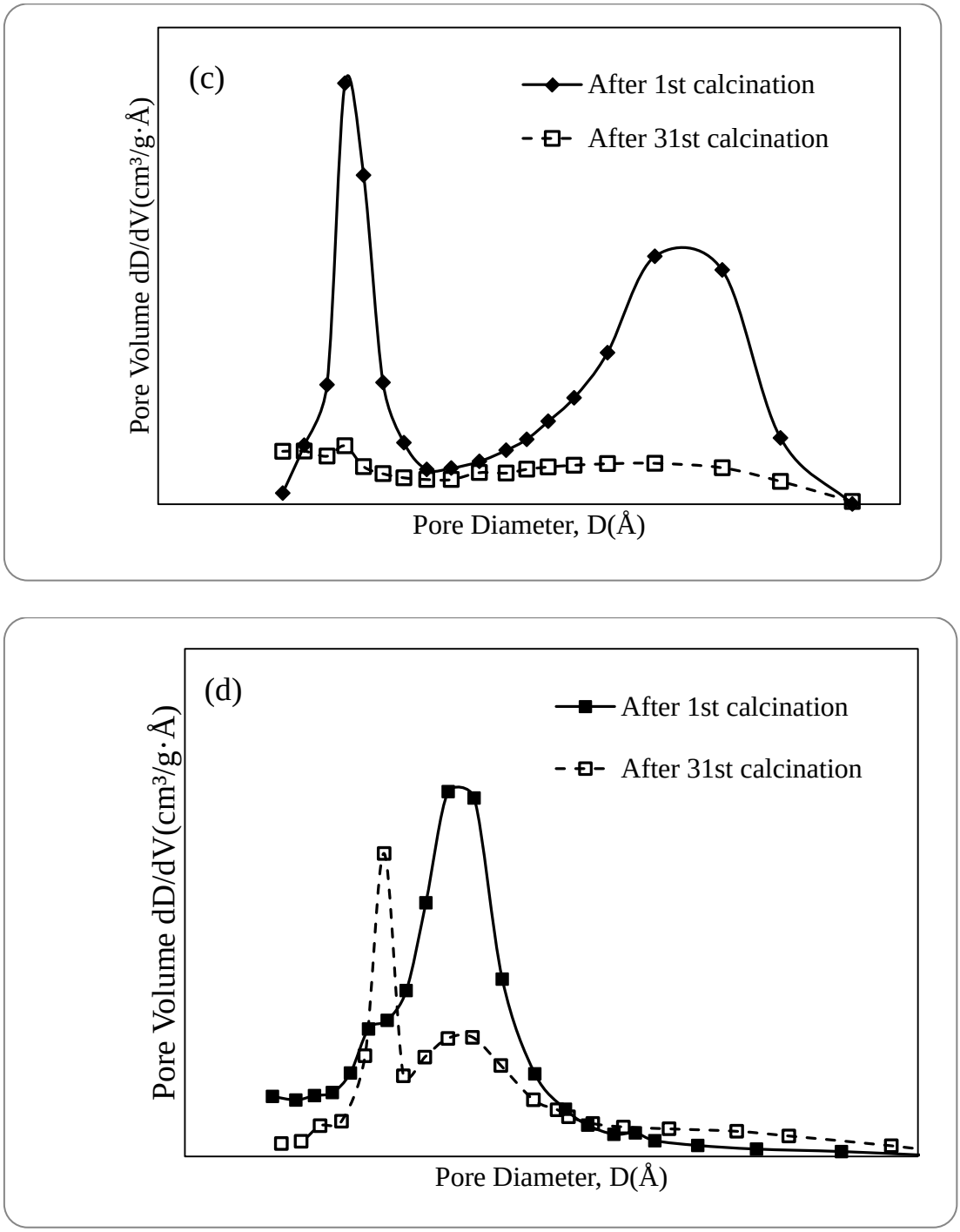

Fig. 5.7 BJH desorption pore volume distribution of calcined sorbent samples before and after 31 calcination/carbonation cycles: (a) CD, (b) CD-CA-14, (c) CD-Si, (d) CD-CS.

These results suggest that the mesopores formed as a result of calcination were of smaller volumes, which may be associated with a slower release of CO_2 from the core material due to resistance to outward CO_2 flow by the silica shell. Thus, the macropores that formed in the other samples from calcination would be associated with the mechanical constraints resulting from a high CO_2 release flow rate.

After calcination at 850°C, similar values of S_{BET} were obtained (14-17 m^2/g) for all samples. This suggests that the pore surfaces generated as a result of calcination were mostly associated with the CO_2 removal process. From Table 5.4, the average pore diameter of the CD-CS sorbent decreased significantly from calcination, and the macropores present before calcination were converted to mesopores after calcination.

Table 5.4 BET surface area and BJH pore size of sorbent samples before calcination and after 1st and 31st cycles.

	Before calcination			After 1st calcination			After 31st calcination		
Sample	S_{BET} (m^2/g)	Average pore diameter (Å)	Pore volume (cm^3/g)	S_{BET} (m^2/g)	Average pore diameter (Å)	Pore volume (cm^3/g)	S_{BET} (m^2/g)	Average pore diameter (Å)	Pore volume (cm^3/g)
CD	0.5	35.1	0.00	13.8	343.3	0.12	6.4	327.2	0.05
CD-CA-14	17.3	271.3	0.13	16.7	251.4	0.11	9.1	285.7	0.06
CD-Si	11.4	246.2	0.11	16.9	224.1	0.10	7.1	249.2	0.04
CD-CS	10.2	343.5	0.10	16.8	88.6	0.04	10.7	197.1	0.05

Fig. 5.7 presents the BJH desorption pore volume distributions of the calcined sorbent samples after the 1st and 31st carbonation–calcination cycles. The comparisons of Fig. 5.7(a)-(d) yield information on the deactivation process represented in Fig. 5.4, which was affected by the

binders and the mesoporous shell. In Fig. 5.7(a), the significant change in pore volume was likely associated with the strong activity loss shown in Fig. 5.4. This effect may have been due to sintering, and it may have also been related to a slower CO_2 evacuation, creating less damage to the $CaCO_3$ phase. As seen from the results in Table 5.4, this process also corresponds to lower values of both the specific surface area and the pore volume. Similar trends can also be observed for the CD-CA-14 sorbent in Fig. 5.7(b). The lower relative decrease in pore volume compared to the CD samples was correlated to the lower loss of activity.

In Fig. 5.7(c), the initial pore size distribution of CD-Si was different from the previous two samples, illustrating a low size mode at 30-35 Å, similar to the one usually found in silica gel. This peak disappeared after 31 cycles, and the remaining pore size distribution was similar to those observed in the CD and CD-CA-14 samples.

The pore size distribution of the CD-CS sample was initially dominated by a strong mode centered at 60 Å, which corresponds to the mesopores in the silica shell. After 31 cycles, the 60 Å mode was significantly reduced, suggesting some partial collapse of the shell mesostructure. A minor mode appeared at 30-35 Å, similar to the CD-Si sample. Contrary to the other three samples, the final pore size distribution mode centered at 400 Å showed an increased volume after 31 cycles. It is, therefore, likely that some cracks were formed in the silica shell, creating less resistance to the outward CO_2 flow.

XRD patterns of the four carriers before and after the first calcination are reported in Fig. 5.8(a) and (b), respectively. Before calcination, all four samples yielded the pattern of $CaCO_3$. Only in the case of the CD-CA-14 sample did additional weak lines appear, indicating the presence of some non-converted Mayenite ($Ca_{12}Al_{14}O_{33}$). After calcination, the CD and CD-Si samples still showed essentially the pattern of CaO. This pattern was also found in the CD-CS

sample; however, in this case, the additional lines at 2θ = 29.5, 37.5, 39.6, 42.6, 47.6 and 48.5 degrees were assigned to Larnite ($Ca_2(SiO_4)$) and Spurrite ($Ca_5(SiO_4)_2CO_3$). Note that the broad line of amorphous silica was subtracted from the patterns shown for the CD-Si samples in Figs. 5.8(a) and (b).

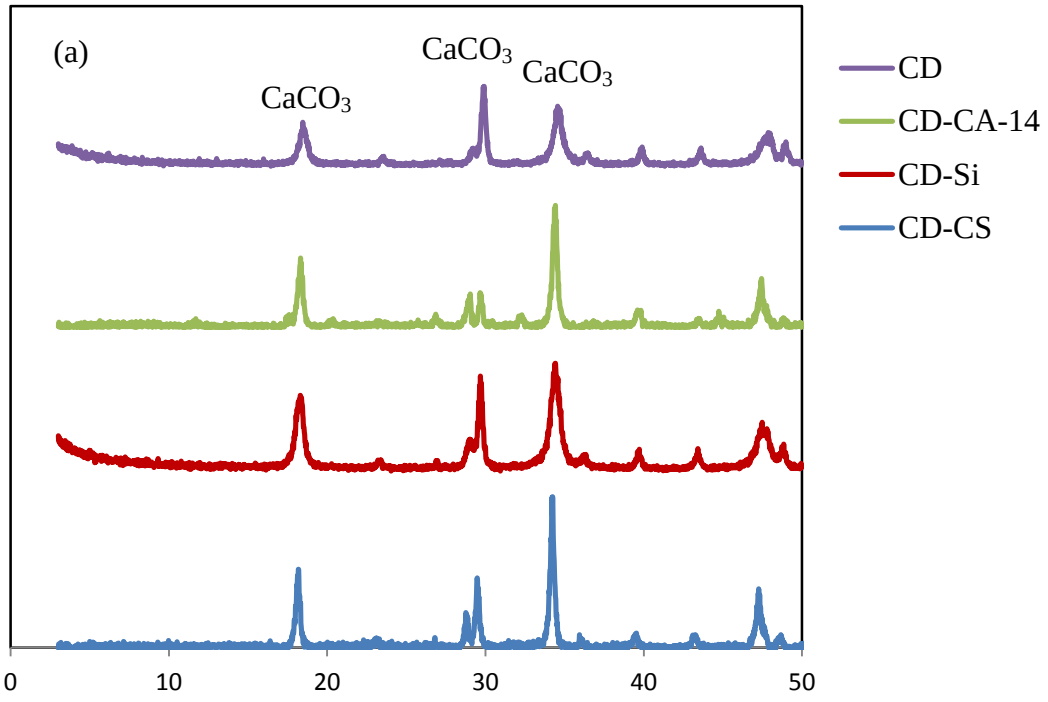

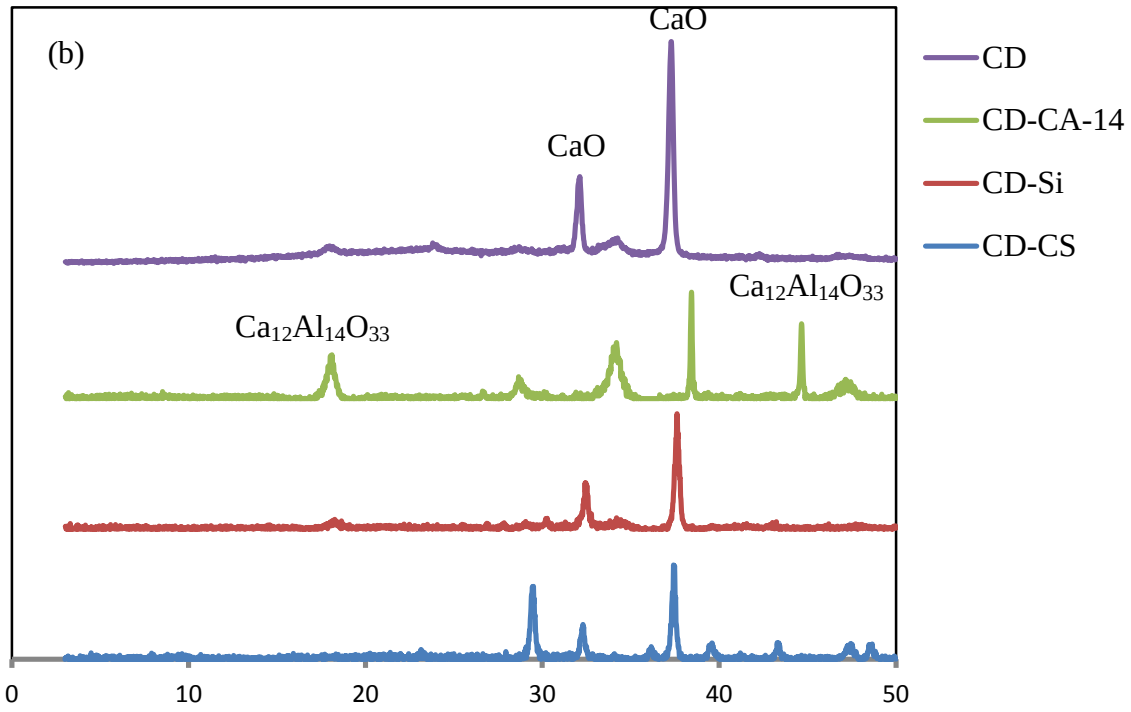

Fig. 5.8 XRD pattern of the sorbent samples before (a) and after (b) calcination at 850°C.

For the calcined CD-CA-14 sample, only the Mayenite was visible with XRD, since the Cadomin/aluminate cement weight ratio was 9/1 in this sample. This result indicates that the major calcined CaO phase was very divided, with crystal domains no larger than 40-50 Å. Manovic and Anthony [28] already demonstrated that the presence of Mayenite enhances the sintering resistance of nano-sized CaO subgrains.

Fig. 5.9(a) and (b) display SEM pictures of the CD-CA-14 and CD-CS samples, respectively, after 10 carbonation–calcination cycles. Both samples showed cracks in the initial particles, which were likely associated with the stress formation upon rearrangement of the particles through calcination or it may be due to the mechanical effect of the outward flow of CO_2 upon calcination. This effect occurred simultaneously with the decrease in activity depicted by Figs. 5.4 and 5.5 and the sintering effect leading to the pore size and pore volume changes

illustrated by Fig. 5.7. In the case of the CD-CS samples, Fig. 5.9(b) shows that the more uniform layer of the mesostructured silica shell had been damaged in the process, showing only patches of the layer on the particle external surface after 10 cycles. As previously discussed, it is suggested that the mesoporous shell regulated this flow rate, yielding less mechanical strains on the reacting solid and a lower volume of mesopores after the first cycle (see Fig. 5.7(d)). Losing the integrity of this shell over the first 5-10 cycles corresponded to a significant loss of activity.

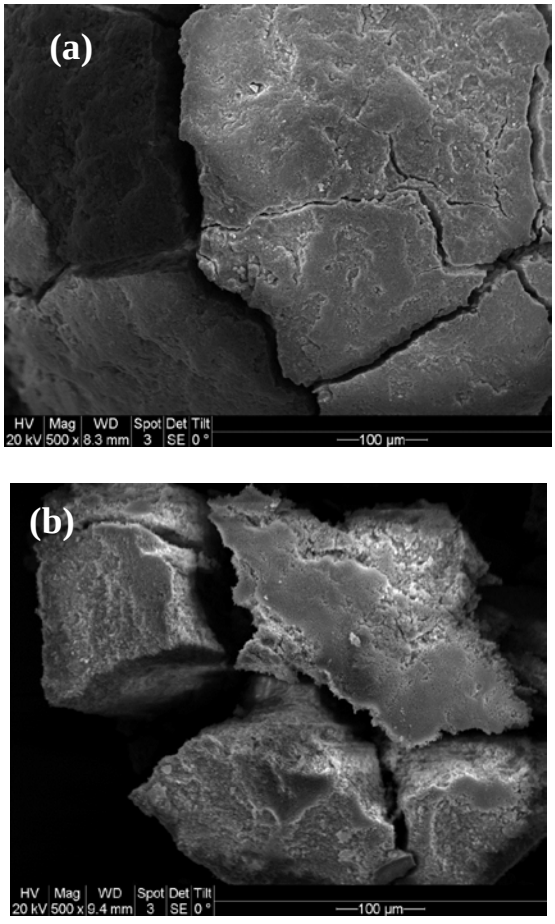

Fig. 5.9 SEM images of (a) CD-CA-14 and (b) CD-CS after 10 carbonation-calcination

Significant gains, therefore, in terms of mechanical and thermal stability of the CO_2 carrier, may be made if the active CaO core particle could be covered with a stronger shell of mesoporous material. However, this shell should not be too thick, in order to maintain a high activity per unit mass of the sorbent.

5.6 Conclusion

Experimental series of 31 carbonation–calcination cycles were performed with CaO-based pellets prepared with different binders (calcium aluminate cement and silica-sol) and different procedures (precipitation and sol-gel). The CO_2 uptake capacity and stability of the modified sorbents were studied using TGA, in order to compare their performances with that of natural Cadomin limestone. The results showed that the modified sorbents improved the CO_2-carrying activity and that the use of binders decreased the negative effect of sintering. Cadomin-calcium aluminate (CD-CA-14) pellets gave both a high CO_2 uptake capacity and a low loss of activity through 31 cycles. XRD patterns of the CD-CA-14 samples identified the presence of a Mayenite phase ($Ca_{12}Al_{14}O_{33}$) in the CaO structure, which led to a reduction in sorbent sintering. The core/shell (CD-CS) pellets had the highest stability with a low CO_2 uptake capacity, due to the high content of binder (43%) in the pellet structure. The surface morphology changes of the sorbent that resulted from sintering through the CO_2 looping cycles were explained using the data obtained from the SEM and BET/BJH analyses. However, the sintering problem of calcium oxide has not been thoroughly addressed. This study showed that the use of silica as a binder and shell for improving the stability of CaO against sintering at high temperatures was not successful. More investigation on sintering is needed to elucidate this phenomenon and to resolve it by employing novel materials as binders and promoters.

5.7 References

[1] Herzog, H., What future for carbon capture and sequestration?. Environ. Sci. Technol. 35 (2001) 148A-153A.

[2] Bachu, S., CO_2 storage in geological media: Role, means, status, and barriers to deployment. Prog. Energy Combust. Sci. 34 (2007) 254-273.

[3] Yang H., Zu Z., Fan, M., Gupta, R., Slimane, R. B., Bland, A.E., Wright, I., Progress in carbon dioxide separation and capture: A review. J. Environ. Sci. 2008; 20: 14-27.

[4] Adanez, J., de Diego, L. F., Garcia-Labiano, F., Gayan, P., Abad, A., Selection of oxygen carriers for chemical-looping combustion. Energy Fuels 18 (2004) 371–377.

[5] Stanmore, B. R., Gilot, P., Review - Calcination and carbonation of limestone during thermal Cycling for CO_2 sequestration. Fuel Process. Technol. 86 (2005) 1707–1743.

[6] Abanades, J. C., Grasa, G., Alonso, M., Rodriguez, N., Anthony, E. J., Romeo, L. M.., Cost structure of a post combustion CO_2 capture system using CaO. Environ. Sci. Technol. 41 (2007) 5523–5527.

[7] MacKenzie, A., Granatstein, D. L., Anthony, E. J., Abanades, J. C., Economics of CO_2capture using the calcium cycle with a pressurized fluidized bed combustor. Energy Fuels 21 (2007) 920–926.

[8] Abanades, J. C., Rubin, E. S., Anthony, E. J., Sorbent cost and performance in CO_2 capture system. Ind. Eng. Chem. Res. 43 (2004) 3462– 3466.

[9] Lin, S. Y., Suzuki, Y., Hatano, H., Harada, M., Developing an innovative method, HyPr-RING, to produce hydrogen from hydrocarbons. Energy Conv. Manag. 43 (2002) 1238-1290.

[10] Weimer, T., Berger, R., Hawthorne, C., Abanades, J. C., Lime enhanced gasification of solid fuel: Examination of a process for simultaneous hydrogen production and CO_2 capture. Fuel 2008; 87: 1678-1686.

[11] Anthony, E. J., Solid looping cycles: A new technology for coal conversion. Ind. Eng. Chem. Res. 47 (2008) 1747-1754.

[12] Romeo, L. M., Lara, Y., Lisbona, P., Martı´nez, A., Economical assessment of competitive enhanced limestones for CO2 capture cycles in power plants. Fuel Proc. Technol. 90 (2009) 803–811.

[13] Lysikov, A. I., Salanov, A. N., Okunev, A. G., Change of CO_2 carrying capacity of CaO in isothermal recarbonation-decomposition cycles. Ind. Eng. Chem. Res. 46 (2007) 4633–4638.

[14] Abanades, J. C., The maximum capture efficiency of CO_2 using a calcination/carbonation cycle of $CaO/CaCO_3$. Chem. Eng. J. 90 (2002) 303– 306.

[15] Burtin, P., Brunelle, J. P., Pijolat, M., Soustelle, M., Influence of surface area and additives on the thermal stability of transition alumina catalyst supports. I. Kinetic data. Appl. Catal. 34 (1987) 225–238.

[16] Powell, B. R., Stabilization of high surface area alumina. Materials Res. Soc. Ann. Meeting, Boston (1980) 16-21.

[17] Kato, A., Yamashita, H., Kawagoshi, H., Matsuda, S., Preparation of lanthanum b-alumina with high surface area by co-precipitation. J. Am. Ceram. Soc. 70 (1987) 157–159.

[18] Arai, H., Machida, M., and Eguchi, K., Effect of additives on the surface area of oxide supports for catalytic combustion. J. Catal. 103 (1987) 385-393.

[19] Beguin, B., Garbowski, E., Primet, M., Stabilization of alumina toward thermal sintering by silicon addition. J. Catal. 127 (1991) 595-604.

[20] Manovic, V., Anthony, E. J., Thermal activation of CaO-based sorbent and self-reactivation during CO_2capturelooping cycles. Environ. Sci. Technol. 42 (2008) 4170–4174.

[21] Wu, Y., Blamey, J., Anthony, E. J., Fennell, P. S., Morphological changes of limestone sorbent particles during carbonation/calcination looping cycles in a thermogravimetric analyzer (TGA) and reactivation with steam. Energy Fuels 24 (2010) 2768-2776.

[22] Pacciani, R., Muller, C. R., Davidson, J. F., Dennis, J. S., Hayhurst, A. N. Synthetic Ca-based solid sorbents suitable for capturing CO_2 in a fluidised bed. Canad. J. Chem. Eng. 86 (2008) 356–366.

[23] Li, Z. S., Cai, N. S., Huang, Y. Y., Han, H. J. Synthesis, experimental studies, and analysis of a new calcium-based carbon dioxide absorbent. Energy Fuels 19 (2005) 1447–1452.

[24] Manovic, V., Anthony, E. J. CaO-based pellets supported by calcium aluminate cements for high-temperature CO_2 capture. Environ. Sci. Technol. 43 (2009) 7117–7122.

[25] Manovic, V., Anthony, E. J., Screening of binders for pelletization of CaO-based sorbents for CO_2capture. Energy Fuels 23 (2009) 4797–4804.

[26] Liu, F. Q., Li, W. H., Lia, R. X. Synthesis, characterization, and high temperature CO2 capture of new CaO based hollow sphere sorbents. J. Mat. Chem. A (2013), DOI: 10.1039/C3TA11369H

[27] Karami, D., Mahinpey, N., Highly active CaO-based Sorbents for CO2 capture using the precipitation method: preparation and characterization of the sorbent powder. Ind. Eng. Chem. Res. 51 (2012) 4567−4572.

[28] Manovic, V., Anthony, E. J., Long-term behavior of CaO-based pellets supported by calcium aluminate cements in a long series of CO_2 capture cycles. Ind. Eng. Chem. Res. 48 (2009) 8906–8912.

[29] Lu, Y., Ganguli, R., Drewien, C. A., Anderson, M. T., Brinker, C. J., Gong, W., Guo, Y., Soyez, H., Dunn, B., Huang, M. H, Zink, J. I, Continuous formation of supported cubic and hexagonal mesoporous films by sol–gel dip-coating. Nature 389 (1997) 364-368.

[30] Sun, Z., Deng, Y., Wei, J., Gu, D., Tu, B., Zhao, D. Hierarchically ordered macro-/mesoporous silica monolith: tuning macropore entrance size for size selective adsorption of proteins. Chem. Mat. 23 (2011) 2176–2184.

[31] Borgwardt, R. H., Sintering of nascent calcium oxide. Chem. Eng. Sci. 44 (1989) 53–60.

[32] Borgwardt, R. H., Calcium oxide sintering in atmospheres containing water and carbon dioxide. Ind. Eng. Chem. Res. 28 (1989) 493–500.

[33] Abanades, J. C., Alvarez, D., Conversion limits in the reaction of CO_2 with lime. Energy Fuels 17 (2003) 308-315.

[34] Fennell, P. S., Pacciani, R., Dennis, J. S., Davidson, J. F., Hayhurst, A. N., The effects of repeated cycles of calcination and carbonation on a variety of different limestones, as measured in a hot fluidized bed of sand. Energy Fuels 21 (2007) 2072-2081.

Chapter Six: **Sorbent enhanced hydrogen production from steam gasification of coal integrated with CO_2 capture**

Int. J. Hydrogen Energy 39 (2014) 10071-10078

6.1 Presentation of the article

This chapter presents the application of the calcium-based sorbents in the gasification process for capturing CO_2 and producing H_2 simultaneously. The steam gasification of Boundary Dam (BD) coal was integrated with CO_2 capture using calcined natural Cadomin limestone in a horizontal fixed bed reactor. The effects of the temperature and the sorbent-to-carbon molar ratio were investigated to recognize basic kinetic information of the process. The concentration of produced gases (i.e., H_2, CH_4, CO, and CO_2) were measured continuously using a micro gas chromatograph/thermal conductivity detector (GC-TCD) during the process. Moreover, the solid residues of all experiments were examined using a TGA and a CHNS (carbon, hydrogen, nitrogen, sulfur) elemental analyzer to determine the composition of solid residues.

The results verified that the presence of sorbent in the steam gasification of coal increased the molar fraction of H_2 to more than 80%, with almost all CO_2 fixed into the calcium-based sorbent. CO was converted to H_2 and CO_2 through the water gas shift reaction.

The main part of this work was performed by Mohammad H. Sedghkerdar, Dr. Nader Mahinpey supervised the work, and Mr. Ehsan Mostafavi helped in conducting the experiments and interpreting the results.

Sorbent enhanced hydrogen production from steam gasification of coal integrated with CO_2 capture

This article has been published in Int. J. Hydrogen Energy journal, 39 (2014) 10071-10078.

Mohammad Hashem Sedghkerdar, Ehsan Mostafavi, Nader Mahinpey*

Department of Chemical and Petroleum Engineering, Schulich School of Engineering, University of Calgary, Calgary, AB, Canada T2N 1N4

6.2 Abstract

In this work, CO_2 capture and H_2 production during the steam gasification of coal integrated with CO_2 capture sorbent were investigated using a horizontal fixed bed reactor at atmospheric pressure. Four different temperatures (650, 675, 700, and 750°C) and three sorbent-to-carbon ratios ([Ca]/[C] = 0, 1, 2) were studied. In the absence of sorbent, the maximum molar fraction of H_2 (64.6%) and conversion of coal (71.3%) were exhibited at the highest temperature (750°C). The experimental results verified that the presence of sorbent in the steam gasification of coal enhanced the molar fraction of H_2 to more than 80%, with almost all CO_2 was fixed into the sorbent structure, and carbon monoxide (CO) was converted to H_2 and CO_2 through the water gas shift reaction. The steam gasification of coal integrated with CO_2 capture largely depended on the reaction temperature and exhibited optimal conditions at 675°C. The maximum molar fraction of H_2 (81.7%) and minimum CO_2 concentration (almost 0%) were obtained at 675°C and a sorbent-to-carbon ratio of 2.

6.3 Introduction

CO_2 is the primary greenhouse gas emitted through human activities that contributes to global warming [1-2]. The growing need for the reduction in anthropogenic CO_2 emissions has led to a global demand towards the development of efficient, economical and realistic carbon capture and sequestration (CCS) technologies for application to fossil fuel based power plants [1].

Three technological thrusts are under development in considering how to best improve CO_2 capture. These are classified as post-combustion capture, pre-combustion capture, and oxy-fuel combustion [3-6]. In post-combustion capture, the CO_2 is separated from other flue gases produced by combustion. Among the post-combustion technologies, amine-based CO_2 wet scrubbing is believed to be the most technologically mature, but it requires high capital and operational costs [7].

In pre-combustion CO_2 capture, the CO_2 is recovered from some process streams before the fuel is burned. Integrated gasification combined cycle (IGCC) supplemented by shift conversion, is a very promising approach for pre-combustion capture. In this process, fossil fuel is gasified to produce synthesis gas (syngas), which is a mixture of mainly carbon monoxide (CO) and H_2. The syngas is sent to the shift reactor to convert the CO to H_2 and CO_2 in the presence of steam. The CO_2 is then separated from H_2 in the separation unit.

In recent years, a new gasification method for H_2 production from coal using a CO_2 solid sorbent, i.e., hydrogen production reaction integrated novel gasification (HyPr-RING), was proposed by Lin et al. [8-11]. The HyPr-RING method includes integrating the steam gasification of coal, the water gas shift reaction (WGS) and CO_2 capture using synthesized calcium oxide (CaO, <325 mesh, Wako Pure Chemical Industries, Osaka, Japan) in a single

reactor at temperature in the range of 600-800 °C [8-11]. The individual and overall reactions are described in reactions (6.1)-(6.4).

Steam char gasification:

$$C + H_2O \rightarrow CO + H_2 \qquad \Delta H^o_{298} = 132\ kJ/mol \qquad (6.1)$$

WGS reaction:

$$CO + H_2O \rightarrow CO_2 + H_2 \qquad \Delta H^o_{298} = -41.5\ kJ/mol \qquad (6.2)$$

CaO carbonation:

$$CaO + CO_2 \rightarrow CaCO_3 \qquad \Delta H^o_{298} = -178\ kJ/mol \qquad (6.3)$$

The overall reaction:

$$C + CaO + 2H_2O \rightarrow CaCO_3 + 2H_2 \qquad \Delta H^o_{298} = -87.5\ kJ/mol \qquad (6.4)$$

where $CaCO_3$ is calcium carbonate. In a continuous operation, the saturated CO_2 carrier sorbent ($CaCO_3$) should be regenerated to CaO in the regenerator at temperature 850-900 °C. The heat required for regeneration of $CaCO_3$ can be obtained from the combustion of unreacted carbon from the gasification reaction.

The negative heat of reaction of the overall reaction shows that the process needs no heat from the combustion of coal in the gasifier and that the heat of the carbonation and WGS reactions are available and sufficient for steam gasification. Lin et al. [10] confirmed that the only gas product from integrated hydrocarbon gasification and CO_2 separation at 700°C and 25 MPa was H_2.

In another study, Lin et al. [11] investigated the effect of pressure (in the range of 0.1-6 MPa) on gas products for the HyPr-RING process on Taiheiyo coal. According to the results, pressure increased the production of H_2 accompanied by methane (CH_4) decomposition.

Thermodynamic studies of the HyPr-RING process by coal gasification at 650°C and 3MPa showed a mixture of flue gas consisting of 91% H_2 and 9% CH_4 (dry basis nitrogen (N_2) free).

Given the advantages of gasification in producing syngas for a range of chemical processes and in terms of overall energy efficiency and environmental factors in power generation, there has been considerable work on the gasification of a wide range of feedstocks. Despite these efforts, there are insufficient experimental data to be able to identify the optimal conditions for conducting steam gasification integrated with an efficient CO_2 capture scheme.

The present work provides a detailed study on H_2 production from the steam gasification of Boundary Dam (BD) coal integrated with CO_2 capture using calcined natural Cadomin limestone in a horizontal fixed bed reactor. In order to identify basic kinetic information, the effects of the reaction parameter such as temperature and molar ratio of sorbent-to-carbon in BD coal ([Ca]/[C]) were investigated. Moreover, the solid residues from all coal gasification experiments were investigated to determine the composition of solid residues using thermogravimetric analyzer (TGA) and a CHNS (carbon, hydrogen, nitrogen, sulfur) analyzer.

6.4 Experimental section

6.4.1 Materials

In this study, BD coal (lignite, Saskatchewan, Canada) was used as a carbonaceous material. The proximate analysis of the BD coal was performed according to the ASTM D-3172 standard using a TGA (TG 209, F1 Iris, Neztsch). In addition, the ultimate analysis of the coal sample obtained using a Perkin Elmer CHNS analyzer (CHNS/O Analyzer Series III, 2400). Tables 6.1 and 6.2 present both proximate and ultimate analyses on dry basis for the BD coal.

Table 6.1 Proximate analyses of the BD coal (Wt%, dry basis)

Sample	VM[a]	Ash	FC[b]
BD Coal	37.6	16.6	45.8

[a] VM: Volatile matters

[b] FC: Fixed carbon

Table 6.2 Ultimate analyses of the BD coal (Wt%, dry basis)

Sample	C	H	N	S	O
BD Coal	58.00	3.38	1.81	1.01	35.80

Natural Cadomin limestone from western Canada was calcined at 850°C under N_2 flow and used as a sorbent for CO_2 capture. The particle size of the calcined limestone (CaO) was less than 250 μm. The chemical analysis of Cadomin limestone can be found elsewhere [12]. The coal was crushed by a milling machine to an average diameter of about 5 μm and then mixed with CaO powder.

6.4.2 Experimental set-up

The schematic diagram of the experimental set-up is shown in Fig. 6.1. A stainless steel tube (length of 100 cm, inner diameter of 2.54 cm) as a reactor was placed in a horizontal electric furnace.

Superheated steam (650-750°C at 1 atm) was generated by forcing water into a coil that was 600 cm long and 0.32 cm in diameter, which was attached to the outside of the reactor and housed in the furnace. The bed temperature was measured with two K-type thermocouples located inside and outside of the reactor.

The flue gases generated by steam gasification were conducted first to a condenser to separate the steam and then to an Agilent micro GC-TCD 490 (gas chromatograph/thermal conductivity detector) to measure the composition of the product gases. A mass flow controller was installed to control the flow rate of N_2 (400 ml/min) in the reactor during pyrolysis and gasification experiments.

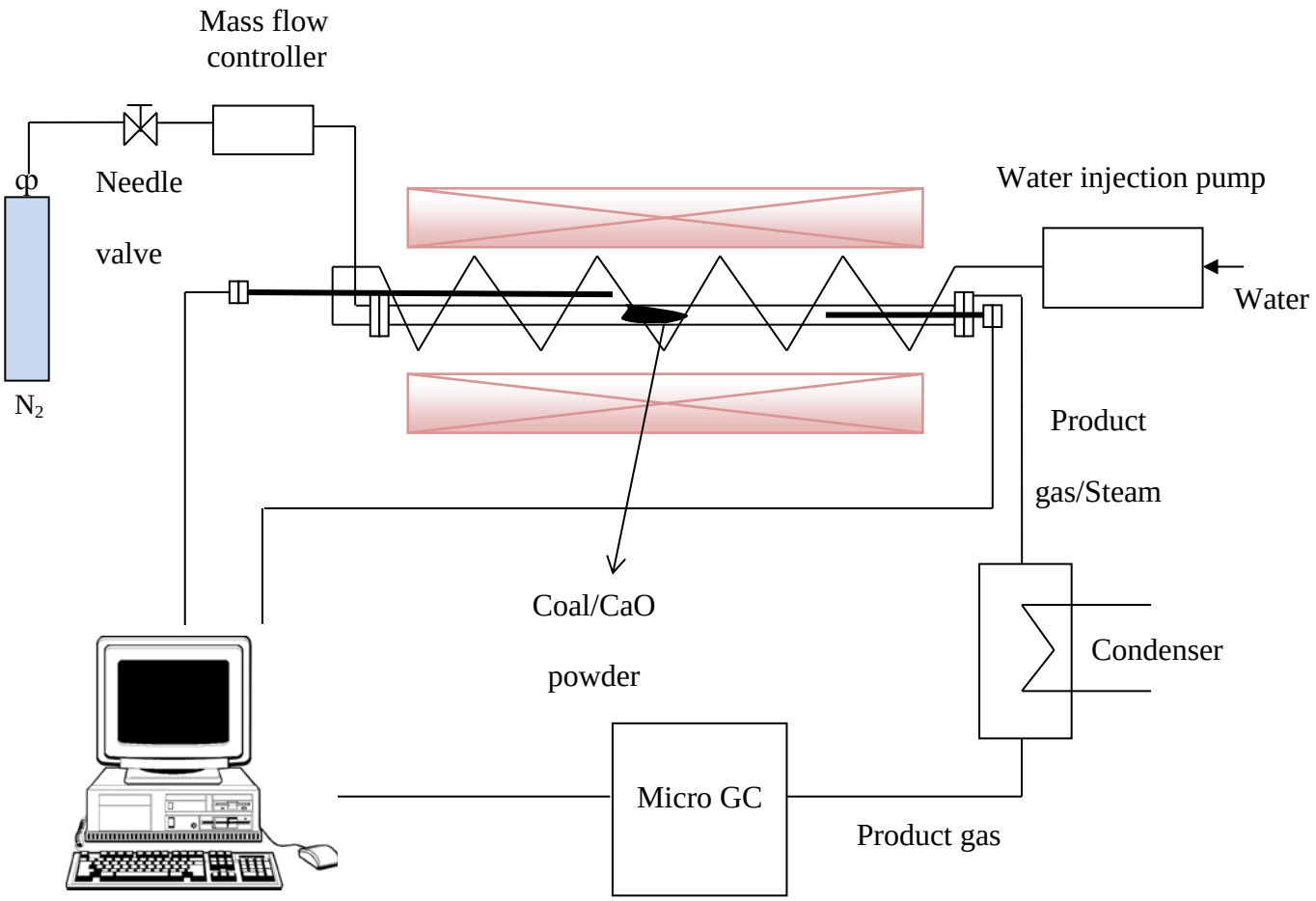

Fig. 6.1 Schematic diagram of the steam gasification of coal experimental set-up

Superheated steam (650-750°C at 1 atm) was generated by forcing water into a coil that was 600 cm long and 0.32 cm in diameter, which was attached to the outside of the reactor and housed in the furnace. The bed temperature was measured with two K-type thermocouples located inside and outside of the reactor.

The flue gases generated by steam gasification were conducted first to a condenser to separate the steam and then to an Agilent micro GC-TCD 490 (gas chromatograph / thermal conductivity detector) to measure the composition of the product gases. A mass flow controller was installed to control the flow rate of N_2 (400 ml/min) in the reactor during pyrolysis and gasification experiments.

6.4.3 Experimental procedure

All experiments used 5 g BD coal. The amount of CaO was added to the coal sample at specific molar ratios of CaO to the carbon in BD coal ([Ca]/[C] = 0, 1, 2). The material was mixed and placed in the middle of the reactor. All experiments were performed at atmospheric pressure, and the temperature was increased by the electric furnace at an average heating rate of 30°C/min. During the heat up stage, pure N_2 was fed into the reactor for pyrolysis of the sample.

When the temperature became stable at the pre-determined gasification temperature (650, 675, 700, or 750°C), the N_2 was switched to steam (75%) and balanced with N_2. The steam was generated by pumping water at a constant rate of 10 ml/min into the hot coil at the desired temperature to start the gasification reactions. The concentrations of H_2, CH_4, CO, and CO_2, produced during pyrolysis and 30 min gasification were measured continuously using the micro GC-TCD. All experiments have performed twice and the results showed less than 5% uncertainty.

6.5 Results and discussions

In this work, the effects of temperature and sorbent-to-carbon ratio ([Ca]/[C]), as the main process conditions of steam gasification of coal, were investigated. Four different temperatures (650, 675, 700, and 750°C) and three different specific molar ratios of CaO (as the CO_2 sorbent) to carbon ([Ca]/[C] = 0, 1, 2) were chosen for the steam gasification of coal integrated with a CO_2 capture process. According to our previous study on calcined Cadomin limestone carbonation, 675°C was found to be the optimal temperature resulting in fastest carbonation reaction rate [13]. Therefore, we considered this temperature as one of operating conditions of experiments for this study.

The experiments in the steam gasification of coal in the absence of CO_2 sorbent were carried out to obtain reference results at each temperature. The gasification process consists of a complex set of reactions taking place in series and parallel. Reactions (6.1)-(6.3) are the main reactions taking place under identical conditions HyPr-RING [8-11]. The use of sorbent moves the WGS reaction forward, leading to higher H_2 production.

Fig. 6.2 illustrates the composition of gas products from pyrolysis and steam gasification at 650°C. The pyrolysis gas contained mainly H_2; and, small amounts of CH_4, and CO_2 were produced starting at 450°C and increased with increasing temperature. Early in the steam gasification stage, the H_2 molar fraction increases sharply with time. Simultaneously, the molar fraction of CO_2 increased in the pyrolysis and then declined towards the end of the pyrolysis

stage.

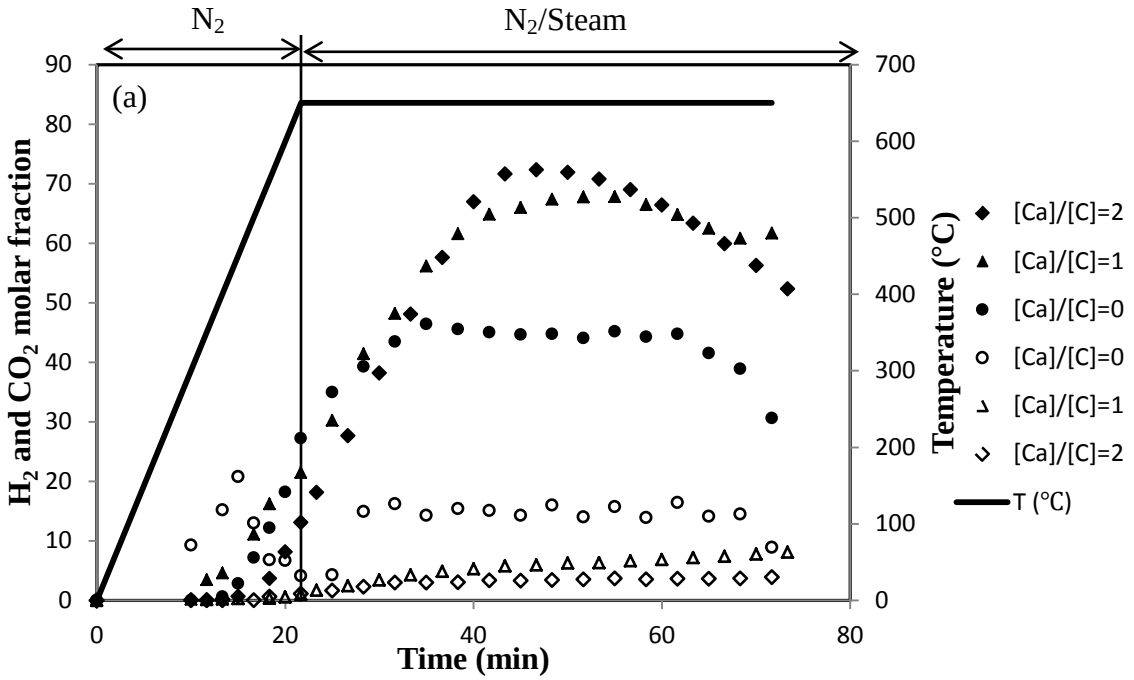
N2
N2/Steam
(a)
H2 and CO2 molar fraction
Temperature (°C)
Time (min)
[Ca]/[C]=2
[Ca]/[C]=1
[Ca]/[C]=0
[Ca]/[C]=0
[Ca]/[C]=1
[Ca]/[C]=2
T (°C)

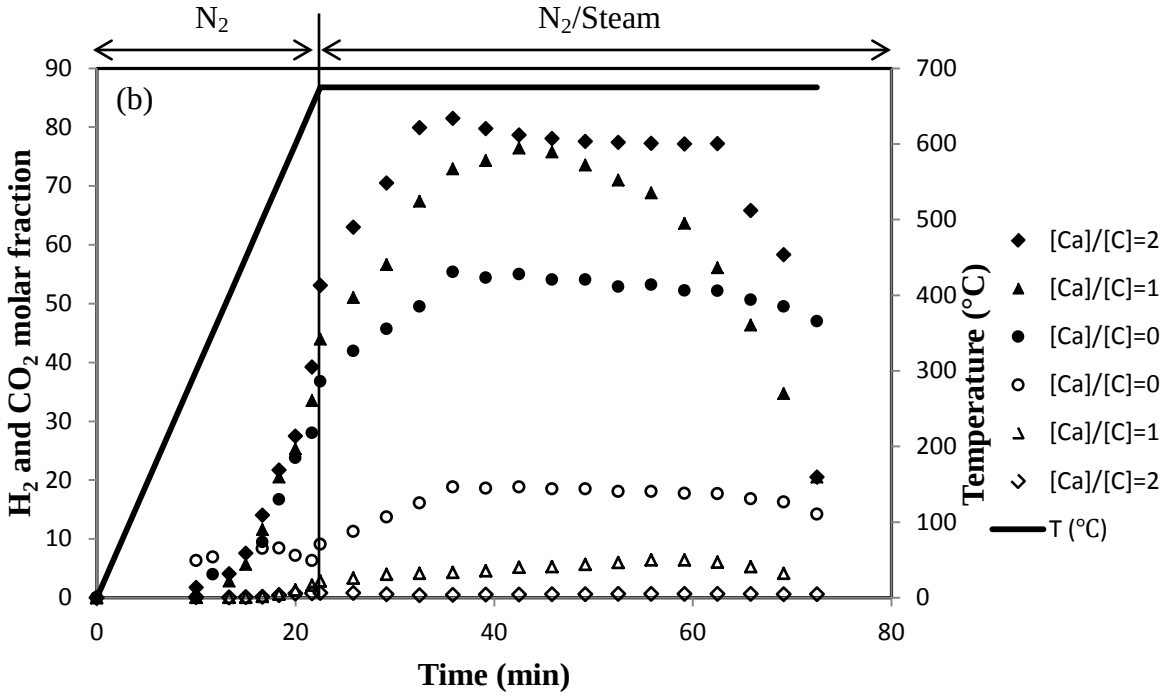
N2
N2/Steam
(b)
H2 and CO2 molar fraction
Temperature (°C)
Time (min)
[Ca]/[C]=2
[Ca]/[C]=1
[Ca]/[C]=0
[Ca]/[C]=0
[Ca]/[C]=1
[Ca]/[C]=2
T (°C)

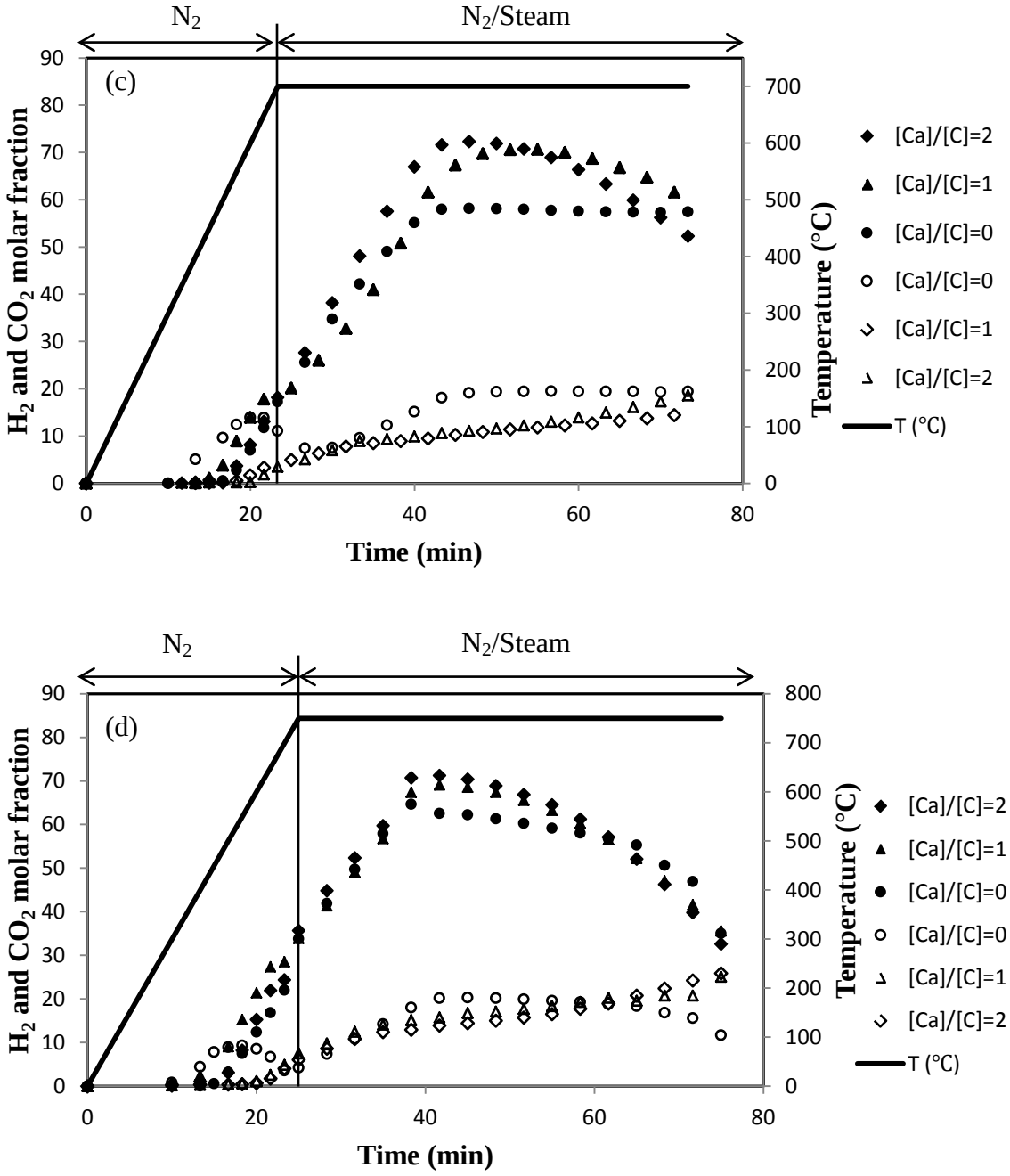

Fig. 6.2 Profile of H_2 (solid fill) and CO_2 (no fill) produced during the pyrolysis and steam gasification of coal with and without sorbent at (a) 650°C, (b) 675°C, (c) 700 °C, and (d) 750°C.

In steam gasification without sorbent ([Ca]/[C]=0), the molar fraction of CO_2 was raised to almost 16% with the injecting of steam into the reactor, implying that a WGS reaction took place and produced H_2 and CO_2 at the same time. After reaching to a certain level of H_2 and CO_2 in the gas phase, the molar fractions of H_2 and CO_2 hovered around a constant value and eventually decreased at the end of gasification. It should be noted that all the results reported in this study were on a dry basis with N_2.

As can be observed in Fig. 6.2(a), increases in the sorbent-to-carbon ratio significantly changed the H_2 production. Introducing sorbent to the steam gasification suppressed CO_2 production and enhanced H_2 production. Consequently, the H_2 molar fraction had higher peaks with time. The difference between H_2 molar fractions for [Ca]/[C] of 1 and 2 was not pronounced well at 650°C. The maximum value of the H_2 molar fraction was the result of shifting from a kinetic to mass transfer limited regime, which was caused by the carbonated layer around the sorbent and by the ash layer around char particles [14]. Indeed, the char gasification reaction decelerated the entire gasification process, particularly the key WGS reaction. Moreover, the highest molar fraction of H_2 (72.3%) and the lowest molar fraction of CO_2 (less than 3.0%) were obtained with in the case of [Ca]/[C] of 2.

Fig. 6.2(b) demonstrates the distribution of product gases H_2 and CO_2 from pyrolysis and steam gasification of coal at 675°C. The maximum H_2 molar fraction (more than 80%) and minimum CO_2 molar fraction (almost 0%) were achieved at 675°C with [Ca]/[C] of 2. In our previous study [13], the calcined Cadomin limestone (CaO) exhibited the best performance in terms of CO_2 capture at 675°C. Similar to Fig. 6.2(a), there was a noticeable gap between the gas products from steam gasification without sorbent ([Ca]/[C] = 0) and with sorbent ([Ca]/[C] = 1, 2). However, the greatest difference among all gasification temperatures occurred at 675°C.

The effect of further increments in temperature on the steam gasification of coal process is illustrated in Fig. 6.2(c) and (d). Although increasing the temperature resulted in higher reaction rates for the same experimental conditions, the maximum H_2 fraction decreased at 700 and 750°C. It is remarkable that increasing the temperature more than the optimal value (675°C) favored the WGS reaction rate such that, in coal gasification without sorbent, more H_2 was produced.

The endothermic steam coal gasification reaction (reaction (6.1)) benefited both kinetically and thermodynamically from higher temperatures. However, the exothermic WGS reaction in the absence of the catalyst never reaches equilibrium at temperatures less than 1123°C [15]. Therefore, the temperature affects the kinetic reaction rate rather than the equilibrium.

The consistency among the H_2 and CO_2 molar fraction trends confirmed the dependency of steam gasification of coal on the temperature and sorbent-to-carbon ratio. It is also worth mentioning that the CO_2 fraction for 700 and 750°C went through upward trends, since the carbonated sorbent began to calcine and release CO_2 into the reacting mixture.

The variations of the produced H_2 and CO_2 against time in the steam gasification of coal at four different temperatures with various molar ratios of sorbent-to-carbon ([Ca]/[C] = 0, 1, 2) are shown in Fig. 6.3. As can be observed from Fig. 6.3(a), the H_2 fraction at the lower temperature of 650°C did not demonstrate a sharp maximum during the steam gasification of coal without sorbent ([Ca]/[C] = 0). Increasing the temperature to 750°C resulted in leveling off the H_2 mole fraction.

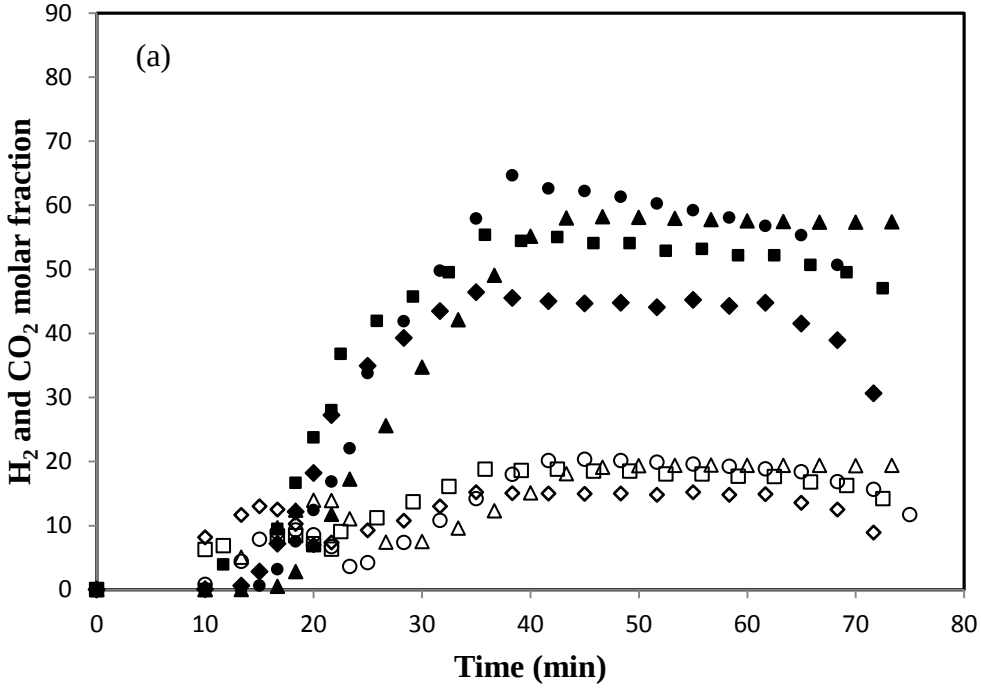
(a)
H_2 and CO_2 molar fraction
Time (min)
0
10
20
30
40
50
60
70
80
90

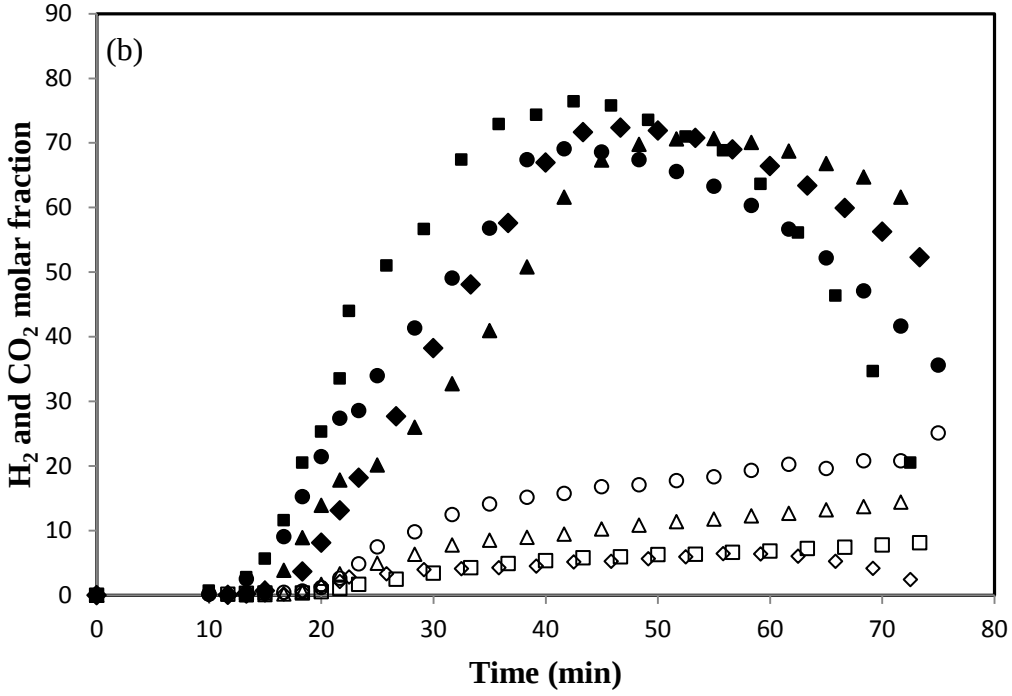
(b)
H_2 and CO_2 molar fraction
Time (min)
0
10
20
30
40
50
60
70
80
90

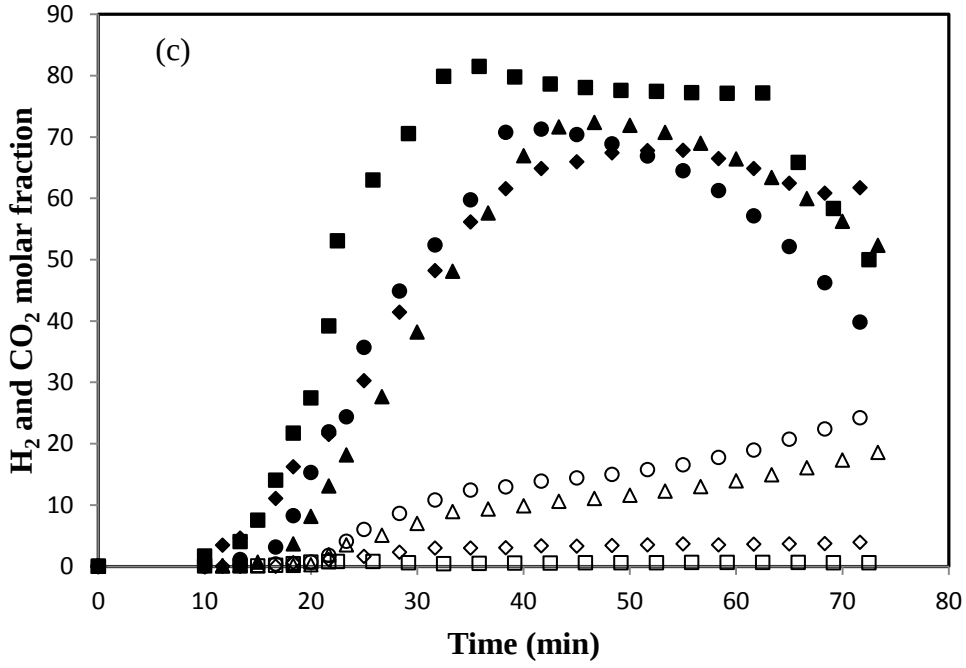

Fig. 6.3 Profile of H_2 (solid fill) and CO_2 (no fill) produced during the pyrolysis and the steam gasification of coal at different temperatures (650°C ♦, 675°C ■, 700°C ▲, and 750°C ●) and with different sorbent-to-carbon ratios (a) [Ca]/[C]=0, (b) [Ca]/[C]=1, (c) [Ca]/[C]=2.

The gap between the H_2 fractions became smaller with increasing temperature. In fact, the major variations in the H_2 fraction took place up to 700°C. After 700°C, the produced gas compositions changed slightly with temperature. This may have resulted from the occurrence of an inverse WGS reaction at temperatures above 700°C. On the other hand, there is also the possibility that WGS reached equilibrium at temperature as low as 700°C (rather than 1123°C) in the presence of the catalyst. With the higher and lower fractions of H_2 and CO_2 at 750 and 650°C (Fig. 6.3(a)), respectively, increasing the temperature improved the efficiency of steam gasification of coal and led to more thermal conversion of coal to gas products.

Fig. 6.3(b), and (c) indicate that the optimal temperature for steam gasification of coal integrated with CO_2 capture sorbent resulting in producing maximum H_2 molar fractions (more

than 81%) and minimum CO_2 (almost 0%) has occurred at 675°C. It is clarified that maximum and minimum molar fractions of H_2 and CO_2 occurred at different time period. This can be attributed to the highest CO_2 capture activity of the sorbent at 675°C. Table 6.3 shows the maximum molar fractions of H_2 produced from all steam gasification experiments. As mentioned before, increasing the temperature for the steam gasification of coal without sorbent enhanced the molar fraction of H_2; however, with the addition of the sorbent into the steam gasification, the molar fraction of H_2 increased with increasing temperature up to 675°C and then decreased with further increases in temperature.

Table 6.3 The maximum molar fractions of H_2 produced from all steam gasification of coal with different sorbent-to-carbon ratios and temperatures.

sorbent-to-carbon ratio / Temperature	0	1	2
	H_2 (%)		
650°C	46.4	67.4	72.3
675°C	55.4	76.4	81.5
700°C	58.2	70.6	70.4
750°C	64.6	69.1	71.2

Lin. et al [8] obtained a molar fraction of H_2 of 85.3% from steam gasification of a subbituminous coal (Taiheiyo coal, Japan) with CO_2 removal at 700°C. The measured H_2 concentration was calculated on a dry basis and N_2 free. However, in the current study, a molar fraction of H_2 of 81.5% was obtained at 675°C on a dry basis with N_2, which is equivalent to more than 98% H_2 on a dry basis and N_2 free. The improvement in H_2 production compared to the study made by Lin et al [8] may be due to the use of a natural active limestone with an

appropriate surface property to capture CO_2 rather than a synthesized CaO. The physical and chemical characteristics of Cadomin limestone were explained elsewhere [13].

The capture of CO_2 using active sorbent shifted WGS reaction forward, resulting in CO consumption and greater generation H_2. In addition, according to ultimate analysis, the BD coal sample used in this work consisted of more oxygen than the Taiheiyo coal used by Lin. et al [8], which may have contributed to producing more CO than CH_4 and leading to the generation of more H_2. The production of CH_4 in the product gas from coal pyrolysis with sorbent is less than that in the product gas from the coal pyrolysis without sorbent. Based on the reaction (6.5), it can be concluded that the reduction of CO due to WGS reaction may enhance CH_4 decomposition to H_2:

$$CH_4 + H_2O \rightarrow CO + 3H_2 \quad (6.5)$$

The molar fractions of CO_2 and CH_4 from steam gasification of coal without sorbent was larger and smaller than those from coal pyrolysis, respectively. CO_2 production occurs during WGS reaction and CH_4 produces through the following hydro-gasification reaction during the gasification.

$$C + 2H_2 \rightarrow CH_4 \quad (6.6)$$

The solid residue obtained from each coal gasification experiment was tested by a TGA to quantify the amount of unconverted carbon and $CaCO_3$ contained in the solid residues. About 20 mg of solid residue was subjected to the calcination condition of heating up to 900°C at 20°C/min in a pure N_2 flow of 50 ml/min. At 900°C, the N_2 was switched to air for burning off the carbon contained in the solid residues. Results are presented in Figs. 6.4, and 6.5.

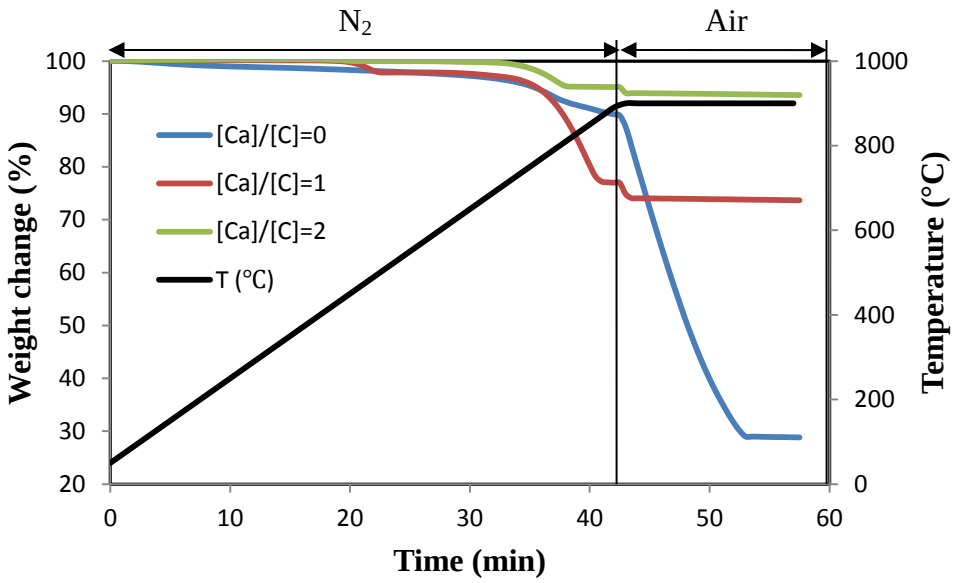

Fig. 6.4 TGA results of the solid residue obtained from the steam gasification of coal with and without sorbent at 650°C.

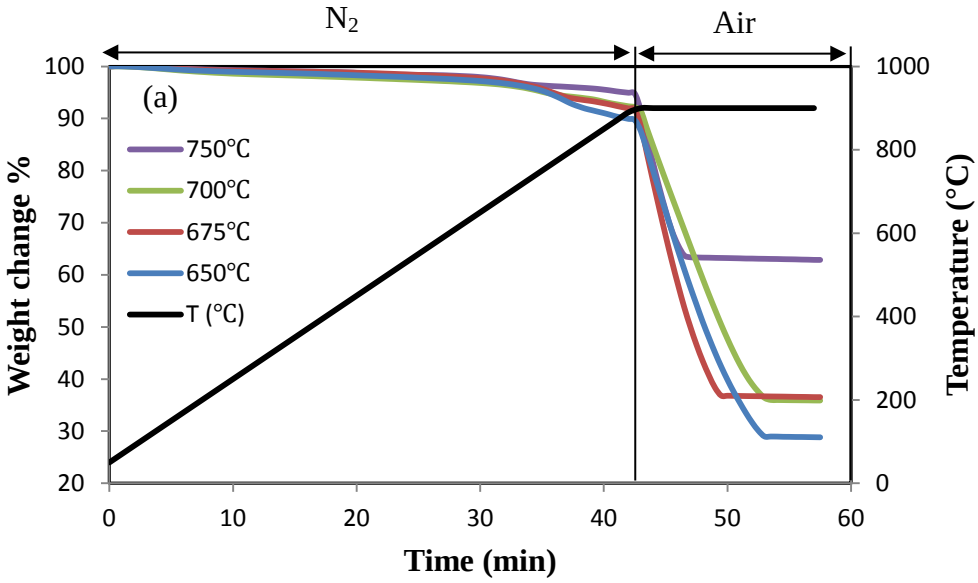

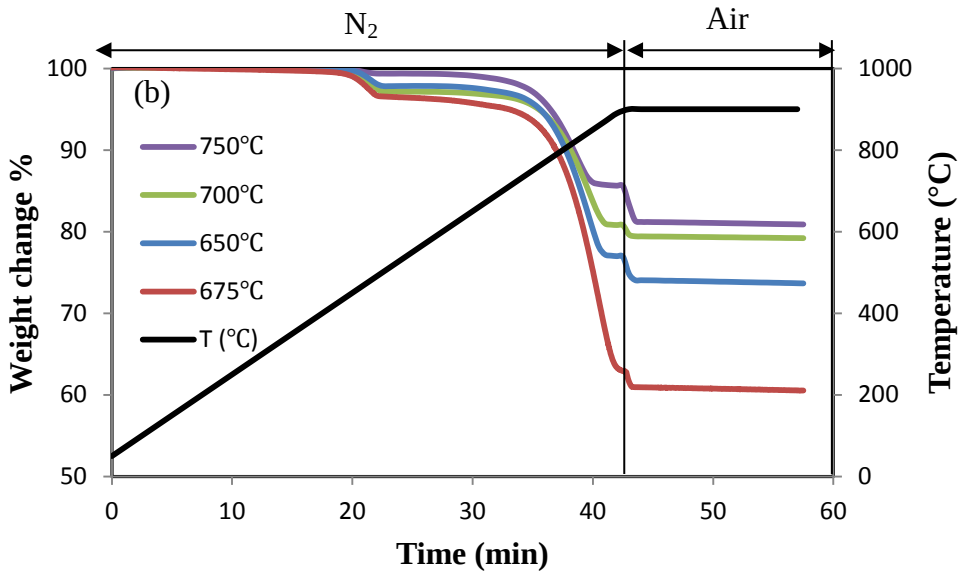

Fig. 6.5 TGA analysis of solid residues from steam gasification of coal at different temperatures and sorbent-to-carbon ratio (a) [Ca]/[C] = 0, and (b) [Ca]/[C]=1.

Fig. 6.4 shows a sample of the results obtained for the residues obtained from steam gasification of coal with three sorbent-to-carbon ratios ([Ca]/[C] = 0, 1, 2) at 650°C. According to Fig. 6.4, the coal pyrolysis and $CaCO_3$ decomposition occurred with increasing temperature up to 900°C under N_2 atmosphere. In this case, there are two steps in the weight loss profiles; the first step reveals the weight loss due to the coal pyrolysis, followed by the second step presenting the decomposition of $CaCO_3$ from capturing CO_2 with CaO in the process. In this figure, it can be observed that the presence of sorbent dramatically improved the coal gasification process, resulting in much lower unconverted carbon after gasification. The unconverted carbon of coal gasification with a sorbent-to-carbon ratio of 2 was slightly less than that of with a sorbent-to-carbon ratio of 1. Table 6.4 shows the weight percentage of unconverted carbon of all solid residues obtained after coal gasification with the different sorbent-to-carbon ratios and temperatures. Therefore, it is concluded that the CO_2 produced during coal gasification was fixed

to the sorbent. According to this figure, the percentage of $CaCO_3$ decomposition of sorbent-to-carbon ratio of 2 was lower than that with a sorbent-to-carbon ratio of 1, due to the presence of double the sorbent mass in the coal gasification.

Table 6.4 The weight percentage of unconverted carbon of all solid residues obtained after coal gasification with different sorbent-to-carbon ratios and temperatures.

sorbent-to-carbon ratio / Temperature	0	1	2
	Unconverted carbon (wt.%)		
650°C	61	32	21.3
675°C	57.5	19.1	22.4
700°C	57.5	18	22.5
750 °C	33.1	26.4	20.9

The TGA results of the solid residues after coal gasification without and with sorbent at different temperatures (650, 675, 700, and 750°C) are presented in Fig. 6.5. As can be seen from Fig. 6.5(a), and Table 6.4, the percentage of unconverted carbon combusted in air decreased with increasing temperature. Therefore, as expected, the coal gasification without sorbent improved when the temperature was increased up to 750°C. In addition, the weight loss of the solid residues before the burn-off stage decreased with increasing temperature, confirming a positive effect of increasing temperature on coal gasification.

Fig. 6.5(b) illustrates the TGA results of the solid residues after the steam gasification of coal with a sorbent ([Ca]/[C] = 1). In this figure, the percentage of $CaCO_3$ decomposition, which means the amount of CO_2 captured by the sorbent, increased with temperature up to 675°C and then decreased with further increases in temperature. These results confirm those of our previous

study [13], which showed that 675°C was the optimal temperature of CO_2 capture using sorbent at 1 atm. Moreover, regarding to carbon combustion part, the steam gasification of coal with sorbent at 700 and 675^{o}C almost completely was occurred as evidenced by the 1.6 and 1.8% of carbon in the residues.

Fig. 6.6 shows the measured unconverted carbon contained in the solid residues after coal gasification at four different temperatures and three sorbent-to-carbon ratios using the CHNS analyzer. As can be seen, the amount of unconverted carbon decreased with addition of CO_2 capture sorbent into the steam gasification of coal process at all four temperatures. In the steam gasification of coal without sorbent ([Ca]/[C] = 0), the unconverted carbon content of the solid residue decreased with increasing temperature, indicating that the steam gasification of coal was improved with increasing temperature. On the other hand, the lowest and highest unconverted carbon contents of the solid residues after steam gasification of coal with sorbent belong to temperatures 675^{o}C and 750^{o}C, respectively. Therefore, the CHNS results verified the TGA results of the unconverted carbon content of the solid residues after the steam gasification of coal with and without sorbent.

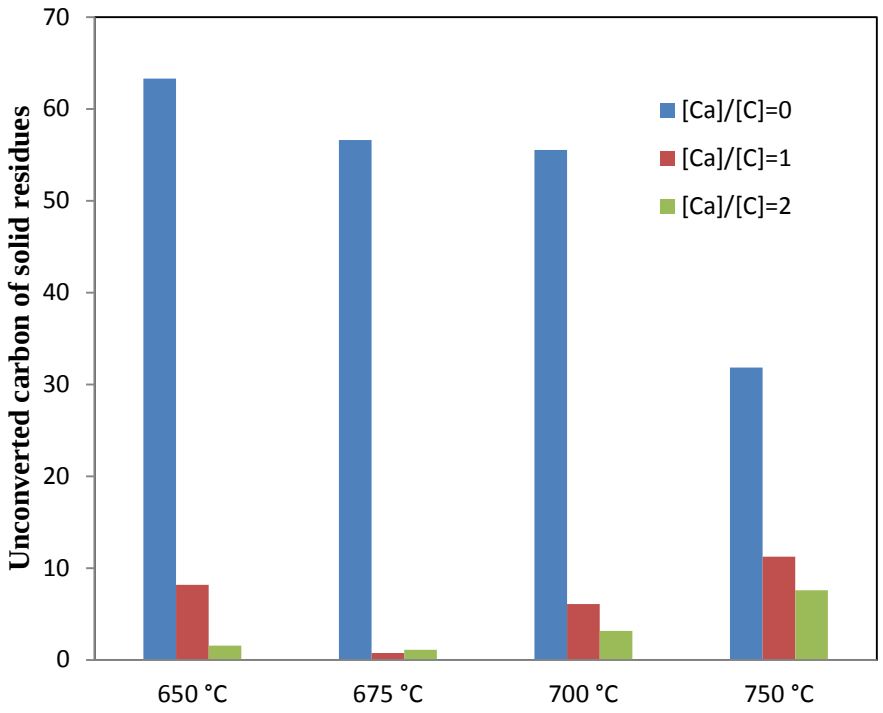

Fig. 6.6 Comparison of the amount of unconverted carbon of solid residues obtained from the steam gasification of coal experiments using CHNS analyzer.

The conversion of coal to gas in all steam gasification experiments was defined on a carbon basis as follows:

$$X = \frac{m_{c_0} - m_{c_r}}{m_{c_0}} \times 100 \tag{6.7}$$

where X is the conversion of coal, m_{c_0} is the mass of the carbon in coal supplied to the reactor, and m_{c_r} is the mass of the unconverted carbon in residues obtained after the steam gasification experiments. Table 6.5 presents the conversion of coal from all steam gasification with different sorbent-to-carbon ratios and temperatures. As expected, in the case of steam gasification of coal without sorbent, increased temperatures resulted in enhanced conversion of coal to the product gas. For instance, the conversion of coal increased from 36.5% to 71% by increasing temperature from 650°C to 750°C. On the other hand, with the addition of sorbent to the steam gasification,

the coal conversion increased dramatically (almost 50%) for temperatures of 650°C, 675°C, and 700°C. However, no obvious improvement could be seen at temperature 750^{o}C.

Table 6.5 The conversion of coal from all steam gasification of coal with different sorbent-to-carbon ratios and temperatures.

sorbent-to-carbon ratio / Temperature	0	1	2
	Conversion (%)		
650^{o}C	36.5	66.7	77.8
675^{o}C	43.5	82.3	76.7
700^{o}C	46.8	85.2	76.6
750^{o}C	71.3	80.1	78.2

As also shown in Table 6.5, the increase of the sorbent-to-carbon ratio from 1 to 2 led a 10% increase in the conversion of coal at 650°C, was almost constant at 675°C, and decreased at higher temperatures (700, 750°C). Therefore, at temperatures higher than 675°C, the addition of more sorbent actually decreased the process efficiency. According to our previous study [13], the calcination reaction was initiated at temperature 700°C and atmospheric pressure, thereby releasing the CO_2 from the sorbent. The release of CO_2 from the sorbent during steam gasification of coal would have an adverse effect on the WGS reaction, resulting in decreased process efficiency and carbon conversion.

6.6 Conclusions

The effects of temperature and sorbent-to-carbon ratio ([Ca]/[C]) on the molar fraction of H_2, the conversion of coal, and the concentration of CO_2 in the steam gasification of BD coal integrated with CaO as the CO_2 capture sorbent at atmospheric pressure were investigated. The

molar fraction of H_2 and conversion of coal were enhanced with increased temperature in the steam gasification of coal in the absence of sorbent. CO_2 was detected in all experiments performed without sorbent. With the addition of sorbent into the steam gasification of coal, the process improved considerably, increasing the molar fraction of H_2 and conversion of coal up to more than 80%. The TGA results of solid residues obtained from the gasification process with sorbent indicated that almost all CO_2 was fixed to the sorbent. The steam gasification of coal with sorbent showed an optimal temperature of 675°C, due to the best performance of the sorbent in capturing CO_2 at that temperature.

6.7 References

[1] Herzog, H. J., What future for carbon capture and sequestration?. Environ. Sci. Technol. 35 (2001) 148A–153A.

[2] Rao, A. B., Rubin, E. S., A technical, economic, and environmental assessment of amine-based CO_2 capture technology for power plant greenhouse gas control. Environ. Sci. Technol. 36 (2002) 4467–4475.

[3] Figueroa, J. D., Fout, T., Plasynski, S., McIlvried, H., Srivastava, R. D., Advances in CO_2 capture technology—The U.S. Department of Energy's Carbon Sequestration Program, Int. J. Greenh. Gas Control 2 (2008) 9–20.

[4] Kanniche, M., Gros-Bonnivard, R., Jaud, P., Valle-Marcos, J., Amann, J. M., Bouallou, C., Pre-combustion, post-combustion and oxy-fuel combustion in thermal power plant for CO_2 capture. Appl. Therm. Eng. 30 (2010) 53–62.

[5] Hossain, M. M., de Lasa, H. I., Chemical-looping combustion (CLC) for inherent CO_2 separations—a review. Chem. Eng. Sci. 63 (2008) 4433–4451.

[6] Scheffknecht, G., Al-Makhadmeh, L., Schnell, U., Marier, J., Oxy-fuel coal combustion—A review of the current state-of-the-art. Int. J. Greenh. Gas Control 55 (2011) 516-535.

[7] Davidson, J., Thambimuthu, K., Technologies for capture of carbon dioxide. Proceedings of the 7th International Conference on greenhouse gas control technologies, Vancouver, Canada (2004).

[8] Lin, S., Harada, M., Suzuki, Y., Hatano, H., Hydrogen production from coal by separation carbon dioxide during gasification. Fuel 81 (2002) 2079–2085.

[9] Lin, S., Suzuki, Y., Hatano, H., Harada, M., Hydrogen production from hydrocarbon by integration of water-carbon reaction and carbon dioxide removal (HyPr-RING method). Energy Fuels 15 (2001) 339-343.

[10] Lin, S., Harada, M., Suzuki, Y., Hatano, H., Process analysis for hydrogen production by reaction integrated novel gasification (HyPr-RING). Energy Conv. Manag. 46 (2005) 869-880.

[11] Lin, S., Harada, M., Suzuki, Y., Hatano, H., Continious experiment regarding hydrogen production by coal/CaO reaction with steam (I) gas products. Fuel 83 (2004) 869-874.

[12] Sedghkerdar, M. H., Mahinpey, N., Sun, Z., Kaliaguine, S., Novel synthetic sol-gel CaO based pellets using porous mesostructured silica in cyclic CO_2 capture processes. Fuel 127 (2014) 101-108.

[13] Sedghkerdar, M. H., Mostafavi, E., Mahinpey, N., Investigation of the kinetics of carbonation reaction with CaO-based sorbents using experiments and Aspen Plus simulation. Chem. Eng. Comm. In press, available online July 1, (2014). DOI: 10.1080/00986445.2013.871709

[14] Mostafavi, E., Mahinpey, N., Manovic, V., A novel development of mixed catalyst-sorbent pellets for steam gasification of coal chars with in situ CO_2 capture. Catal. Today 15 (2014) 111-117.

[15] Corella, J., Sanz, A., Modeling circulating fluidized bed biomass gasifiers. A pseudo-rigorous model for stationary state. Fuel Process. Technol. 86 (2005) 1021-1053.

Chapter Seven: **Conclusions and recommendations for future studies**

7.1 Conclusions

The overall objective of this thesis was the integration of coal gasification and CO_2 capture using a solid sorbent, while producing high purity hydrogen simultaneously. In order to address this objective, two topics were explored. The first topic focused on the CO_2 capture using a solid sorbent through a calcium-looping cycle process, which included investigation of the intrinsic and global kinetics of the carbonation reaction, the effect of the presence of biomass during the calcination reaction on the sorbent surface morphology and the intrinsic kinetics of the carbonation reaction. The performances of different sorbents, i.e., natural and modified calcium-based materials, with respect to CO_2 capture activity and stability throughout the calcium-looping cycle process were also investigated.

The knowledge achieved from the first topic was then applied in the second part of the research which concentrated on the application and integration of the tested solid sorbents in the coal gasification process to capture CO_2 and, consequently, produce high purity hydrogen.

The intrinsic kinetics of the carbonation reaction for two types of calcined limestone (Havelock and Cadomin) was studied based on the grain model, with the following results:

- Both types of calcined limestone showed linear relations between the rate of carbonation reaction and the CO_2 partial pressure at a constant total pressure of 1 atm.
- The first-order carbonation reaction rate at a lower total pressure changed to zero order at total pressures higher than 3 and 4 atm for the Havelock and Cadomin calcines, respectively.
- The carbonation reaction rate showed an increase with increasing temperature in the range of 450 to 675°C, but decreased with further increases in temperature.

- The activation energies were found to be 32.1 and 20.3 kJ/mol for the Havelock and Cadomin calcines, respectively.

The global kinetic study was performed using two mathematical modeling, i.e. the grain and the CGS models, to describe the carbonation reaction, with the following results:

- The CGS model coupled with the variable product layer diffusivity as a function of the overall CaO conversion showed better agreement with the experimental data than the results obtained by the grain model.
- The modeling results showed an improvement in the carbonation reaction rate by increasing the temperature and particle porosity and decreasing the sorbent particle size.
- The comparison between the modeling and experimental results showed that the CGS model was able to predict the behavior of the carbonation reaction more accurately that the grain model.
- The modeling results confirmed that the carbonation reaction consists of two stages; a kinetic controlled stage at the beginning, followed by a diffusion control stage.

The intrinsic kinetic study of the carbonation reaction for calcined Havelock limestone which was calcined with or without biomass (sawdust) under N_2 resulted in:

- The presence of sawdust during calcination decreased the negative effect of sintering by improving the surface morphology of the sorbent based on smaller pore size and higher surface area, which significantly increased the initial carbonation rate, where the reaction is kinetically controlled.

The performances of the natural calcined Cadomin limestone and modified ones prepared with different binders (calcium aluminate cement and silica-sol) and different procedures

(precipitation and sol-gel) with respect to CO_2 capture activity and stability were compared through a series of 31 carbonation–calcination cycles. The results showed that:

- The modified sorbents improved the CO_2-carrying activity and that the use of binders decreased the negative effect of sintering.
- Cadomin-calcium aluminate (CD-CA-14) pellets yielded both a high CO_2 uptake capacity and a low loss of activity through 31 cycles due to the presence of a Mayenite phase ($Ca_{12}Al_{14}O_{33}$) in the CaO structure.
- The core/shell (CD-CS) pellets had the highest stability with a low CO_2 uptake capacity, due to the high content of binder (43%) in the pellet structure.

Finally, the application of the calcium-based sorbent in the gasification process to capture CO_2 in a horizontal fixed-bed reactor at atmospheric pressure, which consequently produced high purity hydrogen, was investigated. This study explored the effects of temperature and sorbent-to-carbon ratio on the molar fraction of H_2, the conversion of coal, and the concentration of CO_2 in the steam gasification of BD coal integrated with CaO as the CO_2 capture sorbent at atmospheric pressure. The results were as follows:

- The molar fraction of H_2 and conversion of coal were enhanced with increased temperature in the steam gasification of coal in the absence of sorbent.
- After adding solid sorbent into the steam gasification of coal, the process improved considerably, increasing the molar fraction of H_2 and conversion of coal up to more than 80%.
- The steam gasification of coal with a sorbent had an optimal temperature of 675°C, i.e., the best performance of the sorbent in capturing CO_2 was at that temperature.

7.2 Relation between chapters:

Fig 7.1 presents all of research concepts of this study and the rationale and relations among them. Two topics have been studied for this research: the first subject is CO_2 capture using calcium-based sorbents; and, the second is the application of calcium-based sorbents into the gasification process for the capture of CO_2. As shown in Fig. 7.1, Chapters 2-5 have investigated the first topic, which included two subtopics – the kinetic study of CO_2 capture through a carbonation reaction (Chapters 2 and 3) and the calcium-looping cycle process (Chapters 4 and 5). The second topic of this thesis is presented in Chapter 6.

In Chapter 2, the intrinsic kinetics of the carbonation reaction is investigated to measure the intrinsic kinetic parameters. Chapter 3 conducts a global kinetic analysis of a CO_2 capture process by applying the intrinsic kinetic parameters obtained from Chapter 2. The results obtained from the kinetic study of CO_2 capture are applied to a calcium-looping cycle process.

Chapter 4 presents the effect of presence of sawdust as a biomass during high temperature calcination on the surface morphology of the sorbent and, consequently, on the rate of the carbonation reaction. In Chapter 5, the performances of different solid sorbents, including natural and modified calcium-based materials, in the calcium-looping cycle process through 31 carbonation–calcination cycles are studied for CO_2 capture activity and cyclic stability.

The results obtained from the kinetic study of a carbonation reaction in Chapter 2 are then applied in Chapter 6 for investigation of the application of the calcium-based sorbets in the gasification process to capture CO_2 and produce H_2.

Continuous gasification integrated with a CO_2 capture process applying the results obtained from Chapters 2 through 6 is recommended for future study.

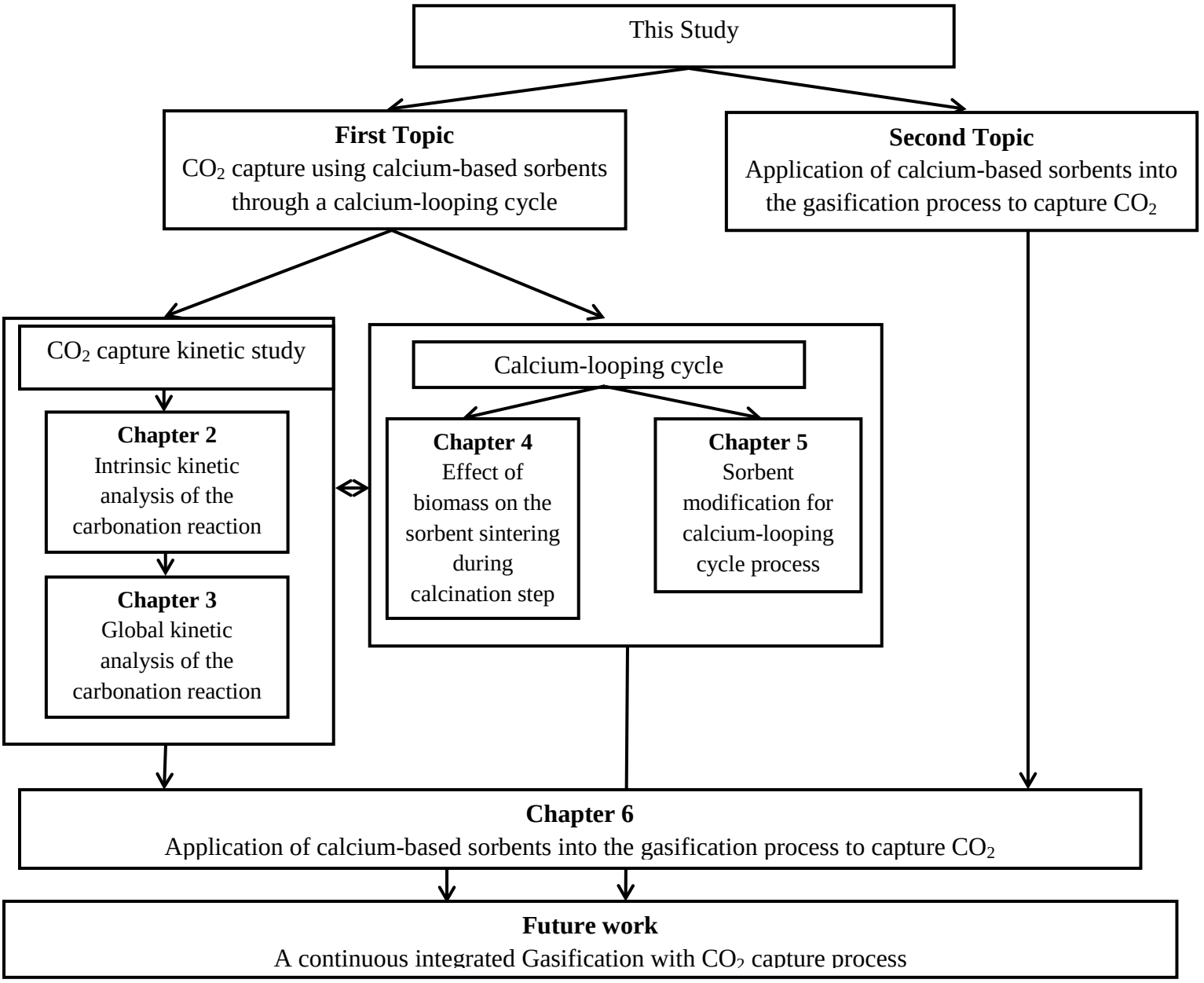

Fig 7.1 Relation between chapters

7.3 Recommendations for future work

Recommendations for future work are listed as follows:

1) Since the sorbent activity plays an important role in the overall calcium-looping cycle process, investigations should be pursued on the preparation of the calcium-based sorbent with a higher activity and slower deactivation rate using different methodologies and materials.

2) The calcium-looping cycle process has been studied for several decades in the bench scale; therefore, scale up studies should be conducted in the future for exploring the process in more real situations.

3) The integrated gasification and CO_2 capture process needs more investigation to clarify the effect of different parameters such as pressure, and steam-to-carbon ratio.

4) A continuous experiment of integrated gasification and CO_2 capture process should be performed by adding a regenerator reactor to the experimental set up.

5) A comprehensive kinetic modeling of the entire integrated gasification and CO_2 capture process including several reactions is highly recommended.

6) Testing the integrated gasification and CO_2 capture process to be conducted in a fluidized-bed reactor instead of fixed-bed reactor to enhance the heat and mass transfer efficiency is recommended.

7) A scale-up investigation should be performed in the future to study the integrated gasification and CO_2 capture process with large quantities of coal and sorbent.

APENDIX A: UNCERTAINITY ANALYSIS

Different experimental facilities were used in this research, which posed uncertainties in the measurement of parameters. TGA was the main experiment used to measure the mass change of the sample versus time at different determined temperatures. In this study, two different types of ATGAs were used; 1) Perkin Elmer TGA 7, and 2) Perkin Elmer STA 6000, with a sensitive microbalance, which is capable of detecting weight changes as small as 0.1 μg. The THERMAX 500 PTGA included a Cahn 100 balance with a sensitivity of 1 μg. In all experiments, there were mostly 5% uncertainty associated with the program temperature and the sample temperature. All experiments have conducted at least twice and the results showed less than 5% uncertainty.

A.1 Uncertainty measurements for activation energy:

In Chapters 2 and 4, the intrinsic kinetic parameters such as activation energy and pre-exponential factor were calculated using the Arrhenus equation (Eq. (2.6)) through a linear regression of the logarithm of a rate constant versus inverse temperature. In Chapter 2, the 21.8% and 16.2% uncertainties were obtained for the measured activation energies of the carbonation reaction using Havelock and Cadomin limestone calcines, respectively. Similarly, in Chapter 4, the 21.6% and 32.3% uncertainties were associated with the activation energies for Havelock limestone carbonation reaction calcined with and without sawdust. The uncertainties are calculated in Excel and correspond to 95% confidence levels. Table A.1 presents a sample of output result from Excel for the linear regression (Eq. (A.1)) that fits the experimental data for the calcined Havelock limestone with the minimum amount of squared variation.

Table A.1 Excel output of linear regression statistics

	Coefficients	**Standard error**	**Lower 95%**	**Upper 95%**
Intercept ($Ln\ (k_0)$)	-8.364	0.991	-11.5388	-5.2288
Slope $(-\frac{E}{R})$	-3867.41	815.321	-6455.0682	-1265.64

$$y = -3867.41\ x - 8.364 \qquad \text{Eq. (A.1)}$$

The standard error which represents the uncertainty for the slop of the linear regression was obtained through Eq. (A.2).

$$\text{Standard error} = \frac{\sqrt{\sum_1^N \frac{(y_i - \hat{y}_i)^2}{N-2}}}{\sqrt{\sum_1^N (x_i - \bar{x})^2}} \qquad \text{Eq. (A.2)}$$

where y_i, $\hat{y}_i$, x_i, and $\bar{x}$ are actual value of y for data i, predicted value of y for data i, actual value for x for data i, and the mean of x data.

APPENDIX B: MATLAB CODE FOR A GLOBAL KINETIC STUDY OF THE CARBONATION REACTION

```
%----------------------Carbonation Reaction Model------------
Tc=550;% Reaction Temperature, C
alphaDg=10.6;%Product layer parameter, dimensionless
delt=0.002;% time step, min
tf=100;% Final time
Dg0=2.5e-11;%diffusivity through the product layer of grain,cm2/min
psize=450;% average particle diameter, micrometer
P1=0.5;%CO2 partial pressure,atm
P=1;% total pressure of the reaction, atm
YCaO=0.42;%weight fraction of CaO in the sorbent
rotrue=2.71;%true density of sorbent limestone,gr/cm3
roCaO=0.06; %molar density of sorbent. mole/cm3
Rp=(psize*1e-4)/2;% initial average radius of particle,cm
T=Tc+273;% absolute temperature
Pe=(10^(7.079-8308/T));%equilibrium pressure of CO2 at T in reaction, atm (ref. Baker)
Cb=P1/(82.06*T);%CO2 concentration in the bulk,mol/cm^3
Ce=Pe/(82.06*T);%equilibrium concentration of CO2at T,mol/cm^3
rc=140e-4;%minimum particle radius regarding to maximum conversion, cm
GP=70;% number of grids used in modeling of entire particle
GPd=65;%number of grids used for inner core of the particle
epsg=0.01;%porosity of product layer
eps0=0.16;%initial porosity of the particle
Sg=13.8e+4;%initial surface area of the particle (BET surface area),cm^2/g
Zvi=2.45;%theoretical expansion factor
vN2=17.9;%molecular volume of N2
vCO2=28.2;%molecular volume of CO2
mN2=28;%molecular weight of N2
mCO2=44;% molecular weight of CO2
error=1e-7;%maximum acceptable truncation error of iteration
%--------------------%Calculating corresponding constants------
Zv=Zvi/(1-epsg);%actual estimated expansion factor
ropart=rotrue*(1-eps0);%actual density of the particle,g/cm3
rg=3*(1-eps0)/(Sg*ropart);%grain radius, cm
Ng=(1-eps0)*Rp^3/rg^3;%number of the grains in the particle
delR1=(Rp-rc)/(GP-GPd);%grid interval(outer shell)
delR2=rc/GPd;%grid interval (inner layer)
Xmax=1;
if Xmax>1.0
   Xmax=1.0;
end
rigmin=rg*(1-Xmax)^(1/3);%minimum theoretical radius of grain after complete conversion
ks=3.0*10^-4*Rg*Texp(-20.3/8.314*T);%cm/s
```

```
ghama=-0.000872*(T/131.85)^3+0.01904*(T/131.85)^2-
0.159732*(T/131.85)+1.273584;%intermolecular potential
Dm=60*0.0018583/(3.839^2)*((1/mCO2+1/mCO2)^0.5)*T^(3/2)/P/ghama;%(1e-
3)*60*T^1.75*0.05844^.5/(P*(vCO2^0.3333+vN2^0.3333)^2); %Molecular
diffusivity,cm2/min
ii=1;
count=1;
%---------Assigning initial guess for grain reaction interface--
for s=1:GP+1
   rig(s)=rg;%variable grain radius within the particle
end
%------------------------Marching through time steps-----------
ff=0;
jj=1;
for t=0:delt:20
   Z=0;%dummy variable to check for total number of iterations
   Cdummy=1.0;%dummy variable for checking the truncation error
   for i=2:GP+1
      X1(i)=1-(rig(i)/rg)^3;%local conversion of grains through the particle
      eps(i)=1-((1-eps0)*(1+(Zv-1)*X1(i)));% local porosity of the particle
      rgd(i)=rg*(1+(Zv-1)*X1(i))^(1/3);%expanded radius of the local grain
      Dk=60*(4/3*(8*8.314e7*T/(3.14*mCO2))^0.5)*(4.7286*(1-eps(i))/eps(i)/rgd(i))^-
1;%Knudsen diffusivity,cm2/min
      De(i)=eps(i)^2*(1/(1/Dk+1/Dm));%effective diffusivity between the grains,cm2/min
      Cnew(i)=((Cb-Ce)*Rp/R(i))*sinh((3*k*rig(i)^2*(1-
eps0)/.08/rg^3)^0.5*R(i))/sinh((3*k*rig(i)^2*(1-eps0)/.08/rg^3)^0.5*Rp)+Ce;
   end
%-------calculating reaction interface (Runge-Kutta method)-----
   sigmaX1=0;
   sigmaX2=0;
   sigmaGama=0;
   sigmaGama1=0;
   for m=2:GP+1
      rn=rig(m);% radius of unreacted core of each grain
      k=ks;
      if m<GPd+2
         R(m)=(m-1)*delR2;
      else
         R(m)=(GPd+1)*delR2+(m-GPd-1)*delR1;
      end
      n1=(-k/roCaO)*(Rp/R(m))*(Cb-Ce)*sinh((3*k*rn^2*(1-
eps0)/.08/rg^3)^0.5*R(m))/sinh((3*k*rn^2*(1-eps0)/.08/rg^3)^0.5*Rp);
      rn2=rn+(n1*delt)/2;
      n2=(-k/roCaO)*(Rp/R(m))*(Cb-Ce)*sinh((3*k*rn2^2*(1-
eps0)/.08/rg^3)^0.5*R(m))/sinh((3*k*rn2^2*(1-eps0)/.08/rg^3)^0.5*Rp);
```

```
      rn3=rn+(n2*delt)/2;
      n3=(-k/roCaO)*(Rp/R(m))*(Cb-Ce)*sinh((3*k*rn3^2*(1-
eps0)/.08/rg^3)^0.5*R(m))/sinh((3*k*rn3^2*(1-eps0)/.08/rg^3)^0.5*Rp);
      rn4=rn+(n3*delt)/2;
      n4=(-k/roCaO)*(Rp/R(m))*(Cb-Ce)*sinh((3*k*rn4^2*(1-
eps0)/.08/rg^3)^0.5*R(m))/sinh((3*k*rn4^2*(1-eps0)/.08/rg^3)^0.5*Rp);
      rn=rn+(n1+2*n2+2*n3+n4)*(delt/6);
      rig(m)=rn;
      if rig(m)<rigmin
         rig(m)=rigmin;
      end
      X1(m)=(1-(rig(m)/rg)^3);
      Gama(m)=(3*k*rig(m)^2*(1-eps0)/.08/rg^3)^.5*Rp;
      if m<GPd+2
         R(m)=(m-1)*delR2;
         dummyX2=X1(m)*R(m)^2;
         dummyGama=Gama(m)*R(m)^2;
         sigmaX2=dummyX2+sigmaX2;
         sigmaGama=dummyGama+sigmaGama;
      else
         R(m)=(GPd+1)*delR2+(m-GPd-1)*delR1;
         dummyX1=X1(m)*R(m)^2;
         dummyGama1=Gama(m)*R(m)^2;
         sigmaX1=dummyX1+sigmaX1;
         sigmaGama1=dummyGama1+sigmaGama1;
      end
   end
   %--calculating the overall conversion and plot the results--
   Gama0(count,1)=(3*delR1*sigmaGama/Rp^3+3*delR2*sigmaGama1/Rp^3);
   Xo(count,1)=(3*delR1*sigmaX1/Rp^3+3*delR2*sigmaX2/Rp^3);
   espss(count,1)=eps(i);
   subplot(2,2,1);
   plot(t+delt,Xo(count,1));
   hold on;
   xlabel('time min');
   ylabel('Overal Conversion');
   if (t==1|t==5|t==10|t==15|t==20)
      for jj=1:GP
         C(ii,jj)=Cnew(jj);
         Xlocal(ii,jj)=X1(jj);
      end
      ii=ii+1;
   end
   subplot(2,2,2);
   semilogy(Xo(count,1),(Dg0*exp(-alphaDg*Xo(count,1))));
```

```
    hold on;
    subplot(2,2,3);
    plot(R,Cnew)
    xlabel('Overal Conversion');
    ylabel('Dg,cm2/min');
    count=count+1;
end
%----------plot the local concentration vs particle radius------
for jj=1:GP+1
    if jj<GPd+2
        R(jj)=(jj-1)*delR2;
    else
        R(jj)=(GPd+1)*delR2+(jj-GPd-1)*delR1;
    end
    hold on;
    axis([0 Rp 0 Rp]);
    axis('auto y');
    xlabel('R.cm');
    ylabel('local co2 concentration, mole/cm3');
    subplot(2,2,4);
    plot(R,Xlocal(ii,jj),'-r.');
    hold on;
    axis([0 Rp 0 Rp]);
    axis('auto y');
    xlabel('R.cm');
    ylabel('local conversion');
end
```